3

NASA CR
147503

E7.6-10206

JET PROPULSION LABORATORY
CALIFORNIA INSTITUTE OF TECHNOLOGY
PASADENA, CALIFORNIA

COMPARISON OF SKYLAB AND LANDSAT IMAGES FOR GEOLOGIC MAPPING IN NORTHERN ARIZONA

Final Report

NASA 7-100

Task Order RD-161

A. F. H. Goetz
M. J. Abrams
A. R. Gillespie
B. S. Siegal

Jet Propulsion Laboratory
California Institute of Technology
Pasadena, California 91103

D. P. Elston
I. Lucchitta
S. S. C. Wu
A. Sanchez
W. D. Di Paola
F. J. Schafer
R. Jordan

U. S. Geological Survey
Flagstaff, Arizona 86001

February 27, 1976

CONTENTS

FIGURES

TABLES

I. INTRODUCTION

A. F. H. Goetz

This report contains a compilation of individual papers on the comparison of Skylab and LANDSAT images for geological mapping on a regional scale. The areas chosen in Arizona were identical to those studied in a previous LANDSAT study (Goetz et al., 1975). In addition several areas in western Arizona were studied early in the program to evaluate the comparative resolution capabilities of the instruments.

Analysis of the Shivwits Plateau area in northwest Arizona was carried out by I. Lucchitta and A. Sanchez. This study focused on the use of Skylab photographic products as very-high-altitude, very-small-scale aerial photographs in geologic mapping. The particular questions treated include: (1) the identification of the smallest features visible, (2) how well do various photogeologic maps correspond to reality, and (3) what are the cost factors in mapping with the various image types.

Analysis of the central Arizona test site, centered on the Verde Valley, was carried out by D. P. Elston and W. D. Di Paolo. This study concentrated on the relative visibility and orientation of lineament systems as observed on Skylab, LANDSAT and RB57 images. This study led to the identification of nineteen orthogonal pairs of lineaments or pairsets which cluster in three major north- and northeast-trending pairset groups. These pairsets are correlated with the trends of major Precambrian faults in central and northern Arizona. A study was made of the biases introduced into the lineament data by image resolution, sun angle and sun azimuth.

The Coconino Plateau test site was studied by M. J. Abrams and B. S. Siegal with the use of computer enhanced and classified LANDSAT images as well as

S190A and S192 MSS data. Field spectral measurements were used to determine the optimum combination of S192 spectral bands for the best discrimination among lithologic units. A detailed field map constructed during the prior ERTS investigation provided concise ground-truth for the evaluation of the Skylab derived information.

Red Lake, Arizona was studied by M. J. Abrams and B. S. Siegal to assess the value of imaging in wavelengths beyond the photographic limit of .85 μm by use of the Bendix 24 channel MSS. Eight features were chosen for determining the discriminability in each of the 13 MSS bands observed. The best three bands for the discrimination of lithologic features in the Red Lake area are in the 1 - 2.5 μm region.

A small photogeologic study by M. J. Abrams, comparing the detectability of lithologic units and faults on S190A and LANDSAT photographic images, was carried out in western Arizona along the Colorado River. Numerical values are assigned to the discriminability of various features to facilitate a more quantitative estimate of the usefulness of the different types of images.

A photogrammetric evaluation of S190B images was made by S. S. C. Wu. This study resulted in a 1:100,000 scale contour map developed from a stereo pair of images of the central Arizona test site. Although a contour interval of 100 feet was determined to be theoretically possible using the AP/C plotter, the errors are great enough to make 500 feet the practical minimum contour interval.

Ground spectral reflectance data of Red Lake was obtained in June and August 1973 during SL-2 and SL-3. These data were taken in the false hope that the S191 spectrometer would be trained on the site. However no S191 data were taken until September 1973 when the ground equipment was inoperable. Since severe thunderstorm activity took place between the August ground measurements

and the September S191 overflight, the extrapolation of the ground data to September did not appear feasible. The subsequent difficulty with the calibration of the S191 instrument and our preoccupation with the S192 noise problems led to the abandonment of our effort to use the S191 data.

Finally a complete compilation of the image processing programs and the processing sequence of S192 data is given. The documentation on the comparable LANDSAT image processing is given in Goetz et al. (1975).

Reference

Goetz, A. F. H., F. C. Billingsley, D. P. Elston, I. Lucchitta, E. M. Shoemaker, M. J. Abrams, A. R. Gillespie and R. L. Squires, "Applications of ERTS Images and Image Processing to Regional Geologic Problems and Geologic Mapping in Northern Arizona," JPL TR 32-1597, 1975.

SUMMARY AND CONCLUSIONS

A. Goetz

This report was assembled from the papers of several independent investigation teams. Each carried out an evaluation of the relative merits of LANDSAT and Skylab data in a different way. The findings agree remarkably well, and in the following discussion these findings will be summarized without regard to author.

A. Image Quality, S190A, B

In general it was found that based on resolution the Skylab S190A products were superior to LANDSAT images. Based on measurements of shoreline features in Lake Mead S190A images had 1.5 - 3 times greater resolution than LANDSAT. The term resolution is used here in its true meaning, not as "instantaneous field of view" as is often the use these days. The red (6000 - 7000 Å) B&W transparency had by far the highest resolving capability (65 m) while natural color was second (130 m). The LANDSAT resolution was approximately 220 m. Of course much smaller high contrast objects, such as roads, were detectable. In the S190A films roads as small as 6 m wide were visible while on LANDSAT products 10 m wide roads were detectable.

In general the higher resolution of the Skylab data yielded better discrimination among rock units, but in the case of structural features, lower sun angle LANDSAT images (50^{o}) were superior to higher sun angle Skylab images (77^{o}).

The most valuable advantage of the Skylab over the LANDSAT image products is the capability of producing stereo images./ This capability is very important in geologic interpretation and not available with LANDSAT. Although the S190B stereo images were superb, aircraft type resolution of 5 meters or better is required. The S190B images, in some cases, were acquired with 60% overlap, allowing the production of topographic maps. In this study a topographic map

of the Verde Valley, Arizona area was produced on an AP/C plotter. A contour interval of 100 feet is theoretically possible, but errors as large as 175 were found. Therefore 500 feet is the practical minimum contour interval which can be used.

B. Spectral Discrimination

Field spectral reflectance measurements on the Coconino Plateau were made in an effort to determine the best spectral bands for discrimination of the six geologic units in question. Linear discriminant analysis applied to the spectral data showed that images taken in bands at 1.3, 1.2, 1.0 and 0.5 μm were the most effective for separation of the units.

The EREP multispectral scanner yielded data with a low signal-to-noise ratio which limited its usefulness for image enhancement work. However, it provided unique data beyond 0.9 μm heretofore unavailable from a space platform. The results were very encouraging from the standpoint of being able to choose an optimum set of bands from field spectral data and producing a color composite of those bands which yielded excellent discriminant data. This operation was carried out for an image of the Coconino Plateau, an area extensively studied during the previous ERTS study (Goetz et al., 1975). Although the S/N was not great enough to allow a suitable ratio image to be formed, a color composite formed from bands near 1.3, 1.0 and 0.5 μm provided better discriminability among lithologic units than highly enhanced LANDSAT color ratio composites. The apparent good correlation between portable spectrometer data and satellite spectral images bodes well for the quantitative determination of optimum spectral bands for future missions.

The three S-192 bands chosen for high discriminability among units on the Coconino Plateau are not unique for all geologic provinces. Each geologic

setting will require imaging in a different set of bands to obtain optimal discrimination. However, it appears that bands in the 1.0 - 2.5 μm region are most often required, with a band at 1.6 μm consistently in the top three.

The thermal band was not tested in this study. It is doubtful that a single thermal measurement would be meaningful in separating geologic units because of the effects of topography, albedo and thermal inertia on the data.

In this study no attempts were made to register temporal data for use in separating geologic units based on sun angle, seasonal variations or vegetation anomalies.

C. Geologic Evaluation

The Shivwits Plateau area was again studied to evaluate the suitability of various types of images, including high altitude aircraft photos, for geologic mapping. The suitability of the image type depends strongly on the scale at which the mapping is to be carried out. LANDSAT and Skylab images cover a large area and have low resolution and therefore are totally unsuited for mapping of small areas at high resolution (for example 7½ and 15 minute quads.), for which conventional aerial photographs are much more appropriate. Conversely, LANDSAT images, especially when enhanced, are well suited to the areal coverage and detail required by mapping at 1:250,000 and smaller scales. Under optimum conditions LANDSAT images may be adequate for mapping at 1:125,000. This scale, on the other hand, is well suited to Skylab S190A photographs which may be usable even at 1:62,500 for non-detailed mapping. RB-57 images offer a remarkable combination of resolution and aerial coverage, and are thus usable for a wide variety of mapping scales ranging from 1:24,000 to 1:125,000.

In central Arizona a thorough study of lineaments visible on LANDSAT, Skylab and RB-57 images was undertaken. Detailed mapping of lineaments and

fractures has revealed that the strongly developed lineaments accurately reflect important through-going fracture systems in the bedrock. Analysis of lineaments has provided an azimuthal-frequency framework for evaluating fracture system trends that are related to different structural episodes. A discrete series of fractures was successively impressed on the Precambrian terrain and these breaks served to localize subsequent structural adjustments.

Mapping in the Coconino Plateau was done with S190A, S192 and LANDSAT data. Structural information was equally well seen on all three types of images. The major faults were accurately identified in all cases. LANDSAT false-color ratio composites, an S192 false color composite created from three IR bands, and an S190A false-color infrared composite were compared. All three provided accurate enough data for a geologic reconnaissance map.

Thematic maps produced by the three classification algorithms analyzed were not as accurate as the maps produced by photo interpretation of composites of enhanced images. This result agrees with a previous study (Goetz et al. (1975), which indicates that the spatial relationships in the image can be used to advantage by the interpreter. The computer classification, on the other hand, uses only the spectral reflectance information. In a geologic analysis computer enhancement with human interpretation appears to produce the best product.

Skylab images in general are superior to LANDSAT data but suffer from lack of availability due to absence of coverage in many areas. However one major advantage of the Skylab imager is the stereo coverage in selected areas. This additional type of information makes possible lithologic separations even when spectral data do not reveal differences. The S192 multispectral information has shown the potential of imaging data in the 1 - 2.5 μm region and this part of the spectrum should be emphasized on future missions.

Reference

Goetz, A. F. H., F. C. Billingsley, D. P. Elston, I. Lucchitta, E. M. Shoemaker, M. J. Abrams, A. R. Gillespie and R. L. Squires, "Applications of ERTS Images and Image Processing to Regional Geologic Problems and Geologic Mapping in Northern Arizona," JPL TR 32-1597, 1975.

II. GEOLOGY

II-A. Schivwits Plateau

I. Lucchitta and A. Sanchez

1. INTRODUCTION

Most geologic work requires observations at a variety of scales. The field geologist, for example, is concerned with megascopic observations (an entire mountain chain), mesoscopic observations (an outcrop, a bed, a hand specimen), and microscopic observations (thin sections, microprobe, and so on) (Fig. II-A-1). Each scale of observation provides context for the others, and all are integrated into a whole representing that particular geologist's best interpretation of the geology and geologic history of the area of study. In general, the more general, regional observations tend to provide a context for the more detailed and less embracing ones.

Man always has been able to operate directly at the mesoscopic scale because that is his own scale, the one at which he has evolved. The microscopic and megascopic scales, conversely, have to be converted to the mesoscopic one by means of suitable translating instruments in order for man to make use of these scales. These translating instruments have been in use for less than 150 years. The megascopic scale first became attainable in a primitive way only in the late 1930s when aerial photographs came into general use: each photo showed a substantial amount of terrain from a more favorable perspective than can be obtained from the ground; and several photos could be mosaicked together to cover larger areas in a relatively crude way. A true megascopic and synoptic perspective, in a variety of spectral bands, has become available only in the early 1970s through high-altitude and high-resolution aircraft photographs (U-2, RB-57), earth-orbiting satellites (LANDSAT, formerly ERTS), manned earth-orbiting satellites (SKYLAB), and in the most extreme case of viewing the entire earth

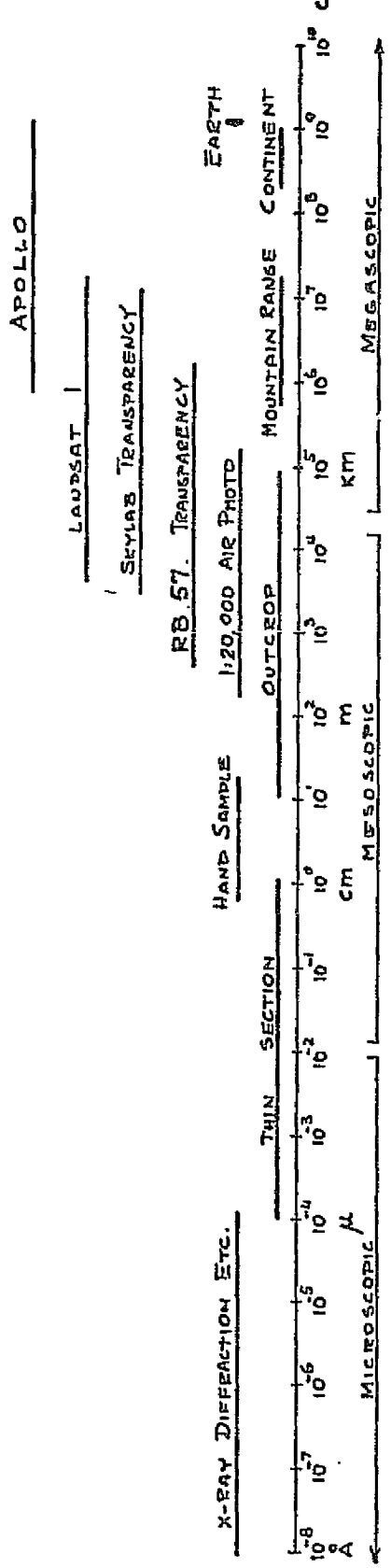

Fig. II-A-1. Scales of observation, size of common geologic objects, and size range of objects visible on various types of imagery.

in one frame, the Apollo missions. The ranges in size of objects that can be viewed by the various translating devices are shown in Fig. II-A-1.

The uses and applications of conventional air photos are well known. What is not well known are the most profitable and appropriate uses of the LANDSAT, SKYLAB and high-altitude aircraft imagery, in part because this imagery involves a far greater array of sensors than was available previously, in part because the imagery can be manipulated in the computer to provide a great variety of derivative images, in part because the megascopic scale requires a change of objectives and of thinking. It is the latter aspect that has provided the main thrust of our study; the other aspects have been investigated extensively elsewhere and the results abound in the literature.

In essence, we have viewed the satellite and aircraft images as very-high-altitude, very-small-scale aerial photographs whose unique attribute it is to furnish a synoptic view of large areas. We have used them in the same manner that geologists have long used aerial photographs in the field: for mapping and to solve geologic problems. Within this context, we have asked the following questions:

1) What is the smallest feature that can be recognized?

2) What is the smallest <u>geologic</u> feature that can be recognized?

These two questions together determine the lower boundary of applicability of the images.

3) How well can photogeologic maps be made on the various bases?

4) How well do the various photogeologic maps correspond to reality?

5) What is the relation between the detail of photogeologic mapping and correspondence to reality?

6) What is the best imagery to use for a specific type and scale of project?

7) What is the best mix, if any, of image types to use?

8) What are the cost factors of the various image types?

This study is a continuation and outgrowth of a previous investigation on the application of LANDSAT images to geologic problems of regional scale (Lucchitta, 1975). In that investigation, I. Lucchitta and R. Jeanne did the field mapping, analyzed LANDSAT images, and prepared photomaps on that base. These results are incorporated in the present study, which includes analysis of SKYLAB, RB-57 and LANDSAT images carried out chiefly by A. Sanchez.

2. IMAGERY

This study focuses on a comparative analysis and evaluation of geologic uses for images from earth-orbiting satellites as well as from high-altitude aircraft. The geographic area selected for the study is the Shivwits Plateau, in the Western Grand Canyon region. This plateau is well covered by the various types of images and has been mapped in detail, thus providing good ground control.

LANDSAT I images studied include 7.3" x 7.3" black and white paper prints of bands 5, 6, 7, and positive transparencies in false-color infrared, both at a scale of 1:1,000,000.

SKYLAB photographs were taken by the 70 mm multispectral cameras and were enlarged as positive transparencies to a scale of approximately 1:720,000.

High-altitude aircraft photographs consist of RB-57F 9" x 9" positive transparencies with an average scale of 1:110,000.

3. EQUIPMENT

Photographs were viewed either directly or with the aid of equipment that is easily available to the geologist. Elaborate or specialized equipment

was avoided in order to evaluate the usefulness of the various images under typical and general conditions. Equipment used is described briefly below:

Light sources: After some experimenting with several kinds of light, fluorescent light was selected because it is the whitest and most natural-appearing light and because it produces the least eye strain.

Light tables: Two light tables, both with fluorescent lighting were used for viewing color transparencies. One, a 16-1/2" x 18" portable light table with a frosted white plastic surface, was used only for single frames. The other was a Richards model GFL-940 MCE light table. This is a semi-portable unit capable of accepting either single frame film or roll film up to 9" wide. The viewing surface is clear glass with an additional frosted glass diffuser underneath. The table is equipped with zoom binocular heads for monoscopic or stereoscopic viewing. Also provided is a rheostat for varying the light intensity.

Magnifying lenses: When it was necessary to view prints or transparencies under magnification, we used a standard single-lens 5X reading glass, a 10X Hastings Triplet hand lens, and the monoscopic binocular head on the Richards light table, whose magnification ranges from 10X to 60X, depending on the eyepieces and zoom setting.

Optical comparators: A commercially available 6X optical comparator with inch and mm scales was used extensively for measuring

very small distances on both paper prints and transparencies.

Stereoscopes: Two kinds of stereoscopes were used. One was a standard 2.25X field pocket stereoscopic, the other a variable-magnification stereo head for use with the Richards light table described above. Magnification for this head varied from 2X to 16X, depending on the eyepieces used.

4. PROCEDURES

The first step was to inspect all images, determine the exact geographic area covered by each image, and then select one photograph from each of the ERTS, SKYLAB and RB-57F suites with the greatest geographic coincidence. These three photographs, depicting approximately the same area on the ground, were subsequently studied intensively.

Several images were studied in order to determine their scale and resolution. Black and white paper prints were studied with overhead fluorescent lighting, positive transparencies were viewed on a light table. Scale was determined by measuring the separation of specific features on the photos and comparing it with the separation of the same features on published maps. Five to ten scale determinations were made for each type of image. The results were compared with published scales, if any.

All images were studied in order to determine maximum "geographic" and "geologic" resolution. "Geographic" resolution pertains to the ability of seeing geographic or cultural features, "geologic" to discriminating geologic features. This was done by studying imagery under various magnifying devices, primarily the Richards light table. A glass reticle with mm and inch scales

was placed on the photograph. Both were then viewed through the monoscopic viewing head on the Richard light table with magnification ranging from 10-60X, depending on the feature being measured. Features as small as .04 mm or .002 inches can be measured with the reticle at 60X magnification.

Detailed photogeologic and photolineament maps were prepared from LANDSAT black and white paper prints, false-color infrared positive transparencies, and from SKYLAB true-color positive transparencies. These are described and presented below.

5. PRODUCTS

Photogeologic and photolineament maps showing different degrees of mapping detail were prepared on LANDSAT and SKYLAB bases. Two photolineament maps were constructed for the same geographic areas, one using LANDSAT and the other SKYLAB photocoverage. All recognizable lineaments were mapped and classified according to definition, which ranges from sharp to very diffuse. The lineament map constructed from the LANDSAT image (E-1051-17432) is shown in Fig. II-A-2. Mapping was done at a scale of 1:1,000,000 on a black and white paper base, Fig. II-A-3. The photolineament map prepared from the SKYLAB true-color transparency (SL3 RL28-060) is shown in Fig. II-A-4. The base used for this map is shown in Fig. II-A-5. Photogeologic maps, accompanied by detailed descriptions of each photogeologic unit, were prepared on the same base as the photolineament maps above. Several maps at various levels of detail were prepared in order to determine the level of detail that yields the most complete and accurate representation of the actual geology while at the same time minimizing photogeologic units that have no correspondence to reality.

Definition and description of photogeologic units are based on many photographic characteristics. These include color(s); geomorphic position; contact(s)

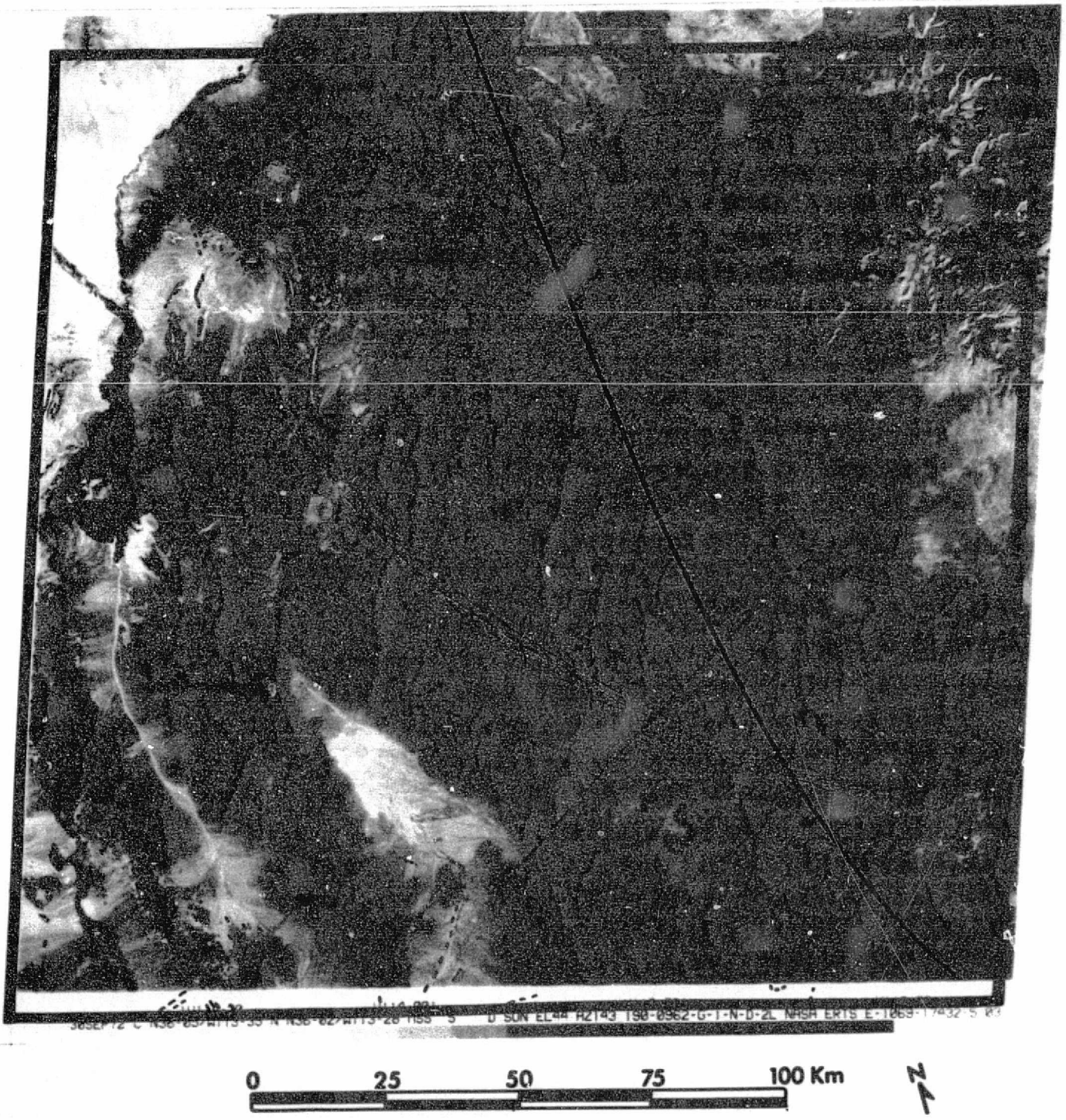

Fig. II-A-2. Photolineament map compiled on base used for maps shown in figures 6 and 10. Base is shown in Fig. II-A-3.

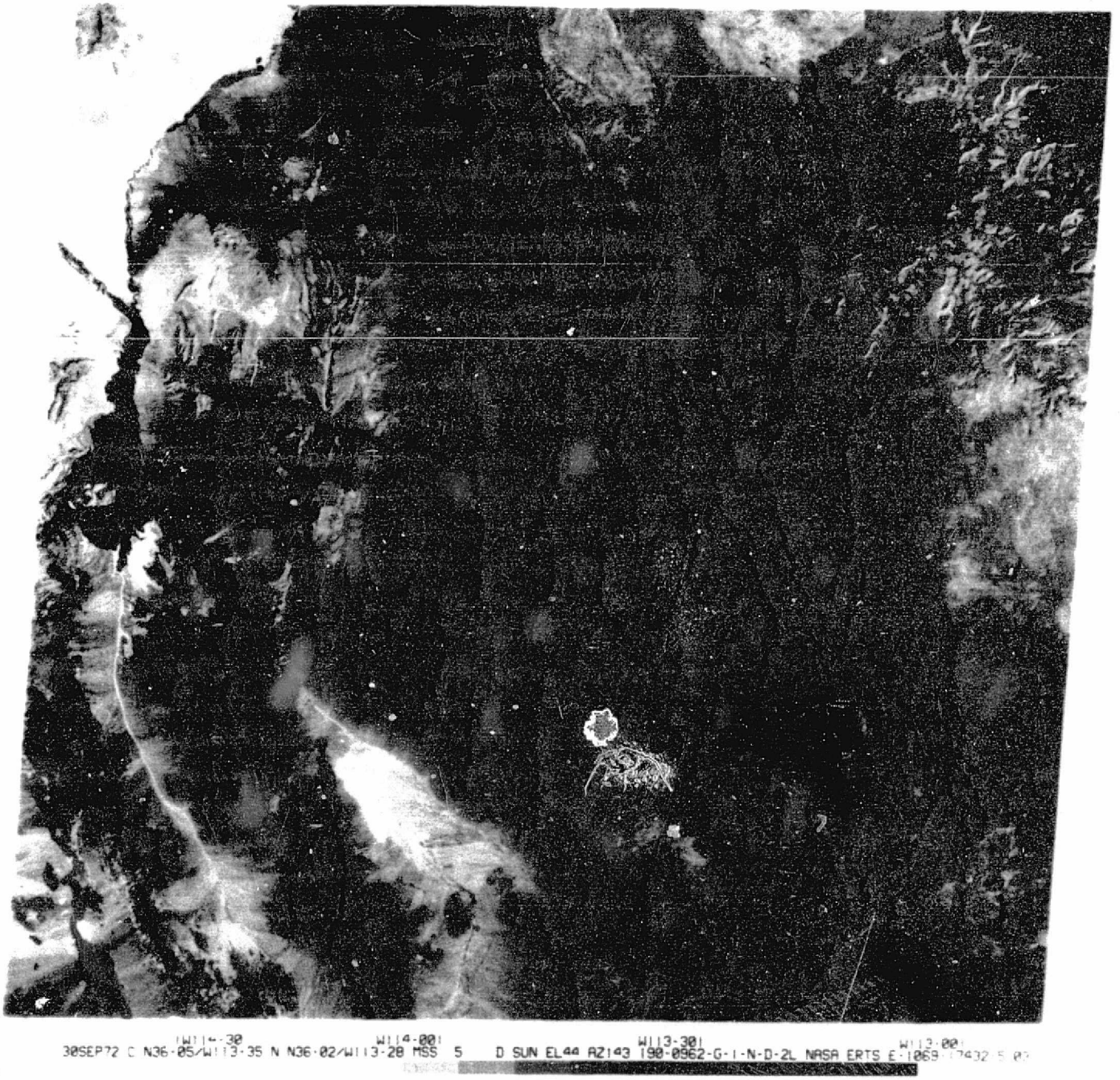

Fig. II-A-3. LANDSAT photo used in compiling Fig. II-A-2 and II-A-6. Photo No. E-1015-17432, band 5.

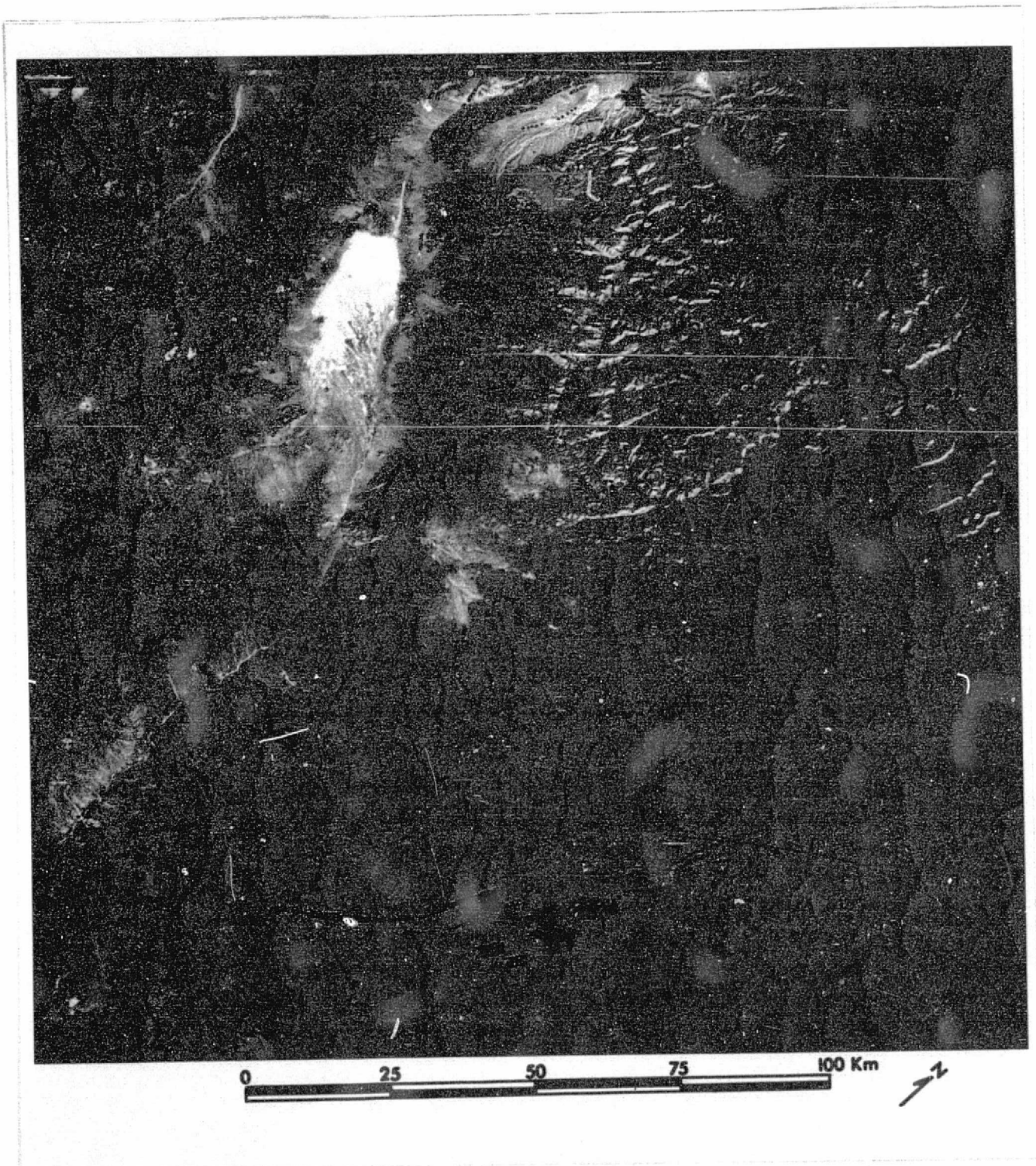

Fig. II-A-4. Photolineament map compiled on base used for map shown in Fig. II-A-7. Base is shown in Fig. II-A-5.

Fig. II-A-5. SKYLAB 3 photo used in compiling Fig. II-A-4 and II-A-7. Photo No. SL3 RL28 060.

with surrounding units; linear features related to the unit; and distinguishing characteristics. Also included are drainage patterns, weathering characteristics, bedding, foliation, and so on.

The photogeologic maps were preared on the same bases used for the photolineament maps. The photogeologic maps made on LANDSAT and SKYLAB bases are shown in Fig. II-A-6 and II-A-7, respectively. The base for the LANDSAT map was a 1:1,000,000 scale black and white paper print (Fig. II-A-3), and the SKYLAB mapping base was a true-color positive transparency at a scale of 1:720,000. Figure II-A-5 is a color print of this base. Both photomaps show all visible detail. Appendices A and C are descriptions of the resulting units.

A simpler and much less detailed photogeologic map was also compiled from the LANDSAT black and white paper print (E-1015-17432). Figure II-A-8 shows this photogeologic map, which portrays the areal distribution of major rock groups. These groups consist of alluvium and basin fill, tabular volcanic rocks, crystalline or massive rocks, and bedded or foliated rocks.

6. RESULTS

Resolution

1. LANDSAT

A brief description of the process by which LANDSAT images are generated is appropriate because it influences strongly the resolution of the images.

LANDSAT images are generated by a computer that places individual points, called pixels, onto a regular grid. Each pixel represents a square on the ground that is approximately 80 metres on a side. The MSS averages the tonal values of all features within each 80 m square and assigns the entire square this average value, represented as one of 64 gray levels that

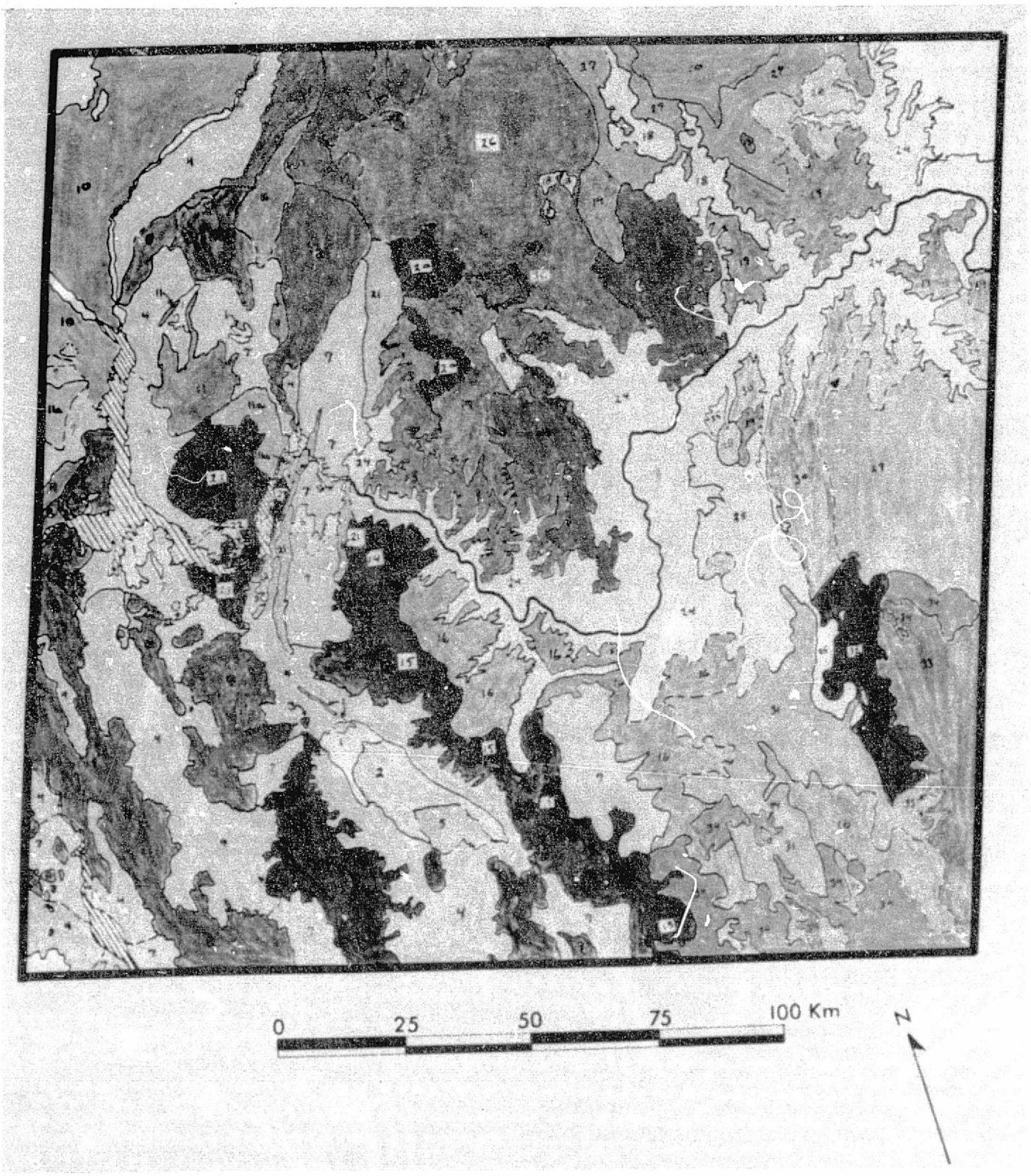

Fig. II-A-6. Photogeologic map of Shivwits Plateau; base is LANDSAT frame 1015-17432 .

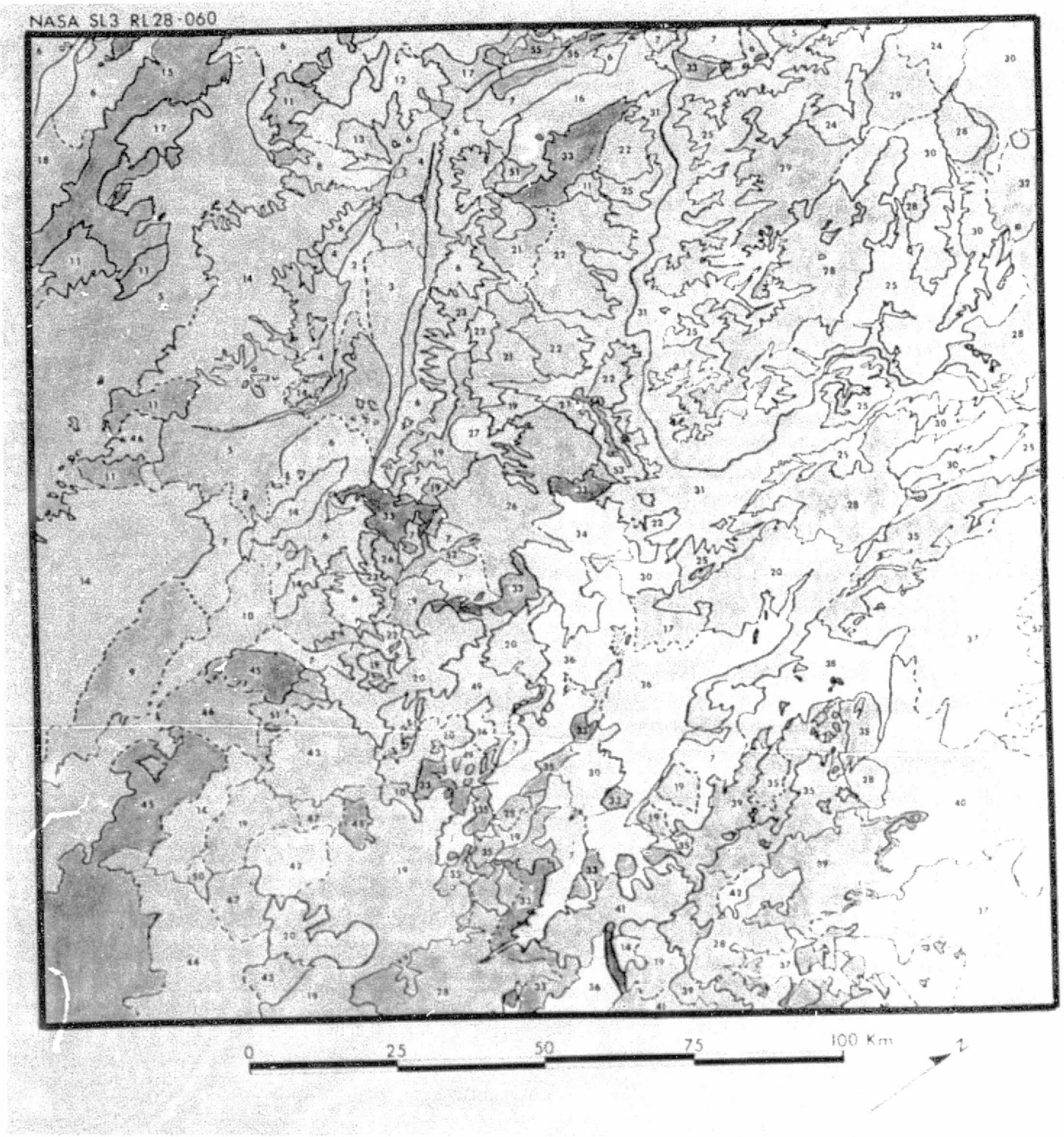

Fig. II-A-7. Photogeolic map of Shivwits Plateau; base is SKYLAB 3 color transparency.

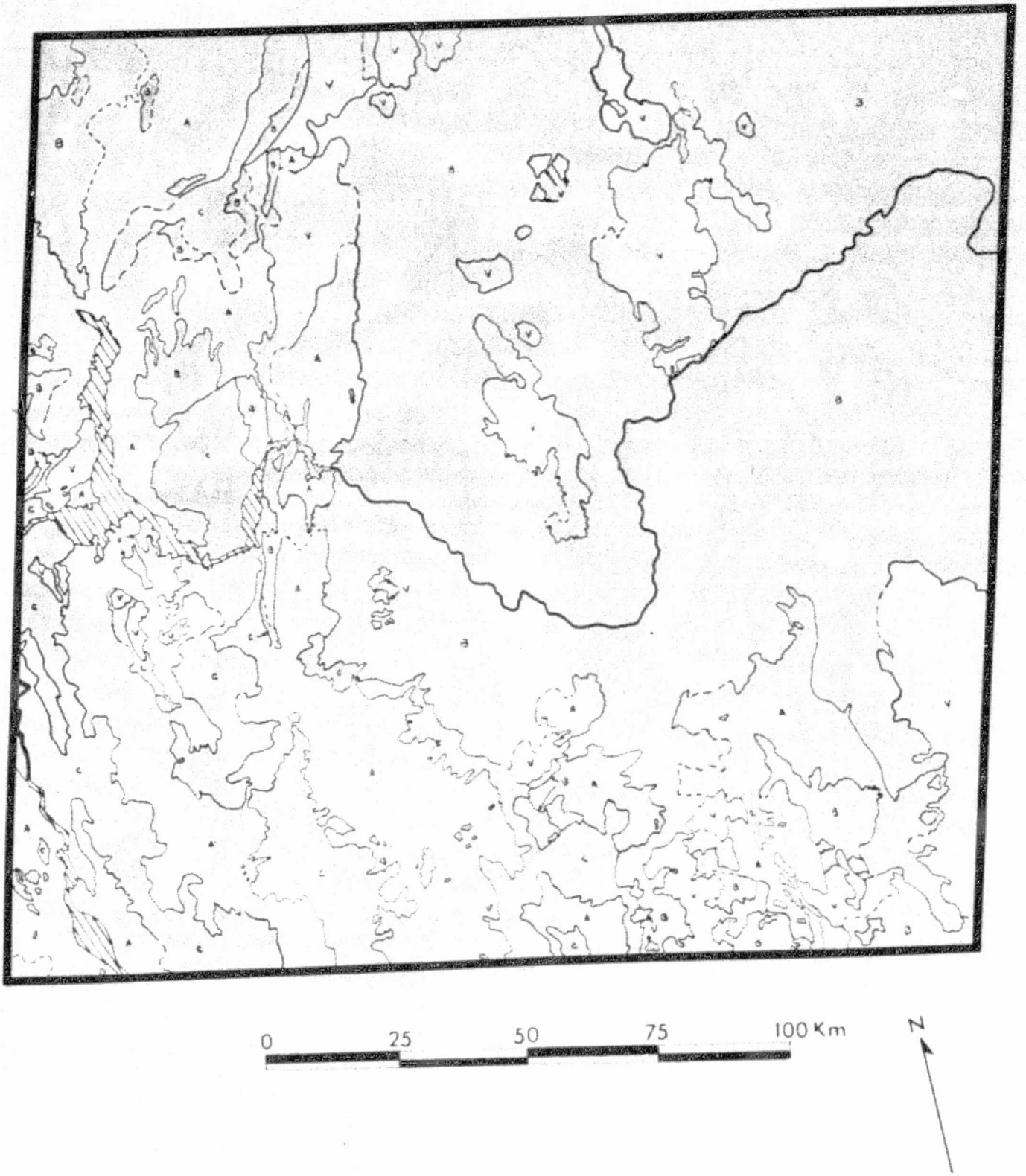

Fig. II-A-8. Photogeologic map of Shivwits Plateau, showing (V) volcanic, (C) crystalline, (B) bedded or foliated, (A) alluvial. Base is LANDSAT frame 1015-17432.

cover the tonal range between black and white inclusive. A picture is formed when all the pixels are placed in the proper position with respect to each other. Consequently, it is possible to detect a feature measuring less than 80 metres on a side if it contrasts strongly in tone with its surroundings, because the feature will affect the tone of the entire pixel. As an example, consider several 80 m squares that are black and one square that is black but contains a white 10 x 25 m rectangle. The computer will take the average of this last pixel and assign it a lighter value than surrounding pixels. This will be detectable on the image as a light spot. Consequently, it will be possible to recognize that the image contains an anomalous area, but it will not be possible to determine the location of the white rectangle within the pixel, nor its size or shape. This property of LANDSAT images is what we call "Apparent Resolution", as contrasted with "True Resolution", which pertains to actually determining the size, shape, and location of an object.

Because of apparent resolution, a long linear feature of narrow width may be visible while an equidimensional feature of the same width may not. This is because a linear feature traverses many pixels and thus produces a band of anomaly, whereas the equidimensional feature can only be averaged and compared with its immediate surrounding, which are uniform, and thus may sink below the level of detectability.

A careful preliminary inspection of the different types of images showed that certain kinds of manmade and geologic features were likely to yield estimates of the maximum resolution capabilities of the different images. These are discussed below.

The smallest linear features detectable on LANDSAT paper prints and transparencies are two-lane paved highways whose widths average 10 m. The smallest recognizable non-linear features are cultivated fields. Near Cedar

City, Utah, for example, the smallest recognizable fields are approximately 200 x 200 m square. No buildings are discernable either on the paper prints or on the color transparencies.

At Zion National Park in southwestern Utah, numerous parallel fractures trending northwest are clearly visible. The narrowest measure 160 m in width, and represent the narrowest linear features that can be detected. Other linear features, defined by color or tonal differences, vegetation changes, or breaks in slope were considered unreliable and not taken into account. The smallest non-linear geologic features that were recognized are hillocks located on the floors of basins such as the Hualapai Valley in northwestern Arizona. These hillocks are about 400 meters in diameter.

Large geologic features are well visible on LANDSAT images. These include numerous fault scarps, some extending for tens of kilometers, and fault-controlled canyons and mountain ranges. In some instances it is possible to detect sequences of layered rocks, even though individual beds or even formations are not visible. This is especially true where the strata are upturned and where the sun angle is favorable. Thus, bedding generally is not visible in the Grand Canyon of Arizona, but is visible along the Hurricane fault, near Cedat City, Utah, where the strata are contorted.

LANDSAT false-color infrared transparencies differ little in resolution from black-and-white prints, but do make certain units and textures stand out better. The reddish tone of vegetation in infrared images is of help in some instances.

2. SKYLAB

Skylab imagery used consists of normal photographic images recorded on 70 mm film and enlarged optically to a scale of about 1:720,000. No computer

or other electronic processing is involved. Consequently, resolution of the images depends on the characteristics of the optic train, the grain size and acutance of the film, and atmospheric haze.

The smallest resolvable manmade linear features are dirt roads about 6 meters wide. The smallest resolvable manmade equidimensional features are buildings, the smallest of which is at the airport in Kingman, Arizona. It measures 73 x 100 meters as scaled from the photo.

Many geologic features are well expressed on SKYLAB images. Even relatively small fault scarps in various stages of erosion, other lineaments, and drainage systems can be seen readily. Bedding is clearly defined, especially when it is not horizontal. In contrast to LANDSAT, however, bedding can be seen even if subhorizontal, as exemplified by the vicinity of Saint George, Utah, where at least seven beds can be seen in a steep exposure. Lithologic units can be discriminated in many instances, typically on the basis of morphology, texture, and color. The latter was made less useful in our case because the transparencies were marred by a bluish cast that markedly reduced color contrast.

3. RB-57F

The high-resolution photographs taken by United States Air Force high-altitude RB-57F reconnaissance aircraft are the product of relatively conventional techniques involving an optic train and sophisticated film. No electronic processing is involved.

Resolution of geographic and geologic features is an order of magnitude better than for LANDSAT or SKYLAB. The smallest manmade linear features detectable on the RB-57F color transparencies are the most freshly painted crosswalks on the streets of Saint George, Utah, which are about three meters wide. Automobiles, which are the smallest resolvable equidimensional features that are

man-made, can be seen easily with 18X magnification. Buildings, parking lots, parks, and large trees can all be seen and recognized.

Resolution of geologic features is excellent. Near Vulcan's Throne, on the north rim of the Grand Canyon, two very fine parallel joint sets are perpendicular to each other and form a grid pattern when viewed from above. These joints are about 5.5 meters wide and clearly visible at 10X magnification. The smallest recognizable equidimensional geologic features are hillocks, the smallest of which was 16.7 meters in diameter. Other features that can be seen and recognized include joints, scarps, blocks that have been dislodged from cliff faces, the plunge pools of Mooney and Havasu falls in Havasu Canyon, which measure 45 and 55 m respectively, and are clearly visible without magnification, drainage systems, and bedding, both horizontal and upturned. Indeed, individual beds can be traced for several kilometers when they are sufficiently distinctive in color. We believe that individual formations and, under favorable conditions, individual beds can be mapped on these photos.

All three types of imagery were viewed with various stereoviewers. The lack of stereo viewing in LANDSAT images is a serious handicap for geologic interpretation. A computer program has been written that introduces appropriate parallax displacements into LANDSAT images and thus produces a pseudo stereo image of usable quality. SKYLAB and RB-57F images yield excellent stereo, and are thus well suited for geologic interpretation. Paper prints would be required for field work.

Geologic Mapping

The usefulness of the LANDSAT and SKYLAB images for geologic mapping was determined by making various photogeologic maps of the same area. The area selected is Shivwits Plateau and vicinity, in Northern Arizona, which includes

a variety of sedimentary, igneous, and metamorphic rocks, as well as basin fill. The area is also characterized by excellent exposure, many structural features, and the availability of detailed ground control for verification and calibration purposes.

Photolineament and photogeologic maps were constructed at different scales and degrees of detail in order to determine what combination of these factors results in the most accurate and useful geologic map. It was clear at the outset that small-scale and low-resolution images such as those of LANDSAT and SKYLAB would be inappropriate for large-scale mapping of relatively small areas, for which conventional air photographs are much more suitable. What was not clear was whether the images would be suitable for small-scale mapping, especially of unknown areas, whether they should be used alone or in conjunction with other images, to which they would add regional perspective, and whether the resulting geologic maps should be detailed as possible or relatively generalized.

1. Photolineament maps

Photolineament maps were compiled on 1:1,000,000 LANDSAT and 1:720,000 SKYLAB bases. Lineaments were subdivided and mapped according to sharpness and definition. All recognizable lineaments are shown, including faults, fractures, foliation, bedding, dikes, topographic features, and vegetation lines. Comparison of the two maps, Fig. II-A-2 and II-A-4, shows that major lineaments such as scarps and fault-controlled canyons agree well, and that the agreement decreases and eventually vanishes as the lineaments become more vague, suggesting that the vaguer lineaments do not correspond well to reality.

Photolineament maps of the type discussed can be used to determine preferred orientation and local concentration of fracturing. Their use for

tectonic analysis is risky. The usefulness of the maps can be increased greatly by eliminating or at least clearly identifying the questionable lineaments and by separating linears into those that are concordant with structural and topographic grain and those that cut it. The latter linears are most likely to be faults.

2. Photogeologic maps

Photogeologic maps were compiled at various scales and on several mapping bases, including those used for the photolineament maps. The purpose was to determine what level of mapping detail would produce the most complete and accurate maps.

LANDSAT maps were compiled at 1:1,000,000 scale on black and white paper prints and a false-color infrared transparency. Two photogeologic maps, each at a different degree of detail, were made from the same black and white paper print.

One map, Fig. II-A-8, shows generalized photogeologic units including alluvium and basin fill, bedded or foliated rocks, homogeneous or crystalline rocks, and volcanic rocks or lava flows. This map is uncluttered, easy to read, and corresponds well to the geology of the area. The second map, Fig. II-A-6, shows all units that could be recognized on the basis of the characteristics discussed previously. The map is much more cluttered, but still legible. When compared with the state geologic map, it agrees well in places and poorly in others. This probably results in part from variations in lighting angle and vegetation cover, both factors amenable to control by computer enhancement methods. Nevertheless, the common and unpredictable inaccuracies in the existing map make it suspect and of questionable value.

Computer enhancement can be used to control several factors, such as slope angle, lighting angle, atmospheric haze, vegetation cover, whose effects are superimposed on the geology and in part mask it. As an example, Fig. II-A-9 is a photogeologic map compiled from part of a false-color infrared image.

The results of enhancement vary widely. In some cases, geologic features are better visible than in an unenhanced image, in others less so. Consequently, a variety of enhanced images should be studied carefully when compiling a photogeologic map. For example, we noted lava flows that on the black and white photos are very dark gray with only a hint of detail, but on the false-color infrared image show considerable detail. As another example, infrared images show abundant textural detail in mountain ranges and little textural detail on basin fill units, whereas the opposite is true for black and white unfiltered photographs. The full potential of this type of image processing is being explored and is sure to gain importance in future geologic mapping.

A SKYLAB true-color 9" x 9" film transparency at a scale of 1:720,000 was used as the base for another photogeologic map showing all recognizable photogeologic units, which were defined in the same way as those of the LANDSAT map. Several more units were recognized on the SKYLAB base than on the LANDSAT, probably because SKYLAB imagery is at a larger scale than LANDSAT, because variations in tone are more easily detected on the color film transparencies than on black and white paper prints, and because the SKYLAB imaging system has a greater inherent resolution than that of LANDSAT.

The map is fairly easy to read and for the most part correlates well with the 1:500,000 geologic map of Arizona, although some areas are overmapped and result in meaningless clutter. Comparison with the 1:125,000 geologic map of the Shivwits Plateau by Lucchitta and Jeanne (1975), shows very close

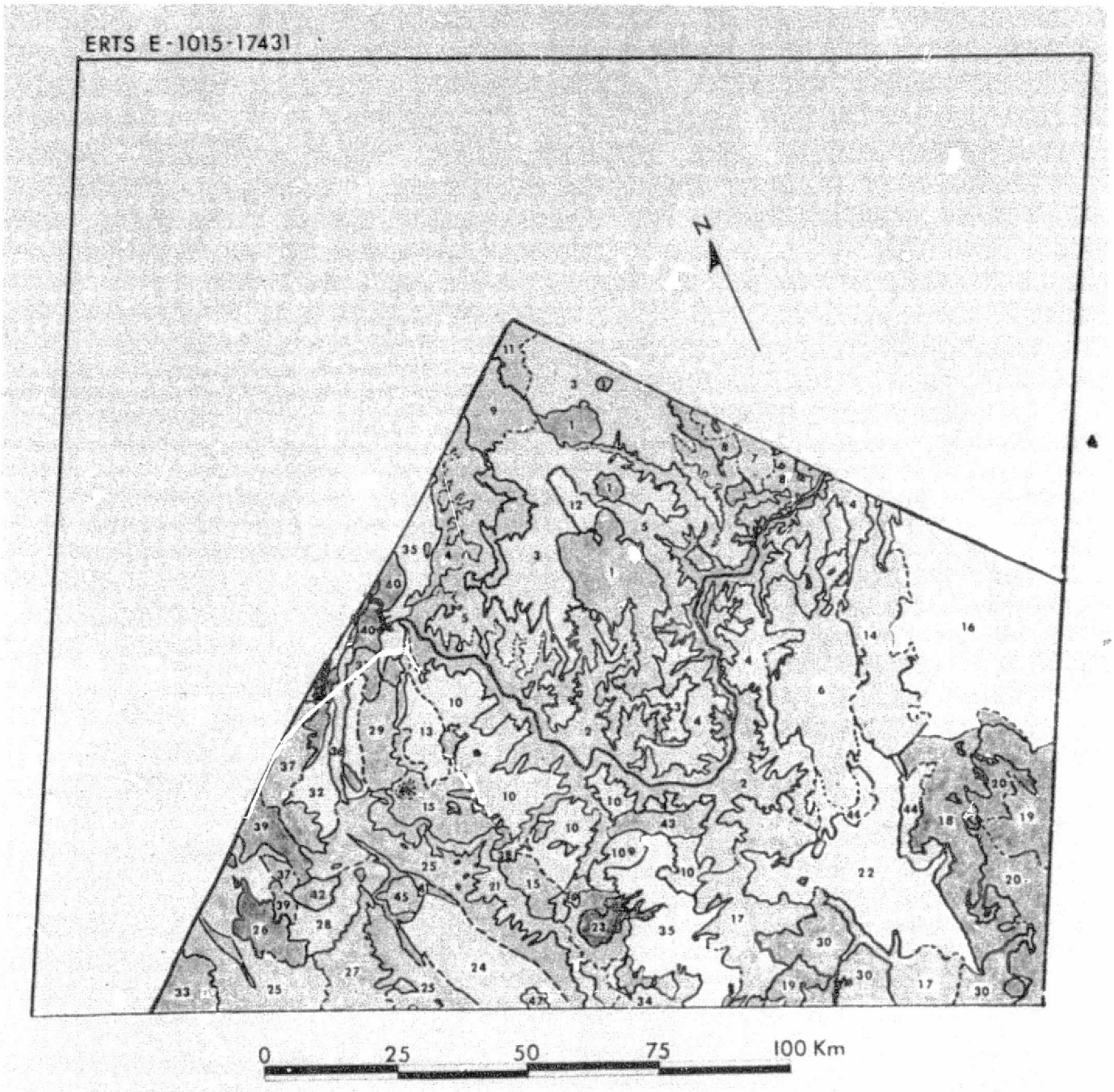

Fig. II-A-9. Photogeologic map of part of area covered by Fig. II-A-10. Base is LANDSAT 1015-17431.

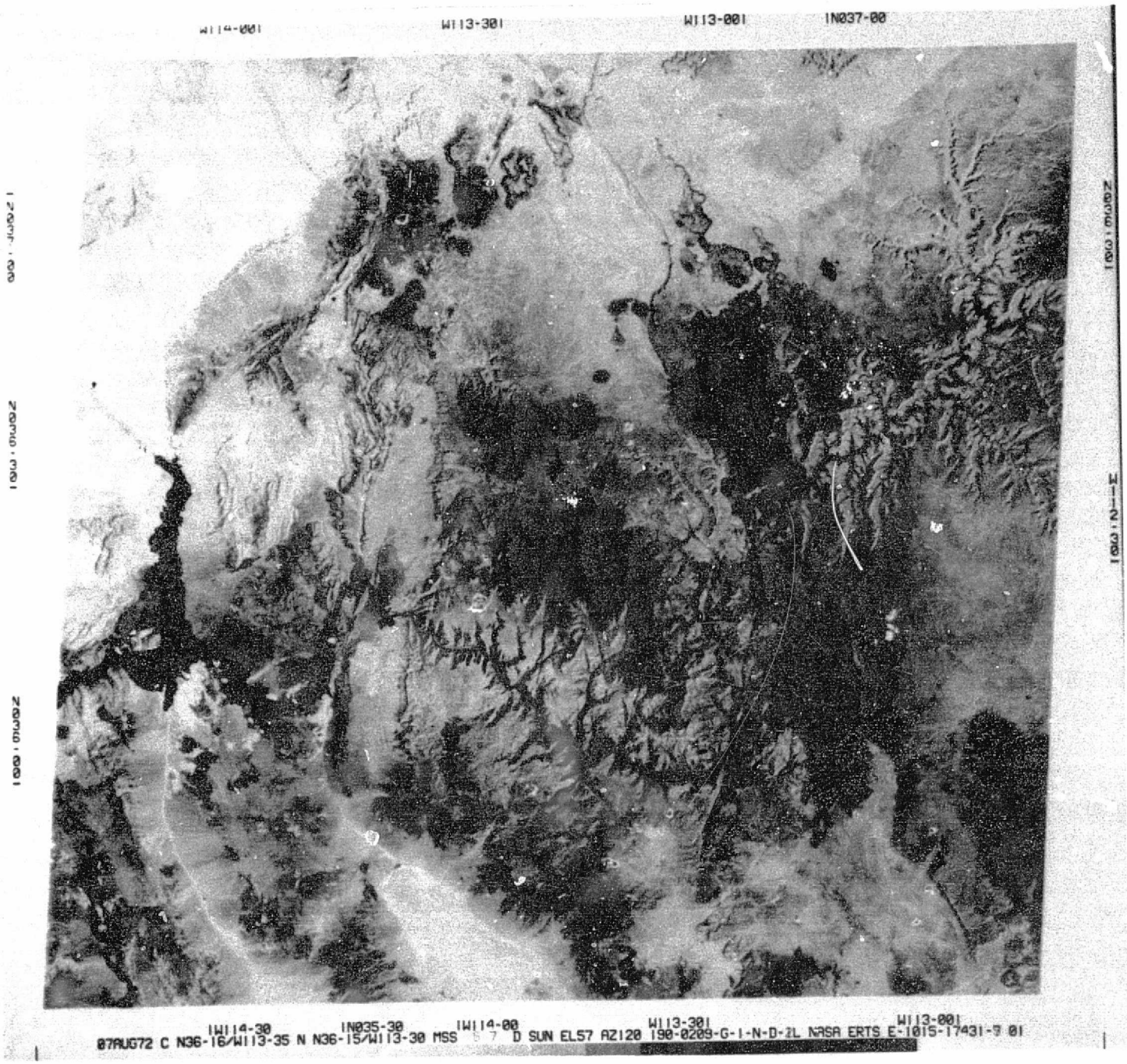

Fig. II-A-10. False color LANDSAT composit used for compiling Fig. II-A-9. Photo No. 1015-17431.

correlation between all major geologic units and some secondary ones as well, although in this case also the correlation decreases with the fineness of the detail mapped.

No geologic maps were compiled from the 1:110,000 RB-57F photographs because of lack of time. Detailed study of some of the photos has shown, however, that they are well suited to the production of accurate and reliable photogeologic maps. Printed on paper, these photos would make an excellent supplement or indeed substitute, for conventional aerial photographs. This is illustrated by the fact that features visible on 1:50,000 conventional aerial photos are clearly seen on the 1:110,000 scale RB-57F color photos. In cases where subtle color differences are involved they are visible even better than on ordinary photographs.

7. CONCLUSIONS AND RECOMMENDATIONS

The imagery that was analyzed in this study falls into two groups whose characteristics differ greatly: LANDSAT and SKYLAB on the one hand, RB-57F on the other. LANDSAT and SKYLAB differ but little in scale, area covered, and resolution, but both differ from the RB-57F imagery by one to several orders of magnitude (Table II-1). Consequently, LANDSAT and SKYLAB have approximately the same uses, which differ radically from those of the RB-57.

The applications to which the imagery is most likely to be put are of two kinds: studies in which the imagery provides regional perspective, a synoptic view, and a context of framework into which individual pieces of geologic information are to be placed; and studies in which the photographs are used directly for mapping. The two differ radically and must be considered separately.

Table II-1. Salient Characteristics of the Various Image Types

	SCALE	AREA COVERED	LINEAR RESOLUTION	AREAL RESOLUTION
LANDSAT	1:1,000,000	32,400	10 m wide	200x200 m
SKYLAB	1:720,000	25,000	6 m wide	73x100 m
RB-57	1:110,000	625	3 m wide	2x3 m

LANDSAT images cover an extremely large area; owing to the very high flight height of the satellite, they have minimal distortion and so can be mosaicked readily; and their relatively low resolution acts as a noise filter that removes local features and therefore emphasized major, regional features. Consequently, these images are a superb tool for a variety of geologic studies--for example regional tectonics and geomorphology--that depend on placing far-flung geologic features into proper geographic perspective. The user can mosaic his own photographs--usually only a few--or purchase one of the several excellent mosaics already available, and thus view at one glance a very large region. This enables him to determine the relation between the area of his interest and its surroundings, and to place it in regional perspective.

The slightly larger scale and better resolution of SKYLAB images and their availability in stereo do not constitute a significant advantage for regional analysis; their spotty availability is a considerable drawback. They should be considered, however, if the same images are to be used for mapping purposes. RB-57F do not cover a sufficiently wide area to provide a truly synoptic perspective, although they are much better in this respect than conventional air photos. In view of their high cost, they should not be used for this purpose.

In summary we recommend that LANDSAT images in black-and-white and in color be obtained in all cases for the area of interest and its surroundings. The cost is minimal and the amount of information that can be obtained is huge. One SKYLAB photo centered on the area would probably be useful. RB-57 photos are not indicated.

For geologic mapping, the suitability of the various types of images depends directly and strongly on the scale at which the mapping is to be carried out. LANDSAT and SKYLAB images cover a large area and have low resolution and therefore are totally unsuited to mapping of small areas at high resolution (for example 7-1/2 and 15 minute quadrangles), for which conventional aerial photographs are much more appropriate. Conversely, LANDSAT images, especialy when cleaned up and enhanced, are well suited to the areal coverage and detail required by mapping at 1:250,000 (2°) and smaller scales. Conventional aerial photographs cover too small an area and are too detailed to be completely satisfactory at these scales. Under optimum conditions LANDSAT images may be adequate for mapping at 1:125,000. This scale, on the other hand, is well suited to SKYLAB photographs which, with their better resolution, may be useable even at 1:62,500 for non-detailed mapping. RB-57 images offer a remarkable combination of resolution and aerial coverage, and are thus useable for a wide variety of mapping scales ranging from 1:24,000 to 1:25,000. The main disadvantage at the smaller scales is that several images are needed, whereas in the case of LANDSAT and SKYLAB only one may suffice to cover the map area.

Stereo coverage is of great value in geologic mapping. LANDSAT images do not provide it, whereas SKYLAB and RB-57 generally do. Programs are currently being developed that will provide LANDSAT images with computer-generated false stereo. This should make them considerably more useful.

The detail at which geologic mapping should be carried out depends on a variety of factors including vegetation cover, geologic terrain, sun angle, and the amount of ground control. All effect one's ability to define and identify photogeologic units that correspond to meaningful lithologic units on the ground. The cardinal rule is to minimize the number of units whose reality is suspect, because a photogeologic map that contains a large and unknown amount of such units is misleading and in fact useless no matter how impressive it may appear.

In areas where conditions are unfavorable and where there is little or no ground control, units mapped on LANDSAT and SKYLAB bases should be kept simple and generalized. The suggested categories of alluvium, surficial deposits and basin fill; massive or crystalline rock; bedded or foliated rocks; and volcanic rocks is one that works well. A map showing these units as well as major structural features probably corresponds well to reality and constitutes a very large increase in knowledge over no map at all, the common situation in many unexplored areas.

The calibration provided by even minor ground control permits a marked increase in the detail of photogeologic mapping. Under favorable conditions, a large area could be mapped quickly and efficiently on LANDSAT and SKYLAB bases by using photogeologic mapping anchored by suitably spaced ground traverses. RB-57 images are so sharp and have such color separation that units can be identified readily, thus needing much less ground control.

In conclusion, our recommendation, based on our experience and on the cost factors shown in Table II-2, are as follows:

All geological mapping projects should be provided with LANDSAT coverage of the region. This coverage should consist of black and white paper prints of selected spectral bands, and of false-color IR prints and transparencies.

Table II-2. Cost Factors for Various Types of Images

Image Base	Type of Mapping Base	Size area to be covered	Photo Scale (Average)	Minimum No. of Photos Req. for Complete Coverage		COSTS (Approximate)		
				Mono-scopic	Stereo-scopic	Per Photo	Total Monoscopic Coverage	Total Stereoscopic Coverage
Conven-tional Aerial	9" x 9" Black & White Paper Prints	2° Quad.	1:60,000	112	532	$ 2.00	$ 224.00	$ 1,064.00
		15' Quad.	1:40,000	12	48		$ 24.00	$ 96.00
		7-1/2' Quad.	1:20,000	12	48		$ 24.00	$ 96.00
	9" x 9" Color Positive Transparency	2° Quad.	1:60,000	112	532	$12.00	$1344.00	$16,128.00
		15' Quad.	1:40,000	12	48	$12.00	$ 144.00	$ 576.00
		7-1/2' Quad.	1:20,000	12	48	$12.00	$ 144.00	$ 576.00
ERTS	7.3" x 7.3" Black & White Paper Prints	2° Quad.	1:1,000,000	1	2+	$ 2.00	$ 2.00	$ 4.00
		15' Quad.		*	*			
		7-1/2' Quad.		*	*			
	7.3" x 7.3" False Color Composite	2° Quad.	1:1,000,000	1	2+	$12.00	$ 12.00	$ 24.00
		15' Quad.		*	*			
		7-1/2' Quad.		*	*			
SKYLAB	9" x 9" Color Positive Transparency Enlarged from 70 mm frame	2° Quad.	1:700,000	1	3+	$ 5.00 for 70 mm $30.00 enlarge-ment	$ 35.00	$ 105.00
		15' Quad.		*	*			
		7-1/2' Quad.		*	*			
RB-57F	9" x 9" Color Positive Transparency	2° Quad.	1:110,000	40	132	$12.00	$ 480.00	$ 1,584.00
		15' Quad.	1:110,000	2	14	$12.00	$ 24.00	$ 160.00
		7-1/2' Quad.	1:110,000	1	6	$12.00	$ 12.00	$ 72.00

+ Not recommended for detailed mapping

* Not recommended for detailed mapping at these scales

The cost for these items is minimal, their usefulness great. Computer-enhanced images should be acquired if they are already available or if the project can afford the cost of custom enhancement. The specific enhancement obtained depends on the focus of the study, the terrain, vegetation cover and so on. It should always include atmospheric correction and noise removal.

The finest base on which to carry out mapping at intermediate to large scales is undoubtedly the RB-57 color imagery, which provides excellent resolution, color, stereo, and coverage at large areas per frame. This imagery is so good that it obviates the need for conventional air photographs entirely, making the cost quite acceptable. The mapper should obtain 9" x 9" positive color transparencies for photogeologic mapping in the office, and color prints on paper, or preferably, plastic base, enlarged to the proper scale and cut into manageable pieces, for mapping in the field. The main difficulty with RB-57 imagery is that it is only available for small parts of the country.

For small-scale mapping, especially of remote areas, SKYLAB and LANDSAT images are quite adequate. SKYLAB offers better resolution, LANDSAT the opportunity for a wealth of enlargements. The specific images that should be used depend on the characteristics of the mapping projects. Whereas LANDSAT covers the whole world, the distribution of SKYLAB coverage is spotty. If SKYLAB images are available, they provide real advantages and should be used.

8. APPENDICES

APPENDIX A

Description of Photogeologic Units - Map 4

UNIT

1. Light to gray to white, mottled on a medium scale. Forms smooth uniform surfaces. Present in lowest part of interior drainage basins, as well as in scattered areas of low relief possibly subject to periodic flooding. Light tone may be due to playa materials, which make unit lighter colored than other surrounding alluvial units. Contacts with adjacent units are sharp, but mildly diffuse with unit 2.

1a. Similar to unit 1, but not located in interior drainage basins. Drainage channels usually are developed on surfaces of 1a and contacts are more diffuse.

2. Light gray and white in braided pattern, overall tone becomes lighter toward contact with unit 1 and darker toward contact with units 4 and 5. Forms braided surface with very low if any relief. Contacts with adjacent units are sharp but mildly diffuse with unit 1. Gently slopes toward unit 1. Braided drainage channels are lighter in tone than rest of unit.

3. Dark gray with very dark gray patches on some higher ridges, very sharp contacts with all adjacent units. Unit has rugged mountainous relief and is higher than all adjacent units. Structure of unit appears homogeneous, no bedding etc. is visible. Drainage density is high and pattern is coarse, dendritic. No tonal contrast between drainage channels and unit.

4. Light to medium gray, streaked. Streaking traceable to parent rock. Forms gentle uniform slopes in valleys and interior drainage basins, lower than and abutting against adjacent ranges. Contacts with range rocks usually are sharp but may be diffuse with other alluvial deposits. Very low relief. Drainage channels lighter than unit.

5. Light gray and uniform. Contacts with adjacent units are mildly diffuse to sharp. Unit is smooth with very low relief and has some slope and elevation as adjacent units. Very low drainage density on unit. Drainage channels have a reverse dendritic pattern and are darker than unit.

6. Light gray, mottled on a medium scale. Where unit forms ledge above adjacent units, tonal contact is sharp, elsewhere it is diffuse. Forms ledge or bench abutting major N-S trending cliffs, appears to rest unconformably on unit 21, and is covered to the south by material of unit 7.

7. Light to medium gray, streaked, mottled or with tone differences coincident with drainage pattern. Similar to unit 4, but with incised drainage channels developed on surface. Unit is also found on plateau and within some ranges at a higher elevation than unit 4. Drainage channels may be darker or lighter than rest of unit.

UNIT

8. Light to dark gray, banded on a very large scale and mottled on a very large scale in some areas. Very strong topographic and tonal grain roughly parallel to length of exposures. Contacts with adjacent units are sharp, although in some areas units 4 and 7 surround many small stringers and isolated outcrops giving an overall impression of a diffuse contact. Drainage channels are generally poorly developed on unit which is only moderately higher than adjacent units. Relief is moderate to moderately rugged.

9. Medium gray with a few light gray blotches. Borders with adjacent units are diffuse. Unit is moderately higher than adjacent units and relief is moderate. Drainages are of moderate density, are fine and do not contrast in tone with unit.

10. Light gray to white, streaked and mottled on a large scale. Western unit forms a large broad plain, or mesa, the borders of which have been eroded forming a scarp. The tone and texture of the slopes below the scarp are the same as the main body of the mesa. Contacts with adjacent units are diffuse except where unit is truncated sharply by a major drainage. Topography is moderately smooth. Drainage channels in unit are poorly developed and generally darker than unit.

11. Uniformly light gray. Consists of ridges of layered rock dipping steeply to east. Tone almost identical to adjacent units. Ridges have moderately rugged relief and trend roughly N-S. Most ridges are sharply truncated by several NE- and NNE- trending lineaments. Most of the lineaments cannot be traced into adjacent units. Minor drainage channels have developed on the ridge slopes and do not contrast with the unit.

11a. Medium gray, mottled on a medium scale. Ridges of layered rock dip steeply eastward and trend slightly east of those of unit 11. Tone similar to adjacent units. Unit is bounded on NW by NE- trending lineament, but no lineaments pass through the unit itself. Drainage channels are well developed on some ridges and do not contrast with tone of rest of unit. Master drainage in area (Colo. R.) has cut through several of the ridges although several miles downstream it follows a strike valley.

12. Dark gray, nearly horizontal layered rock overlain by a light gray material. Darker layer forms rims or fringes around patches of lighter material. Deeply incised drainages have cut through the lighter unit and in places the darker unit creating a very striking and contrasty dendritic pattern. Contacts between the two layers are sharp but contacts with adjacent units range from sharp to unrecognizable. The unit covers most of the floor of a larger basin. Drainage channels are generally lighter in tone than any other part of unit.

13. Light to medium gray, mottled on a medium scale or where drainages have developed, in a dendritic pattern. Moderately smooth to quite heavily dissected. Unit forms wide platform or bench on north side of lower portions of master drainage. Contact with adjacent units is sharp to very diffuse. Height from floor of canyon to bench is considerably greater than from bench to top of unit 19. Drainage channels are darker in tone than unit.

UNIT

14. Light to dark gray, mottled on a very large scale. Unit forms planar bench on south side of canyon across from unit 13. Drainage pattern much denser than on unit 13 and channels are lighter in tone than rest of unit. Relief is moderate to moderately rugged. Contact with adjacent units is scarp and in places marked by a scarp.

15. Dark to very dark gray, mottled on a medium scale. Unit forms 1st layered rock unit above homogeneous rocks of unit 3. Drainage channels are not as well developed as on unit 3, are darker than the unit, and commonly form fan-shaped watersheds. Contacts with unit 3 are sharp; with other units they are diffuse. Relief is moderate. Much of the surface has a wrinkled appearance.

16. Medium to dark gray, mottled on a large scale. Contacts with adjacent units are diffuse. Appears to rest on top of unit 15. Unit forms planar bench on south side of master drainage and is deeply incised by its tributaries. Compared to unit 14, surface is flatter and minor drainages are more dense but less incised. Medium sized drainages have emphasized structural lineaments; small and large drainages and canyons show less structural control. Some of the drainage channels are lighter in tone than rest of unit.

17. Very dark gray, mottled on a small scale, in places pocked or dimpled, in places uniform. Unit appears as dark patches which often form low platforms above lower units. Contact with other units generally is sharp except for a diffuse contact with unit 18. Where the edges of unit 17 have not been modified by erosion, the outline is lobate. Unit crosses contacts between other units. Although it is generally found at higher elevations, locally it can be traced down into nearby valleys. The larger bodies of the unit are arranged in a pattern of roughly linear and subparallel exposures. The surface ranges from moderately smooth to bumpy. The few drainage channels are darker than unit. Headward erosion by tributaries to master stream has incised the edges of the unit where it is adjacent to unit 24. Relief is moderately smooth to moderately rugged. Unit variously covers and is cut by structural lineaments.

18. Unit consists of material similar to that of unit 17, partially covered by material of lighter tone. In some areas the darker material is visibly only in a narrow exposure which marks the edge of the unit.

19. Medium to dark gray, mottled on a very large scale or dendritic in tone pattern. Contacts with adjacent units are diffuse, sharp or separated by scarps (units 13, 24, and 26). Unit forms planar surfaces at higher elevations, and may in part underlie units 17 and 18. Topography is smooth and relief is very low. Structures are not readily visible within unit, although a structural scarp separates unit 19 from 26 and, in places, 19 from 27. Where erosion has produced scarps along edges of unit, structural influence on drainages may be seen. Drainage pattern on the surface of unit 19 is rugose to dendritic, of moderate density, poorly incised and lighter in tone than the rest of the unit.

UNIT

20. Generally medium gray but in part grades to dark gray. Forms very diffuse contact with units 19 and 26 and is characterised by very dense, deeply incised, dendritic erosion pattern. Drainage channels do not contrast with unit except in main wash. Topography has brain-like texture and relief is moderate to moderately rugged. This erosion pattern is distinctly different than that of unit 19.

21. Light to dark gray, mottled on a small scale. Forms cliffs which are moderately to very dissected. Probably correlative with units such as 13, 14, 15, from which it probably differs only in manner of exposure. Forms a scarp that bounds a plateau.

22. Light gray to white. Unit forms small, light, patches in homogeneous rocks and in alluvium. Contact with these units range from sharp to mildly diffuse. No structures are visible in units. Washes have developed in some locations. Unit may in part consist of remnants of 1a type material and/or exposures of lighter facies in homogeneous units. Sharp contacts with alluvium suggest that unit is more indurated than unit 1a.

23. Medium to dark gray, mottled on a medium scale. Contacts with adjacent units are sharp. Unit forms moderately rugged to rugged mountains, roughly equivalent in elevation to unit 3. Stands above all other adjacent units. Drainages do not contrast in tone with unit.

24. Unit exposed in canyons related to master drainage of the area. Probably consists of unit already defined, but not identifiable here because of canyon exposure. Unit ranges in tone from light to medium gray, and is mottled in places. A striking tonal texture consists of a dendritic pattern which is emphasized by shadow, rock type and possibly vegetation. Etching out of structural lineaments by erosion leads to a greater density of structural information in this unit than in any other. Relief is rugged. Contact with other units is commonly marked by a scarp.

25. Very dark gray, mottled on a large scale. Unit forms relatively high planar surface. Surface appears wrinkled, which may be due in part to erosion. Contacts with adjacent units are sharp to diffuse. Although in some areas unit is higher than surrounding units, generally it is at the same elevation unless offset by a scarp. Drainage density is moderate, drainage channels are both lighter and darker than unit. Unit is dissected by several north-trending lineaments, some of which have offset parts of the unit, or have separated it from other units. Relief is moderately rugged.

26. Light to medium gray, very large scale and small scale mottling. Combination of drainages and mottling give unit a leather-like appearance. Surface texture varies from uniform in trough-like and irregular depressions to rough on adjacent and slightly higher surfaces. Drainage density is moderate, drainage channels are light gray to almost white and generally dendritic. Uniform surfaces are lighter than adjacent rough surfaces. Contacts with units 17 and 18, and those offset by scarps are sharp, others are diffuse. Relief is moderate. Unit is bounded on the east by a scarp that separates the unit from units at higher elevation. Several valleys and troughs

UNIT

suggest a structural control that is also reflected in several canyons at the edges of the unit.

27. Medium gray, mottled on a medium scale. Surface topographic texture is uniform and relief is low. Drainage channels are generally absent. Unit forms planer surfaces at higher elevations similar to those of unit 19. Probably underlies unit 18 in part. Appears to overlie unit 10 to north. Two structural lineaments which intersect at about 90° are visible. One of the lineaments separates portions of unit 27 and 19. The scarp on the east side of unit 26 also forms the western edge of unit 27.

28. Unit characterized by dense, lacy drainage pattern. Otherwise similar to units 19 and 27. Some of the canyons related to the Colorado River and cutting laterally into the unit show evidence of structural control.

29. Light to medium gray, mottled on a medium scale. Tonal texture is fluffy, somewhat like cirrus clouds. Contacts with unit 25 are sharp, all others are diffuse. Topographic texture varies from uniform in shallow depressions to moderately rough on adjacent higher areas. Relief is moderately smooth. Drainage channels are poorly developed. Unit forms planar plateau, equivalent in elevation to units 19, 30 etc. Structural lineaments are evident only at edges of unit where they are emphasized by canyon development.

30. Dark gray, mottled on a small scale. Unit appears to be transitional between units 25 and 29. May result from partial removal of material of unit 25 and exposure of material of unit 29. Contact with adjacent units is diffuse except to the south where it is sharp. Topographic texture is dendritic to reticulate, relief is moderate. Unit is roughly equivalent in elevation to units 25 and 29. The unit is bounded on the west by a structural lineament. At its northern end, canyons reflect structural control.

31. Light to medium gray, mottled on a medium scale. Forms planar surfaces lower than surrounding units. Contact with adjacent units generally is sharp. Topographic texture is uniform and relief is moderately smooth. Unit is bounded on the east by a structural scarp. To the south, contacts with units 32, 25 and 36 appear to be structurally controlled. Few if any structural lineaments are visible within unit. Drainage channels are inconspicuous, except for a major wash roughly parallel to the base of the eastern scarp. Where visible, drainages are both lighter and darker than rest of unit.

32. Medium gray, mildly mottled on a medium scale. Unit forms planar bench on upligted side of scarp bounding eastern edge of unit 31. The bench dips gently eastward. Unit is roughly equivalent in elevation to unit 30. Contacts with adjacent units generally are sharp. Relief is moderate. No structures are visible within the unit. Drainage is characteristically down dip, joining a subsequent drainage at the contact with unit 33.

33. Medium to dark gray, intensely mottled. Contacts with adjacent units are sharp. Unit forms low, linear platforms trending NNW and separated by

UNIT

trough-like depressions. Unit is roughly equivalent in elevation to adjacent units. Relief is moderate. Few structures are visible within the unit. Drainage channels are poorly developed. Southwestern contact of unit is lobate and fringed, very much like unit 18.

34. Dark to very dark gray. Forms irregular patches on top of several other units, at different elevations and widely separated localities. Contacts with other units are usually sharp. Low domelike patches have moderate relief and typically are featureless except for some drainage development. Some patches are bounded by structural lineaments; no lineaments are visible within the patches.

35. Very dark gray; uniform tonal texture. Contacts with adjacent units are sharp. Unit is found in narrow exposures as a sloping surface below units 17 and 18 and above unit 26. Structural lineaments which can be traced across the unit are not visible within it.

APPENDIX B

UNIT

1. Olive-gray average color, appears to form a relatively flat plateau with lobate form. Drainage is indistinct, contacts with surrounding units vary from moderately sharp to very sharp where unit forms cliffs. Several linear features are visible within the unit. Distinguishing features: one of the darkest units on photo, displays very little or no relief.

2. Grayish yellow to grayish blue-green, forms a very large, complex canyon system with one major canyon and several branching, secondary, smaller canyons. High relief. Drainage is master drainage of area and well developed. Contact with surrounding units varies from moderately diffuse to very sharp. Numerous linear features are visible throughout the unit. Distinguishing features: associated with master drainage in area. Large canyons, linear features abundant.

3. Mottled grayish yellow-grayish red. Forms a large, broad, flat plateau with very gentle relief. Drainage is mostly fine, moderately well developed, denritic, with some well developed medium drainage forming canyons cut into the unit and usually lighter than rest of unit. Contacts with surrounding units vary from very diffuse to very sharp. Distinguishing features: lighter and larger than any other plateau-forming unit on photo.

4. Moderate yellow-grayish green. Forms a low plateau related to master drainage of area, with moderately rough relief. Highly dissected by well formed, medium, dendritic drainage darker than rest of unit. Contact with surrounding units is moderately sharp to very sharp. Linear features are abundant and clearly visible. Distinguishing features: plateau-forming unit. Highly dissected by drainage. Linear features are clearly visible in some areas.

5. Moderate yellow-green to grayish-green; forms a plateau similar to unit 4, with a gently sloping surface away from next higher plateau and local low, moderately sharp ridges. Drainage varies from non-detectable to well formed. It is fine dendritic, usually lighter than rest of unit. Contact with surrounding unit varies from moderately diffuse to very sharp. Distinguishing features: low plateau-forming unit. Lighter than most plateau-forming units. Complete lack of drainage in some parts of unit.

6. Mottled grayish red to moderate red (this red coloring is a vegetation signature). Consists of a relatively flat surface interrupted in places in scarps. Drainage is well formed, fine, distributary, dendritic, locally becomes medium, well formed around the edges. Contact with surrounding units varies from very diffuse to sharp. Linear features, scarps, large washes, are fairly abundant and trend north-south. Distinguishing features: reddest unit on photo. Flat surfaces interrupted by scarps. Fine well-formed drainage.

7. Overall grayish red; mottled moderate red locally (vegetation). Consists of a fairly flat area with numerous low rounded hills (domes) and small

UNIT

sharp ridges. Drainage is non-detectable. Contact with other units is moderately sharp to sharp. Distinguishing features: darkest unit on photo. No visible drainage. Small rounded hills.

8. Dark green, forms gently sloping surface with small, low hills locally. Drainage varies from non-visible to very fine, poorly developed. Contact with surrounding units is moderately sharp to very sharp. Several areas along the contact exhibit a lobate form. Distinguishing features: very dark green color. Lobate forms along contact.

9. Overall medium yellow with a medium red overcast locally. Appears to be a highly dissected transition zone between plateau and basin. Consisting mostly of small undulating hills and occasional ridges separated by gullies. Drainage is very well formed, fine to medium, lighter than rest of unit. Contact with surrounding units varies from diffuse to very sharp. Distinguishing features: located along basin-plateau transition. Very highly dissected by fine drainage.

10. Mottled grayish yellow-medium yellow. Consist of a gently sloping unit forming several flat surfaces separated by drainage or other units. Has numerous low well rounded hills and ridges throughout. Drainage appears to be fine, well developed, dendritic (?). Contacts are variable from very diffuse to very sharp. This unit may be related to unit 4 though not as deeply eroded. Distinguishing features: plateau-forming unit, consisting of numerous well-rounded hills and ridges, with well developed fine drainage.

11. Grayish yellow, consists of a fairly flat unit with numerous small hills, giving the unit a speckled appearance. Drainage is difficult to detect, however appears to be very fine poorly developed, lighter than rest of unit. Contact with other units is very diffuse. Distinguishing features: plateau forming unit, very difficult to distinguish from adjacent units except for very small hills, giving a somewhat speckled appearance.

12. Olive gray color, with gray yellow patches locally. Very similar to unit 1 but does not appear as massive or fresh. Does not exhibit much relief, except for what appear to be local rounded hills. Drainage appears poorly developed, probably dendritic. Lighter than rest of unit. Contact with surrounding units is moderately diffuse to very sharp, with lobate pattern on a small scale. Distinguishing features: one of the darkest units on photo with a patchy yellow pattern locally.

13. Mottles medium yellow with small dark grayish blue-green spots. Overall flat surface with numerous small rounded hills throughout. Drainage appears to be fine, well developed, lighter than rest of unit. Contact with adjacent units is generally diffuse to locally sharp. Distinguishing features: light plateau-forming unit with small darker hills throughout.

14. Mottled pale brown with pale yellow and green patches. Appears to be a planer feature with a gentle slope and little relief. Drainage is fine, well formed, dendritic primarily, with some rectangular drainage; lighter

UNIT

than rest of unit. Contact with surrounding units varies from moderately sharp to very diffuse. Some of the drainage is very linear and may represent structural control. Distinguishing features: medium dark unit on photo, fairly flat, dissected by much lighter color fine drainage.

15. Mottled moderate brown to dark yellowish orange. Appears at the edge of a major plateau. A moderately gentle sloping unit with moderate relief, has numerous subdued hills and ridges. Drainage is very difficult to detect, but appears fine, poorly developed. Contact with surrounding units varies from very diffuse to very sharp. Only small linear features representing ridges are visible within the unit. Distinguishing features: brown color. Found at the edge of a major plateau. Very poor drainage.

16. Mottled yellow to yellowish green, forms a large flat, broad basin. Drainage appears to be fine to medium, moderately well developed rectangular, somewhat difficult to see. Contact with surrounding units diffuse to very sharp. Linear features which are represented by drainage are visible in most of the unit. Distinguishing features: basin-forming unit with difficult-to-see, moderately well developed rectangular drainage.

17. Mottled brownish gray to greenish gray. Represented by a subdued but topographically higher area than surrounding units. Mountainous region with numerous small ridges giving the unit a slightly hummocky appearance. Drainage is fine to medium, well developed, lighter and darker than rest of unit. Contact with surrounding units is moderately diffuse to sharp. Distinguishing features: mountain region. Well developed fine drainage. Subdued, hummocky appearance.

18. Dusky yellow, forms the edge of a plateau and is truncated on one side by a scarp. Displays very little relief. Drainage appears fine, well developed, dendritic, lighter than rest of unit. Contact with surrounding units varies from very diffuse to very sharp. Distinguishing features: part of a flat plateau-forming unit. Fine distributary and dendritic drainage.

19. Very mottled grayish brown-dusky brown-pale brown-dusky yellow green. Forms a flat unit that rises above the surrounding plains, has abundant small rounded hills and lobate ridges on its surface. Drainage appears to be poorly developed, fine, lighter than rest of unit. Contact with other units varies from moderately diffuse to very sharp, has some lobate contacts giving the impression of a flow. Distinguishing features: darker and topographically higher than surrounding units. Varigated appearance. Has lobate edges locally.

20. Overall grayish green with small pale green patches locally. Appears to form a topographically high plateau unit that rises above the surrounding plains. Does not appear to have much relief. Drainage is poorly developed, fine, unpatterned. Contacts with surrounding units vary from moderately sharp to very sharp, and appear very lobate and fluid, like a flow. Distinguishing features: dark plateau unit. Has very lobate contacts especially with surrounding plains units.

UNIT

21. Dusky green to moderate yellow green. Represented by long fingering sharp ridges and numerous short more concentrated sharp ridges and patches of rounded hills separated by gullies. Drainage is well formed fine to medium dendritic, lighter and darker than rest of unit. Contact with surrounding units is sharp. Represents the transition zone between platea, and basin and is probably the most eroded part of the Plateau. Distinguishing features: location at a basin plateau transition. Consists of numerous long finger-like ridges.

22. Overall greenish yellow, with occasional faint moderately yellow strips (representing major drain). Occupies a basin and appears to have little or no relief. Drainage is well developed, fine with several larger braided stream channels. Lighter than rest of unit. Contact with surrounding units is sharp (moderately). Distinguishing features: basin-fill unit. Braided stream channels that give the unit a faint striped appearance.

23. Grayish brown to pale brown. Consists of several long, sharp ridges grading into smaller ridges some of which are part of a semicircular structure. Drainage is well formed, medium, darker than rest of unit. Contact with surrounding units is moderately sharp to very sharp. Linear features represented by ridges are clearly visible. Distinguishing features: darker than surrounding units. Groups of several long and short sharp ridges giving a hummocky appearance.

24. Mottled moderate greenish yellow with grayish yellow patches. A basin fill unit with little or no relief. Drainage is very fine to fine, well developed, lighter than rest of unit. Appears braided giving the unit a stringy texture. Contact with surrounding units is very diffuse. May represent a unit formed during flooding of basin. Distinguishing features: very light, flat, basin-fill unit. Braided channels give a faint stringy appearance.

25. Pale green to moderate yellow green. Appears to be a gentle sloping pediment surface in the higher parts of a basin-fill unit. Drainage difficult to detect to very fine, lighter than rest of unit. Contact with surrounding units very diffuse to very sharp. Distinguishing features: mottled pale to medium yellow basin-fill unit. Lack of relief. Absence of features.

26. Grayish green with some very pale green patches. Forms a group of low mountains rising from a fairly flat area. Consists of numerous small knobby hills giving a very soft appearance as well as several large high ridges. Displays some change in relief. Drainage appears medium to coarse, well formed, lighter than rest of unit. Contact with surrounding units is sharp. Some linear features represented by ridges are visible. Most of unit looks very broken up. Distinguishing features: low mountain-forming unit that appears to be highly fractured.

27. Mottled pale green to grayish green (brownish red vegetation). Rugged mountain-forming unit, higher than surrounding terrain around its edges, with several sharp ridges seperated by gullies and some peaks. Drainage is well formed, medium to coarse, rectangular to dendritic. Contact with surrounding units is sharp to very sharp. Lineaments represented by ridges

UNIT

are numerous. Distinguishing features: mountain-forming unit with very rugged relief. Numerous ridges and hills rising from a basin.

28. Pale green to moderate yellow green. Appears to be a gently sloping pediment filling the gap between two mountain units. Drainage is fine, well-formed distributary and dendritic, lighter than rest of unit. Contact with surrounding units very diffuse to very sharp. Distinguishing features: inter-mountain basin-fill unit with well developed fine drainage.

29. Pale green with patches of grayish yellow green. Basin-forming unit, gently sloping with little or no relief. Drainage is well formed, distributary with some braided stream channels visible, all darker than rest of unit. Contact with surrounding units very diffuse to very sharp. Distinguishing features: basin-forming unit, with well developed fine dendritic and distributary drainage.

30. Overall grayish yellow, with a few blotches of pale green. Forms a flat basin with no relief. A very non-descript unit. Drainage is very fine to fine, poorly developed, lighter than rest of unit. Contact with surrounding units is moderately sharp to sharp. Distinguishing features: basin-fill unit. Very flat, no distinguishing features.

31. Pale greenish yellow, lighter than all surrounding units, appears to be a flat basin fill unit with a gentle slope, some arroyos and washes formed by drainage which appears to be well formed fine to medium, rectangular (?), distributary, darker than rest of unit. Contact with surrounding units is moderately sharp to sharo. Linear features represented by drainage are visible in places. Distinguishing features: very light colored basin unit. Stands out against darker surrounding units. Does not display much relief.

32. Overall pale green, forms a gently sloping flat pediment surface. Drainage is very fine to fine, lighter than rest of unit. Contact with surrounding units varies from moderately sharp to very sharp. Distinguishing features: uniform pale green pediment surface. Light-colored drainage.

33. Mottled grayish green to light green. Forms a mountain range composed of numerous small hills and several small parallel ridges. Drainage is undetectable. Contact with surrounding units appears sharp. Lineations represented by ridges are moderately well defined. This unit appears highly fractured and foliated on a large scale. Distinguishing features: low mountain-forming unit. Numerous parallel ridges giving a slightly foliated appearance.

34. Grayish green with patches of dusky yellow. Forms a mountainous blocky-appearing unit with moderate relief. Consists of well rounded mounds and rounded ridges. Drainage appears poorly developed, medium. Contact with surrounding units is moderately sharp. Distinguishing features: mountain-forming unit. Very mottled blocky appearance.

UNIT

35. Overall greenish yellow with moderate yellow stringers and patches. Basin fill unit with minor slopes and no other relief. Drainage fine, well developed, distributary, lighter than rest of unit, giving a stringy appearance. Contact with surrounding units is sharp to very sharp. Distinguishing features: basin-fill unit. Well developed fine drainage giving a stringy appearance.

36. Overall dark green, with random patches of pale green. Appears to form a long mountain range consisting of a long sharp ridge several smaller parallel ridges, and numerous small knobby hills. Moderately rugged relief. Drainage is fine, well developed dendritic and parallel to some extent, lighter than rest of unit. Contact with surrounding units is sharp. Linear features are represented by the major ridge system of the unit. Distinguishing features: elongate mountain range with long parallel ridges as the main component.

37. Mottled pale green with small diffuse patches of grayish green. A low mountain-forming unit consisting of numerous closely spaced parallel, subdued, ridges, and several larger widely spaced subrounded hills. Drainage appears primarily fine, well developed, dendritic lighter than unit. Contacts very diffuse to moderately sharp. Numerous small linear features suggesting slight foliation. Distinguishing features: very low mountain range. Numerous parallel ridges suggesting foliation.

38. Overall olive green. Occurs as several small patches. Includes areas that vary from very flat with almost no relief to areas with alternating, subdued ridges and gullies. All are on a plateau unit. Drainage is fine, some medium, poorly developed, lighter than rest of unit. Contact with surrounding units is sharp. Only linear features are occasional subdued ridges. Distinguishing features: occur as small dark patches with sharp contacts. Found only on or near the edge of a plateau unit.

39. Overall moderate yellow green with faint linear patches of moderate yellowish green. Appears to consist of numerous small subdued hills and ridges. Has moderate relief, foliated appearance. Drainage is fine, well developed. Lighter than rest of unit. Contact with surrounding units is diffuse. Distinguishing features: low mountain unit with moderate relief. Numerous fine ridges giving a subdued foliated appearance.

40. Overall pale green, flat basin unit with some minor relief consisting of occasional small, sharp ridges and small hills. Drainage is moderately well developed, fine to medium, distributary, faintly rectangular, lighter than rest of unit. Contact with surrounding unit is sharp. Faint linear features are evident in the larger drainage channels. Distinguishing features: basin unit with some low relief. Very faint rectangular drainage.

41. Plae greenish yellow, part of a basin unit, occurs in the lowest parts of a basin. Has an overall elongate appearance like a pair of horns. Little or no relief. Drainage on surface not evident, but itself appears to be part of a drainage system originating in unit 45. Contact with surrounding units is diffuse to sharp. Appears to be related to flooding and drainage

of the basin. Distinguishing features: very light colored unit that occupies the very low part of a basins.

42. Mottled grayish green, patches of moderate yellow green. Small group of mountains with rugged relief. Consists of elongate sharp ridges and separated by gullies. Drainage is medium, well developed, lighter and darker than rest of unit. Contact with surrounding units is sharp. Linear features are visible in the form of ridges. Distinguishing features: small group of sharp ridges forming a rugged patch of mountains rising out of a basin unit.

43. Mottled yellowish gray with grayish yellow patches. Appears to be an old partially refilled canyon, with walls that are highly eroded by present day drainage and whose floor has been filled by debris, off the walls. Drainage is fine to medium, well developed, distributary and parallel, darker than rest of unit. Contact with surrounding unit is moderately sharp. Distinguishing features: looks like a partially refilled canyon with a relatively flat floor and well developed drainage from the higher parts of the unit.

44. Pale brown, consists of a fairly flat unit with a gentle slope terminated by a sharp scarp on one side. Drainage is fine, well developed, dendritic, lighter than rest of unit. A very large scarp truncates part of the unit. Distinguishing features: dark unit with minor relief and well developed, light colored, fine drainage.

45. Very pale green, flat basin unit with no relief in lowest part of basin. No drainage visible. All contract diffuse. Unit may be related to basin flooding. Distinguishing features: occurs in lowest part of basin. Light color. Diffuse contacts.

46. Pale green. Forms a single butte, no drainage visible. Contact with surrounding units is moderately sharp. Distinguishing features: butte former.

47. Pale green. A small non-descript patch of rounded hills in a basin. No drainage visible, very diffuse contacts. Distinguishing features: very small patch of rounded hills in the bottom of a basin.

48. Pale green to yellowish green. Consists of a single sharp ridge half-buried by sediment. Drainage very fine, well developed, appears dendritic, darker than rest of unit. Contacts very diffuse. Crest of ridge forms a linear feature. Distinguishing features: single sharp ridge appears to be partially buried by its own sediment.

APPENDIX C

UNIT

1. Mottled pale pink to grayish pink, appears to form a smooth, flat surface in the lower part of an inner mountain basin. No drainage visible on surface. Contact with adjacent unit varies from sharp to moderately sharp. May represent an evaporite deposit. Distinguishing features: almost white color. Almost flat relief found in basins.

2. Pale pink to grayish purple, little or no topographic relief. Very fine drainage visible on some areas of the unit. Darker than rest of unit. Contact with surrounding units varies from moderately sharp to very diffuse. Found in an inner mountain basin. Formed in the low flood stage of unit 1. Distinguishing features: mottled pinkish color. Low topographic relief found in basins. Associated with unit 1.

3. Mottled pale pink-grayish purple-grayish blue. Little or no topographic relief found in basin. Fine to medium drainage (braided) lighter than rest of unit. Contacts with surrounding units varies from sharp to very diffuse. Formed during medium flood stage of unit 1. Distinguishing features: mottled white to pink basin association. Braided drainage associated with unit 1.

4. Pale red purple to a very dusky red purple. Very gentle sloping on the lower part of a pediment surface. Very fine to fine parallel drainage, lighter than rest of unit. Contacts moderately sharp, diffuse feather edging. Formed during high flood stage of unit 1. Distinguishing features: associated with unit 1. Feather edging of unit associated with basins.

5. Reddish pink to grayish blue, forms a gentle sloping surface of pediment between mountain ranges. Fine to medium distributary drainage usually lighter than rest of unit. Contacts with surrounding units very diffuse to sharp. May represent the alluvial surface formed by deposition of material by higher surrounding units. Distinguishing features: major reddish unit in inner mountain basins distributary drainage. Formation of pediment surfaces.

6. Pale reddish pink to grayish blue. Appears to be smooth with gradual sloping down toward basins. Unstable changing part of a pediment surface. Drainage varies from none visible to fine parallel-distributary, generally lighter than rest of unit. Contacts vary from sharp with mountain ranges to diffuse with other basin fill units. Similar to unit 5 but less stable. Distinguishing features: filament drainage on most of unit. Associated with basin fill at foot of mountain ranges.

7. Reddish pink to pale bluish cast with occasional light patches. Consists of low moderately sharp ridges at the foot of several mountain ranges continuing into basins. Fine to medium distributary and dendritic drainage, usually darker than rest of unit. Contact with surrounding units, sharp at foot of mountains, to diffuse with other basin fill units. (May represent the most eroded parts of the present mountains.) Distinguishing

UNIT

features: low moderately sharp ridges along the lower parts of several mountain ranges. Fine drainage throughout.

8. Mottled reddish pink to pale blue. Appears to form in moderate sloping surfaces that represent the major drainage from higher areas. Well developed medium distributary drainage darker than rest of unit. Contact with adjacent units, moderately sharp. Distinguishing features: inner mountain valley location. Well developed drainage (distributary).

9. Mottled reddish pink to medium blue. Consists of moderately sharp to sharp ridges forming the lower parts of a mountain range. Displays well developed-medium pinnate and distributary drainage. Darker than rest of unit. Contact with surrounding units, moderately sharp with basin-fill units to diffuse with mountain units. Possible related to unit 7 although not as eroded. Distinguishing features: sharp ridges along lower parts of mountain range, separated by well developed drainage.

10. Pale blue overall forms in basins. Fairly flat with gentle slope and swales locally. Well developed fine drainage usually darker than rest of unit. Contact with adjacent units moderately sharp. Appears to be an area much affected by drainage from higher areas. Distinguishing features: forms in basins. Well developed fine drainage.

11. Very dark red to blackish red. Consists of a cluster of small well rounded hills and elongate smooth ridges in mountain regions. Coarse, poorly developed drainage. Contacts with adjacent units moderately sharp to very sharp. Distinguishing features: darkness of unit with surrounding area. Elongate ridges.

12. Overall pale to medium blue with reddish pink patches. Forms low rounded hills with higher moderately sharp ridges. Occurs as the lower part of a mountain range. Moderately well developed medium to find drainage generally darker than rest of unit. Contacts with adjacent units moderately diffuse to sharp. Distinguishing features: mountain former (low) moderately well developed drainage separating sharp ridges.

13. Pinkish red to medium blue. Consists of several rather elongate some flat top, ridges (cuestas). Occurs as part of a mountain range. Coarse moderately well developed drainage, generally darker than rest of unit. Contacts with other units varies from moderately sharp to very sharp. May represent slightly dipping beds with drainage cutting surfaces. Distinguishing features: closely space elongate flat topped ridges (cuestas).

14. Overall dark blue with some pale blue areas. Consists of several well developed sharp ridges and smaller knobby mounds with steep slopes. Is major mountain forming unit. Drainage is coarse to fine well developed throughout in a rectangular to dendritic pattern. Contact with adjacent units is moderately sharp to very sharp. Distinguishing features: major mountain forming unit. Well dissected drainage on elongate sharp ridges. Topography high.

UNIT

15. Mottled medium red to deep blue with white patches throughout. Is a low mountain forming unit consisting of numerous small rounded knobs with low elongate moderately sharp ridges irregularly spaced. Medium, moderately well developed drainage. Contact with adjacent units sharp. May represent fractured jointed rock, appears to be foliated on a large scale. Distinguishing features: low mountain former. Knobs and elongate ridges forming a foliated appearance.

16. Pale pink with pale blue patches locally. Forms the basin between two small mountain forming ridges and has a flat gentle slope. Fine to coarse, well developed braided and dendritic drainage. Contact with adjacent units diffuse to sharp. May represent sedimentary rocks that have been cut by drainage from surrounding high areas. Distinguishing features: basin fill character. Well dissected by erosional streams.

17. Pale blue and pale red. Flat gentle sloping basin filling unit. Fine braided drainage darker than rest of unit. Contact with adjacent units moderately sharp. May represent a moderately stable pediment surface. Distinguishing features: basin filler with braided dry washes.

18. Mottled light and dark pink with some dark blue locally. Over a gentle sloping surface with low elongate hills (swales). Appears to be a transition between mountains and basin fill. Fine to medium dendritic drainage. Contact with adjacent units moderately sharp. May represent highly eroded part of unit 17. Distinguishing features: only basin unit with well developed elongate swales. Very well developed drainage for basin fill unit.

19. Dusky red, forms flat surface on higher units, almost like a large mesa. Drainage is medium dendritic, well developed, darker than rest of unit. Contact with adjacent units moderately sharp to sharp. May represent nearly horizontal beds more resistant than surrounding units. Distinguishing features: position along mesa type units well developed drainage. Dusky red color.

20. Grayish purple, consists of numerous rounded hills and ridges. Medium moderately well developed drainage, darker than rest of unit. Contacts with surrounding units, moderately well developed drainage, darker than rest of unit. Contacts with surrounding units, moderately sharp. Distinguishing features: fairly dark units. Forms rolling hills. Topographically high.

21. Dark red to dark blue appears to form part of a large plateau. Cut by drainage forming elongate rounded swales. Drainage is fine to medium, moderately well formed, dendritic pattern, darker than rest of unit. Contact with surrounding units is diffuse to moderately sharp. Distinguishing features: very dark. Relatively flat with good drainage. Occasional elongate swales.

22. Mottled medium red to medium blue, forms fairly flat unit on top of a large plateau. Dissected by numerous fine well formed, dendritic and

UNIT

sinuous dry washes. Contact with surrounding units moderately sharp. Distinguishing features: generally flat plateau. Former highly dissected by fine drainage.

23. Medium to pale pink and dark blue. Consists of long fingering sharp ridges and shorter more concentrated sharp ridges. Forming the transition between basin and plateau units. Drainage fine to medium, well developed dendritic. Contact with surrounding units is sharp. Distinguishing features: long fingering ridges. Transition between basins and plateaus.

24. Mottled dusky blue to pale purple, forms the more eroded part of a plateau. Very highly dissected by fine to medium dendritic drainage, appears darker than rest of unit. Contact with surrounding units is very sharp. This unit is very similar to unit 22, is however more dissected. Distinguishing features: position plateau. Highly dissected.

25. Mottled pale red, moderate red, very dusky red. The outer edges of this unit appear locally, to have a white border. This may however be a function of lighting angle. This unit forms the transition between plateau and canyons which are the major drainage in the area. It is gently sloping with occasional sharp ridges and rounded hills. Drainage is fine to medium distributary, sometimes lighter/darker than rest of unit. Contact with surrounding units varies from diffuse to very sharp. Distinguishing features: red color. Canyon-plateau transition. Very flat unit. Lineament show up well.

26. Mottled pale pink-pale blue. Forms a small basin surrounded on all sides by higher terrain. Consist of fairly flat areas and some small rounded hills locally. Drainage is fine to medium well developed dendritic distributary. Contact with adjacent units is diffuse to moderately sharp. Distinguishing features: basin unit higher than most other basins in area, fine drainage.

27. Very dusky purple unit (in a topographically high area). Consist of several moderately sharp to sharp, elongate ridges and several groups of small rounded lineup hills. Drainage is medium distributary on a large scale. Contact with adjacent units is moderately sharp to sharp. Distinguishing features: very dark color. Sharp elongate ridges.

28. Very dusky blue, form flat topped mesas, with some rough areas in the more eroded area plateaus. _____ is among the topographically highest units recognizable. Drainage difficult to detect but appears fine, dendritic and distributary. Contacts are locally diffuse but regionally very sharp, forming scarps in some areas as well as rounded, lobate contacts where uneroded. (Possibly represent lava flows.) Distinguishing features: distinct plateau former. Darkest unit on photo. Sharp and lobate contacts. Topographically very high.

29. Dusky blue, forms mesas (plateaus) like 28, however at lower level. Drainage is fine, poorly developed, distributary. Contacts are very diffuse more so than 28, to very sharp, forming scarps. May represent older

UNIT

more eroded lava flows. Distinguishing features: very dark color. Distinct plateau former. Sharp contacts.

30. Mottled, dominantly pale blue with patches of dusky blue. Appears to occupy an old plateau, has very undulating somewhat smooth surface, and appears subdued, has numerous rounded hills throughout. Drainage is moderately to well developed very fine to fine. Contacts with other units are diffuse to moderately sharp. This unit may occupy a similar stratigraphic position as unit 22. Distinguishing features: dark color. Subdued appearance.

31. Color is quite variable, white, pale pink, pale blue, maroon, occupies canyons formed by main drainage of entire area, appears stratified horizontally. Color may be somewhat sun angle controlled. Contact with surrounding units varies from moderately sharp to very sharp with gradual to very steep slopes. Very rough. Lineaments easily visible. Drainage very coarse, dendritic. Distinguishing features: occupies large canyon areas. Very rough appearance. Lineaments easily visible.

32. Mottled moderate pink with pale blue patches. Surface is relatively flat with subdued swales. Drainage is fine, poorly developed. Contacts with surrounding units varies from subdued to very subdued. Occupies a plateau position. May be stratigraphically similar to unit 25. Distinguishing features: reddish plateau unit. Fine, poorly developed drainage.

33. Pale to medium blue, forms a knobby unit with subdued ridges and hills. Fine to medium, dominantly dendritic with some distributary drainage, darker than rest of unit. Contact with adjacent units is very subdued to sharp forming scarps locally. Distinguishing features: very knobby texture.

34. Medium blue with patches of grayish blue. Occupies what looks like the eroded part of a basin. Drainage fine to medium, very well formed dendritic, darker than rest of unit. Contacts with surrounding units moderately sharp. Probably very eroded part of a basin. Distinguishing features: high basin location. Well eroded.

35. Mottled, dominantly dusky blue, with some pale blue. Forms a flat area similar to unit 28, however probably more eroded. Drainage appears fine, moderately well developed. Contacts are diffuse to very sharp, probably related to 28, more eroded. Distinguishing features: dark unit. Fairly flat.

36. Moderate red, appears to be a basin fill unit, consists of flat areas with some low subdued hills and large washes. Drainage is fine to medium, poorly to moderately well developed, usually darker than rest of unit. Contacts with surrounding units moderately diffuse to very sharp. Distinguishing features: basin fill unit. Darker than most other basin fill units. Moderately well developed drainage.

37. Grayish red to moderate reddish orange, forms part of a large basin fill unit. Drainage is angular-rectangular medium to coarse well formed, (possibly related to structure in the area). Superposed on this locally

UNIT

onto this is a finer sinuous drainage, much younger. Contacts with surrounding units is very diffuse to moderately sharp. Structural lineaments appear through a majority of this unit. Distinguishing features: dark basin fill unit. Medium to coarse rectangular drainage.

38. Mottled grayish red purple-grayish purple. High basis fill unit, possibly consist of well rounded, elongate ridges, separated by moderately flat areas and dry washes. Drainage is well developed medium, usually lighter than rest of unit. Contacts with surrounding units is moderately diffuse to moderately sharp. Distinguishing features: basin fill unit. Overall subdued appearance. Well developed medium drainage.

39. Dark reddish, maroon, forms a very flat unit on a mesa. Drainage is very fine and appears poorly developed, darker than rest of unit. Contact with surrounding units is sharp to very sharp, lobate in some places. Possibly soil development on top of lava flow. Distinguishing features: forms as a cap on flat mesas. Poor drainage.

40. Grayish red to moderate red, forms pact of basin fill unit in which unit 37 is a major part. Appears overall subdued, and flat with possible gentle sloping toward higher standing units. Drainage is fine, poorly developed, may be superposed on older subdued medium drainage still visible in unit 37. Contact with surrounding units is generally very subdued with other basin units, sharp with mesa forming units. Distinguishing features: basin-forming unit. Fairly flat, subdued, with fine poorly developed drainage.

41. Mottled pale red, moderate red. Forms a knobby uneven surface with rounded hills, ridges, and low mesas. Poorly formed coarse drainage. (Lighter and darker than rest of unit.) Contact with surrounding units is moderately sharp to sharp. Some lineaments visible locally. Distinguishing features: mottled appearance. Rounded knobby ridges, hills.

42. Medium to dusky blue. Consist of radiating sharp ridges that meet to form a high mountain. Drainage is well formed, coarse radial, darker than rest of unit. Contact with surrounding units is moderately sharp. Distinguishing features: sharp radiating ridges.

43. Pale red purple, medium blue. Consist of partially radiating to random, moderately sharp to moderately subdued ridges. Drainage is well formed medium coarse drainage. Contact with surrounding units is moderately sharp. This unit appears similar to unit 42. Distinguishing features: partial radiating pattern (drainage) of moderately sharp subdued ridges.

44. Moderate red, forms a fairly flat surface (plateau) with almost no relief. Drainage is moderately well formed, coarse, darker than rest of unit (shadows). Contact with surrounding units is very sharp to very subdued. Distinguishing features: location on a plateau, reddish color. One of the reddest plateau units.

45. Mottled pale, moderate red to a pale, medium blue. Forms a very textured pediment surface consisting of numerous sharp to subdued low ridges, and

UNIT

numerous low sharp to subdued knobby hills. Drainage is well formed fine-medium darker than rest of unit. Contacts a very sharp to subdued linear features visible locally. Distinguishing features: pediment surface location. Geomorphic variability of low ridges and low rounded hills.

46. Mottled medium-dark red. Forms a surface of numerous low, sharp hills and surrounding moderately sharp ridges and moderately sharp hills. Fine to medium drainage well developed. Contacts with surrounding units is moderately sharp. Distinguishing features: relative lightness of this mountain forming unit as compared to similar high units. Concentration of numerous hills giving a fine texture.

47. Moderate red to dark blue. Consists of moderately sharp radiating parallel ridges. Similar to unit 42 but not as dark ridges also not as sharp. Drainage is medium coarse, well developed, darker than rest of unit. Contact with surrounding units is very diffuse to moderately sharp. Distinguishing features: parallel to radiating moderately sharp ridges.

48. Mottled pale pink to light red. Consist of a flat light patch. Poorly developed dendritic drainage. Darker than rest of unit. Contact with surrounding units is moderately sharp. Distinguishing features: forms light patches in mountainous areas which are generally dark.

49. Mottled medium blue to grayish blue appears to form a gently sloping pediment surface with local _____, sharp ridges in the more mountainous parts of the region. Drainage is fine, well developed distributary, dendritic drainage. Contacts vary from moderately sharp to diffuse. Similar to unit 6 much darker. Distinguishing features: pediment surface (dark) in mountainous regions. Fine drainage.

50. Dark grayish purple, forms on top of a plateau in a single small patch with almost no relief. Drainage is very well formed pinnate, darker than rest of unit. Contacts with surrounding units is moderately sharp. Probably similar to unit 44 with more drainage. Distinguishing features: well formed pinnate drainage.

51. Moderate red to dark blue, this unit is generally associated with buttes or mesas, which are darker than the surrounding area. Drainage is poorly developed, fine. Contacts with surrounding units is diffuse to moderately sharp. Distinguishing features: associated with buttes. Darker than surrounding area.

52. Grayish red forms a small mountain range with several medium sharp to sharp ridges. A main ridge forming the crest. Drainage is dendritic, fine moderately well developed. Contact with surrounding units is moderately sharp. Distinguishing features: darker than surrounding units. Formed by a small discontinuous ridge.

53. Pale gray blue. Forms rounded slopes of the walls of a shallow large dry wash. Drainage is well formed, fine medium distributary drainage. Contact with surrounding units is moderately sharp to sharp. Distinguishing features: well formed medium drainage on the walls of a former wash.

UNIT

54. Mottled medium red to medium blue. Forms the flat alluvial surface formed by erosion of unit 53. Drainage is poorly developed, fine, lighter than rest of unit. Contact with surrounding units is very sharp. Distinguishing features: forms a flat basin fill with no relief. _____ fine drainage.

55. Pale pink, forms the gentle slopes of a small mountain range. Drainage is well developed distributary, darker than rest of unit. Contact with surrounding units is sharp. Distinguishing features: very light color for a mountain forming unit. Darker drainage. Well formed fine dendritic drainage.

56. Mottled _____ red to pale blue medium blue. Consist of several large and small hogbacks. Drainage is poorly developed, fine. Contacts with surrounding units is moderately sharp, to sharp. Distinguishing features: several low hogbacks forming a linear feature.

57. Highly mottled grayish red to a pale pink, forms part of a large basin fill unit. Drainage is distributary, well formed, fine. Contacts with surrounding units are diffuse. Distinguishing features: basin fill unit. Well formed distributary drainage. (Highly mottled.) Light color for a basin fill unit.

58. Pale to medium blue, forms small pointed hills (mounds). Drainage appears fine, radial, well developed. Contact with surrounding units is moderately sharp. May be patches of resistant rocks. Distinguishing features: forms small pointed hills with radial drainage.

II-B. VERDE VALLEY

D. Elston, W. D. DiPaolo

1. INTRODUCTION

Multispectral and color images photographed from spacecraft and from high-altitude aircraft were analyzed for regional structural information in a 9400km^2 area of north-central Arizona. The images reveal the existence of long linear traces that transect geologic terranes of differing ages. Comparison with geologic maps, and field geologic examination, have shown that several of the most strongly developed linear traces coincide with major Precambrian faults. Extensions and apparent offsets of some of the Precambrian linear traces occur in Phanerozoic rocks, which include volcanic and sedimentary strata that are only a few million years old. This attests to recurrent movements on ancient breaks in the crust. Most of the linear traces that can be identified in the younger rocks in orbital images are too diffuse at the normal scale of geologic mapping (1:24,000 and 1:62,500 scales) to be readily recognized on the ground as parts of regional fracture systems, although faults locally have been mapped along parts of some lineament trends.

An objective of this work was to identify the principal lineaments and to examine their relations to the geology and structure of the region. This has been carried out by means of: 1) detailed photogeologic supplemented by field geologic mapping (1:24,000 scale) of the stratigraphy, and of faults, joints, and lineaments in a control area (Sedona area) using high-resolution aircraft images; and, 2) by mapping of stratigraphy and lineaments in a larger area of north-central Arizona from Landsat (ERTS) and from Skylab spacecraft images. Reconnaissance and at places detailed field geologic work has supported the regional photogeologic analysis. Additionally, Precambrian faults in the Grand Canyon of northern Arizona, and some faults in Phanerozoic

rocks in an intervening area south of the Grand Canyon, also were compiled. This has served to place the geology of central Arizona in a broader framework, and to provide a better idea of the regional spacing of major structural discontinuities in the basement. A coherent structural framework for central and northern Arizona emerged when the azimuthal distributions of the faults and lineaments were evaluated with respect to structural events that have been defined from geologic work.

Location and Physiography

The area studied in detail is in north-central Arizona and includes part of the southern Colorado Plateau and part of the adjacent Mountain Region (Fig. II-B-1). The Mountain Region borders the Plateau on the south and although considered to be part of the Basin and Range physiographic province (Ransome, 1903, p. 16), it is in part structurally similar to the Colorado Plateau. The physiographic margin of the Colorado Plateau is a south-facing erosional escarpment called the Mogollon Rim. This margin is not marked by an abrupt change in structural style of the nearly flat-lying Paleozoic strata that underlie the surface of much of the Plateau. Thus, where Paleozoic strata have been removed by erosion in the transition region, and Precambrian rocks exposed, the comparatively complicated structure seen is almost entirely of Precambrian age.

Lineaments

The term "lineament" has been applied in this study to any natural elongate trace that indirectly reflects the existence of single fractures or groups of closely spaced fractures (joints or faults) in the bedrock, or the regional trends of stratification and foliation in metamorphic terrane. Lineaments, as thus defined, were mapped in images at both the detailed (1:24,000)

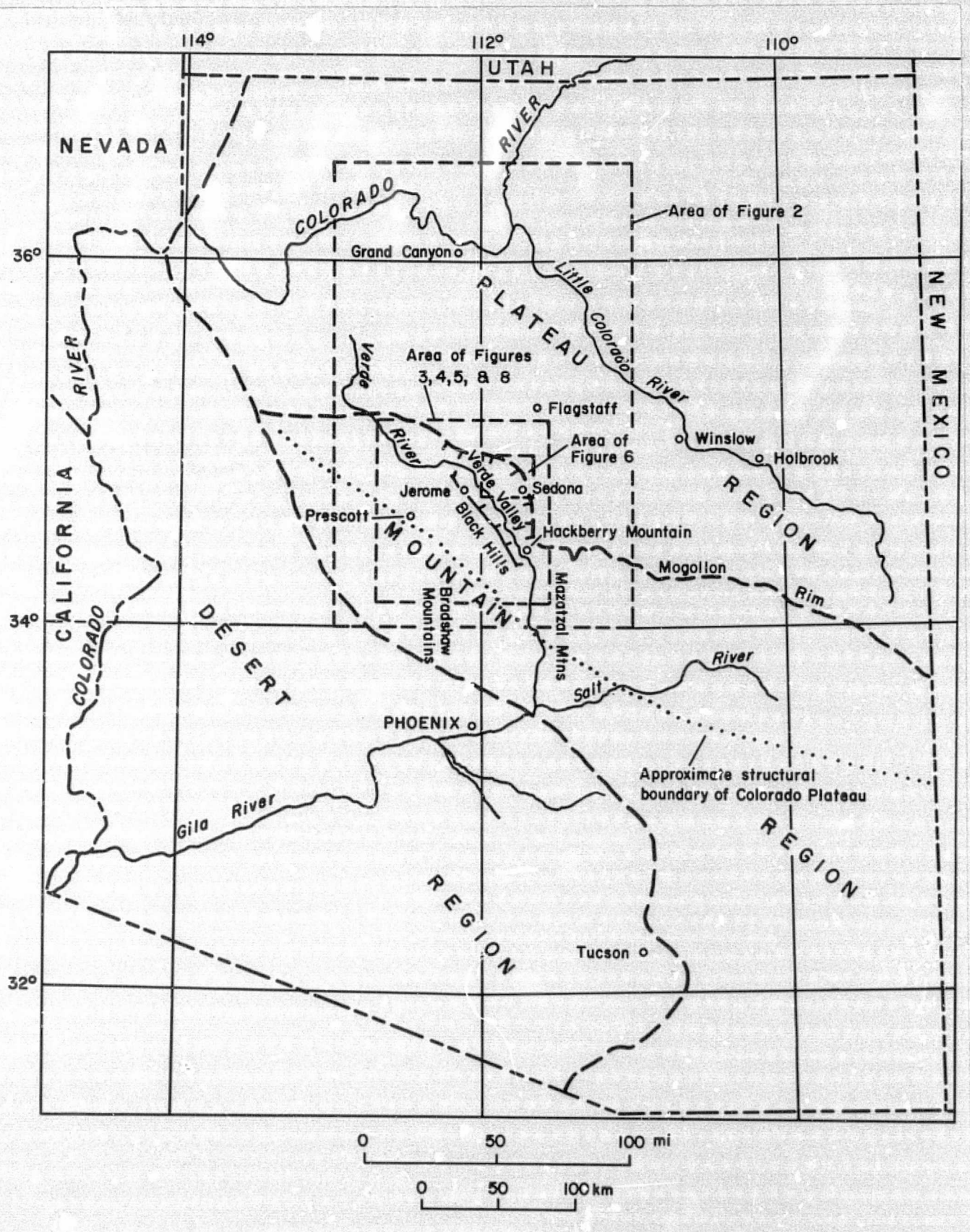

Fig. II-B-1. Physiographic and index map of Arizona.

and reconnaissance (1:200,000) scales. Our definition generally follows the definition of a lineament by W. H. Hobbs (cited in the Glossary of Geologic Terms, 1957), who in 1912 described lineaments as significant lines of landscapes that reveal the hidden architecture of the rock basement. Unlike Hoppin (1974), who makes a distinction between a lineament and a linear, we follow the usage of the Glossary of Geology (1972) in which a tectonic linear is synonomous with a tectonic lineament.

In our detailed mapping (1:24,000) scale, features that we classed as lineaments included: 1) linear topographic or physiographic elements produced by the differential effects of erosion in fractured ground (for example, the straight portions of drainage systems); and 2) in alluviated ground, linear arrays of plants that reflect moisture-bearing fractures in the underlying bedrock. In many cases, features mapped as lineaments were on direct extensions of mapped fractures and groups of fractures. Individual faults, joints, and lineaments were observed in the high-resolution ($\lesssim$3 m), high-altitude aircraft images during the detailed mapping, but expectedly they were not resolved in the orbital images; rather groups of fractures and lineaments resolved in the detailed mapping were recorded only as individual lineaments (if at all) at the 1:200,000 scale mapping. Thus, except for faults known from prior field geologic work and photoidentified on the LANDSAT and Skylab orbital images, linear elements identified in the orbital images were all indirect manifestations of physical breaks in the rocks, and thus all were classed as lineaments. At the reconnaissance scale of mapping, linear elements can reflect linear contacts between contrasting rock types (commonly the result of faulting), laterally continuous zones of fractured ground, and regional trends of stratification and foliation in metamorphic terrane.

2. REGIONAL GEOLOGY

Stratigraphy

The general geology of part of central and northern Arizona is shown in Figure II-B-2. It encompasses an area that extends from near the southern margin of the Mountain Region on the south to the Grand Canyon in the Colorado Plateau on the north. The geology of north-central Arizona, compiled on and in part mapped from Landsat images, is shown in greater detail in Figure II-B-3. The geologic framework of the region is fairly simple and rock units can be assigned to three geologic terranes: 1) Precambrian; 2) Paleozoic and Mesozoic; and, 3) late Tertiary-Recent.

The Precambrian terrain can be subdivided into three broad stratigraphic intervals. The oldest consists of highly to moderately metamorphosed, commonly well foliated, metasedimentary, metavolcanic, and plutonic rocks. Above this are moderately metamorphosed, unfoliated sedimentary and volcanic strata, and plutonic rocks. These, in turn, are overlain by essentially unmetamorphosed, younger Precambrian sedimentary and subordinate volcanic strata. Consistent with the degree of metamorphism, the oldest Precambrian units are highly to moderately deformed, the intermediate units are mostly moderately deformed, and the youngest units are little deformed. Precambrian strata of central and northern Arizona have an aggregate stratigraphic thickness of about 23 km.

Paleozoic and Mesozoic strata of the Colorado Plateau consist of a series of marine, and interfingering marine and continental strata. In the map area of Figure II-B-2, strata that are shown as 'P' are nearly entirely Paleozoic and they form a 1300-m-thick section that is well exposed in the walls of the Grand Canyon. This Paleozoic section is present, although the lower part is less completely preserved, to the south in central Arizona. Paleozoic strata,

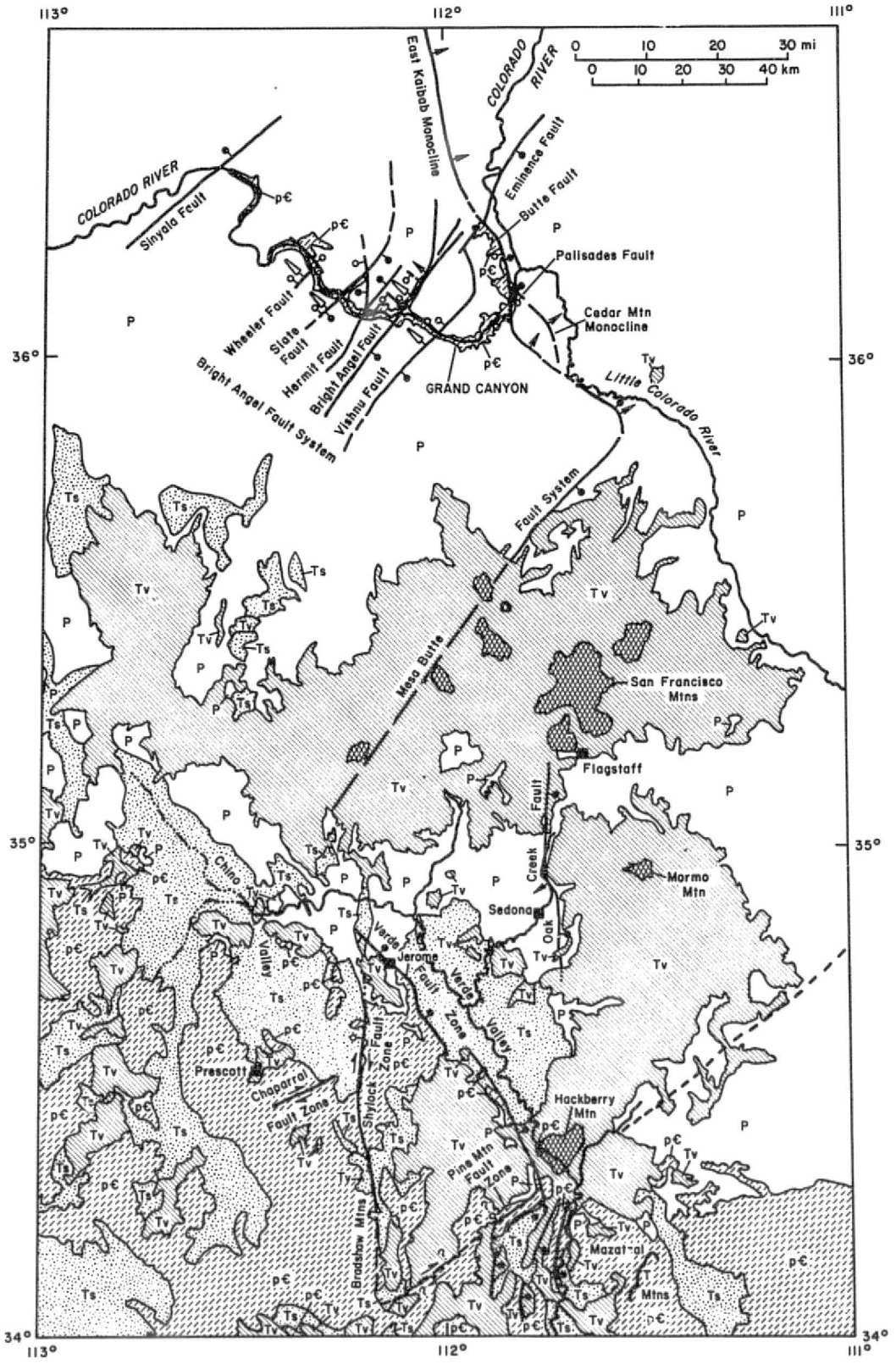

Fig. II-B-2a. Generalized geologic map of part of central and northern Arizona showing principal Precambrian and Phanerozoic faults.

EXPLANATION

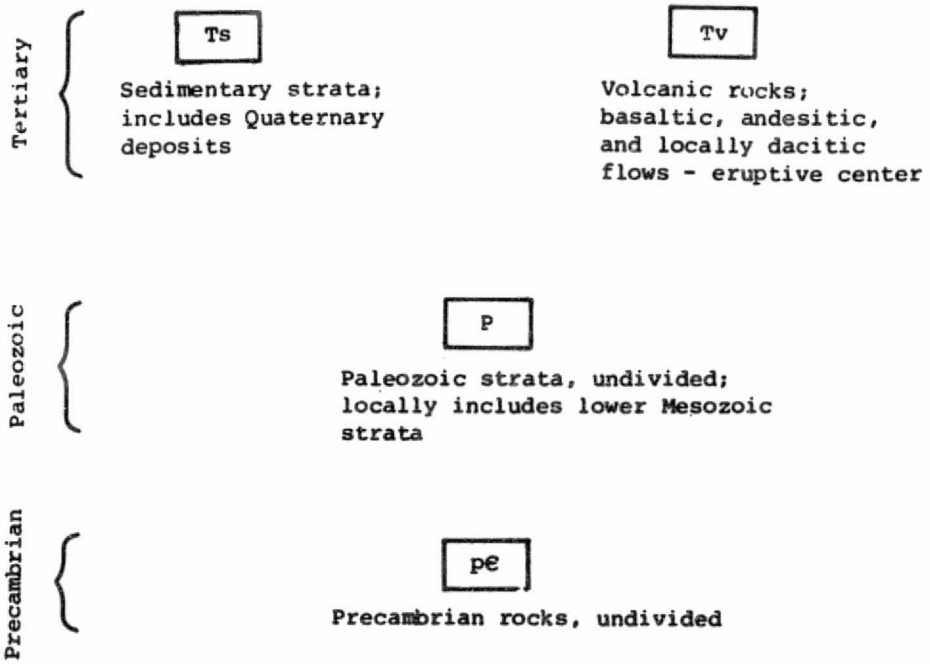

Geology adapted from Arizona Highway Geologic Map (Cooley and others, 1967; 1:1,000,000 scale) with additions from the Geologic Map of Arizona (Wilson and others, 1969; 1:500,000 scale), and maps by Anderson (1967), Canney and others (1967), Maxson (1967, 1969), Sears (1973), and Shoemaker and others (1974).

Fig. II-B-2b. Explanation of Fig. II-B-2a.

which are as old as early to middle Cambrian (∿600 m.y.), are little deformed either on the Plateau or in the Mountain Region. At a number of places, early Paleozoic strata overlie Precambrian faults without break. Such observations have long led workers to conclude that the major structural deformations of the region are of Precambrian age.

The Tertiary record in north-central Arizona (Fig. II-B-3) begins with eruption of latites about 25 m.y. ago near Prescott (Krieger and others, 1971). This was followed in the area of the Black Hills and on the margin of the Colorado Plateau by the deposition of sediments and then eruption of basaltic flows, beginning about 14.5 m.y. ago (McKee and Anderson, 1971). The development of the present topography and much of the recent structure began about 10 m.y. ago (McKee and McKee, 1972). This was a time marked by faulting on the Verde fault, development of a basin and deposition of lake beds in the area of the Verde Valley, and contemporaneous dacitic and basaltic volcanism in the Hackberry Mountain area at the southeast end of the Verde Valley, which ended about 3 m.y. ago (Elston and others, 1974). Eruptions in the San Francisco volcanic field near Flagstaff (Fig. II-B-2) have occurred during the past ∿9 m.y. (Damon amd others, 1974), with the latest eruption occurring at 1064 A.D. (Smiley, 1958). Thus, the laterally extensive cover of basaltic rocks in the region (Figs. II-B-2 and II-B-3) was emplaced principally during the last 15 m.y.

3. FAULTS

Central Arizona

Shylock, Chaparral, and Pine Mountain faults (Precambrian).--Several of the principal Precambrian and Phanerozoic faults of the region are shown in Figure II-B-2. Northeast- and north-trending faults dominate. The oldest faults

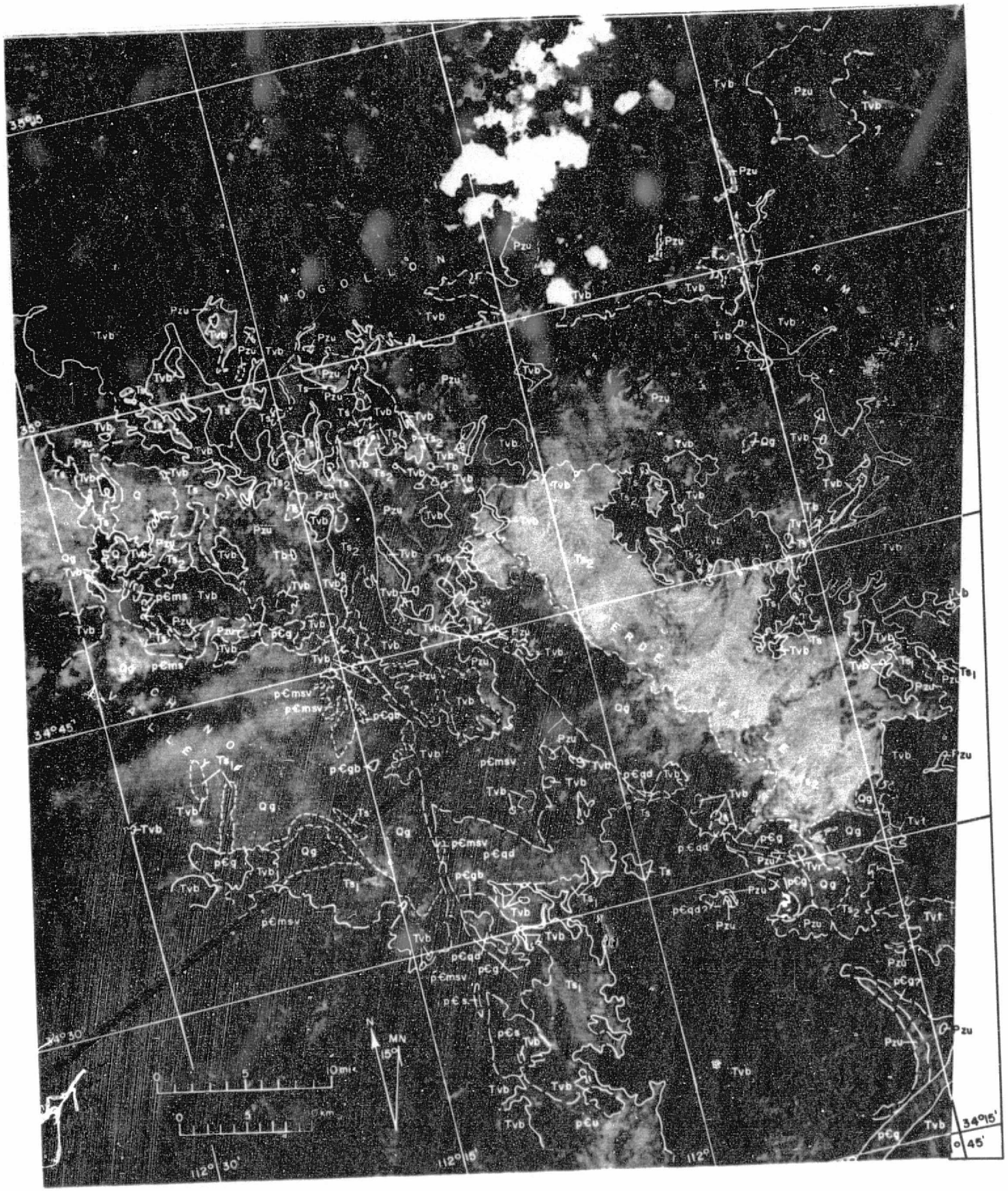

Fig. II-B-3a. Geologic map of north-central Arizona compiled on LANDSAT-1 photobase.

EXPLANATION

SEDIMENTARY ROCKS

Quaternary

Qg

Gravel and alluvium

Tertiary

Ts_2

Sandstone and lake beds

Ts_1

Sandstone

Paleozoic

Pzu

Sandstone and limestone, undivided

Precambrian

pЄms

Quartzite

METAMORPHIC ROCKS

pЄmsv | pЄs

Metasedimentary and metavolcanic rocks, and schist

VOLCANIC ROCKS

Tvb | Tvt

Tvb, basalt
Tvt, tuff

IGNEOUS ROCKS

pЄqd | pЄg

Quartz diorite and granite

pЄu

Undivided

pЄgb

Gabbro

Contact. Dashed where approximately located; short dashed where indefinite

FAULT AND LINEAMENT MAP:

Fault; from published geologic maps. Bar and ball on downthrown side. Dashed where approximately located dotted where concealed.

Lineament. Long traces reflect strongly developed trends, some of which are inferred to be faults. Intermediate and short dashed lines reflect degree of traceability of individual lineaments; dots reflect an alinement of one or more vague linear features.

SCALE OF MAPPING

1:5000

1:24,000

1:31,680

1:48,000

1:62,500

1:375,000 and 1:500,000

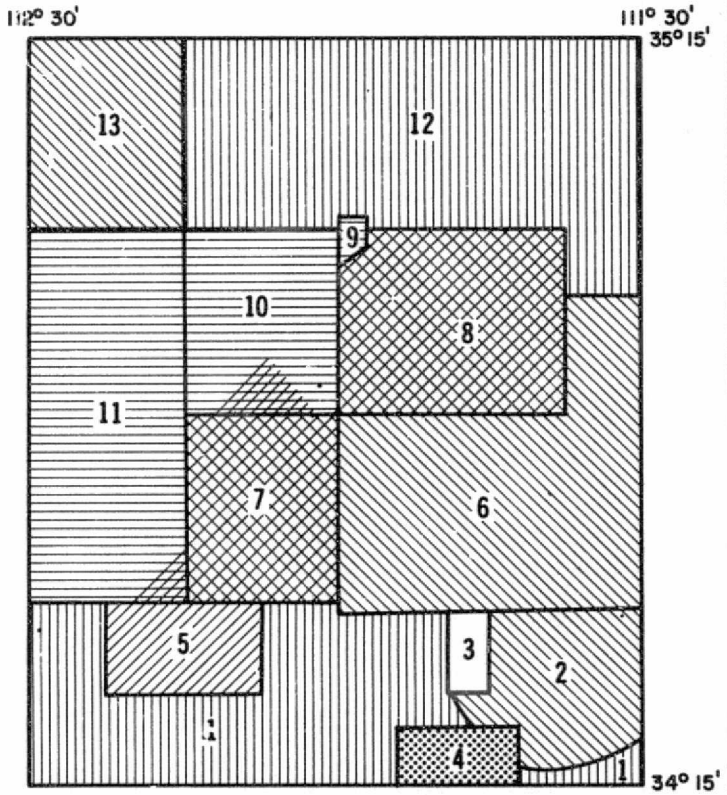

SUMMARY OF DATA

[1] Wilson and Moore, 1958
Wilson and others, 1969

[2] Scott, G.R., and Elston, D.P., 1974 Generalized geologic map of Hackberry Mountain area, central Arizona, in Scott, 1974

[3] Elston, D.P., and Scott, G.R., unpublished map

[4] Canney and others, 1967

[5] Anderson and Blacet, 1972 a & b

[6] Twenter and Metzger, 1963

[7] Anderson and Creasey, 1958, 1967

[8] Elston, D.P., and DiPaolo, W.D., unpublished map

[9] Huff and others, 1966

[10] Lehner, 1958

[11] Krieger, 1965

[12] Moore and others, 1960
Wilson and others, 1969

[13] Krieger, 1967

Index to sources of geology in north-central Arizona

Fig. II-B-3b. Explanation of Fig. II-B-3a.

and folds occur in the Ash Creek Group in the Jerome area, and trend mainly in an east-west direction (Anderson and Creasey, 1958, their Figures 3 and 4).

Somewhat younger Precambrian faults in central Arizona include the north-trending Shylock fault zone and the northeast-trending Chaparral fault zone, both of which are zones of right lateral shear (Figs. II-B-2 and II-B-4). Descriptions and maps of these fault zones are found in Anderson and Creasey (1958), Anderson (1967), Krieger (1965), Anderson and Blacet (1972), and Anderson (1972). Faulting on the Shylock marked the time of development of the latest foliation in the Jerome-Prescott area.

The Shylock fault zone is overlain by unfaulted sandstone of Cambrian age in the Black Hills on the north (Anderson and Creasey, 1958). The Shylock can be traced in Landsat images southward toward Phoenix, Arizona, for a distance of about 75 km, well south of the area of detailed geologic control. Based on the presence of slices of quartz diorite in the Shylock fault zone near the Black Hills, Anderson (1967) estimates a minimum of 8 km right lateral displacement. Transcurrent displacement on the Shylock fault zone is younger than 1760 m.y., the isotopic age of quartz diorite offset by the fault (Anderson and others, 1971). Shoemaker and others (1974) suggest, on the basis of a pronounced aeromagnetic discontinuity across the Shylock, that the total horizontal displacement may have been much greater. Judging from the thickness of the younger Big Bug Group on the west that is in fault contact with the older Ash Creek Group of the east, about 6 km of apparent vertical offset occurs across the Shylock fault zone. The amount of horizontal and vertical displacement on the Chaparral fault zone is not known. The Chaparral either tangentially joins the Shylock fault zone, or is offset by it.

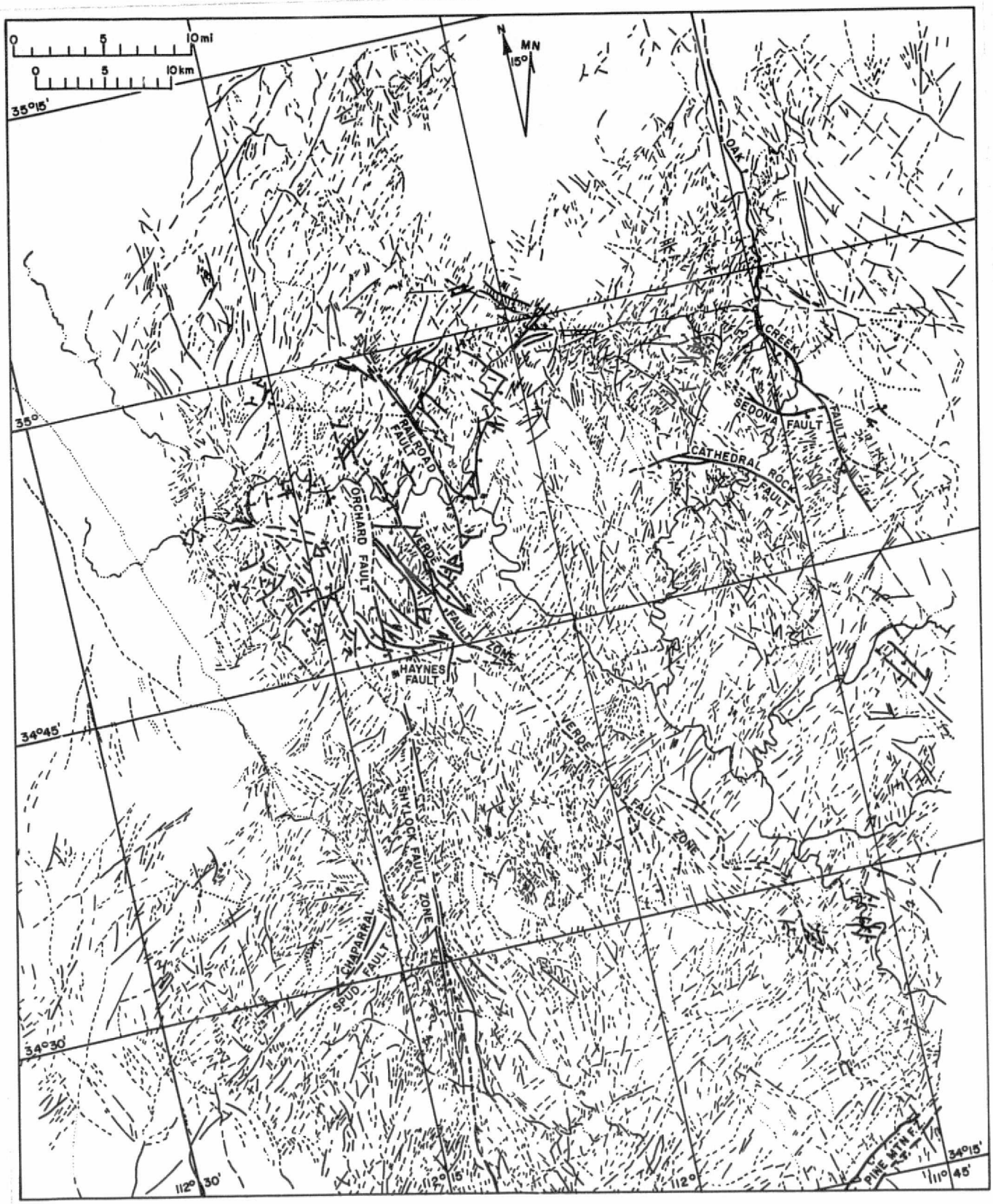

Fig. II-B-4. Faults and lineaments of north-central Arizona compiled on and mapped from LANDSAT photobase.

An essentially vertical, northeast-trending fault zone in Precambrian and Phanerozoic rocks occurs south of Pine Mountain (Canney and others, 1967; Figs. 1, 2, and 4), and it is here named the Pine Mountain fault zone. A distinctively dark reddish granite occurs on the south side of the northern fault strand, and is faulted against a pale reddish granite and highly deformed metavolcanic and metasedimentary rocks on the north (Canney and others, 1967, Plate 1). Near the Verde River, alaskite occurs at least locally adjacent to the fault zone. The trend of the Pine Mountain fault is N50-55°E; similar to the trend of the Chaparral fault zone. A strong aeromagnetic discontinuity occurs along an apparent southward extension of the fault (as seen in orbital images), as the extension approaches the south end of the Shylock fault zone. The southern strand of the fault zone, observed in photogeologic studies by F. R. Twenter (reported in Canney and others, 1967), assumes a more southerly trend and extends for many kilometers to the south. The sense and amounts of Precambrian displacements on the Pine Mountain fault zone are not known, but they may be transcurrent similar to the Chaparral fault zone. If the lateral offset on the Shylock is several tens of kilometers, it is possible that the Pine Mountain fault zone (Fig. II-B-2) is an offset part of the Chaparral fault zone. Such a relationship would imply that strike-slip faulting on northeast-trending faults at least partly predated the latest transcurrent displacement on the north-trending Shylock fault zone. At least 300 m of late Tertiary normal faulting has occurred across the Pine Mountain fault zone, with strata displaced downward on the southeast. As seen in LANDSAT images, a subtle apparent extension of the Pine Mountain fault zone can be traced northeastward in Phanerozoic beds more than 100 km across the Colorado Plateau, passing between Sunset and West Sunset Mountains and trending toward Winslow, Arizona (see Fig. II-B-2 for approximate trace). The trace at places presumably represents a zone of jointing, and perhaps locally of small faults.

Oak Creek and Verde faults (Tertiary and Precambrian?).--Two prominent faults of Tertiary age occur in north-central Arizona: 1) the north-trending Oak Creek fault; and, 2) the northwest-trending Verde fault zone (Figs. II-B-2 and II-B-4). They are normal faults across which Paleozoic and Tertiary strata are displaced downward on the east. The times of most recent faulting, from isotopically dated flows and geologic relationships, lie principally in the interval 10 to 6 m.y. ago (see Elston and others, 1974).

The Oak Creek fault lies south of and may be an extension of the north-trending Butte fault of the eastern Grand Canyon (Fig. II-B-2). If so, the Oak Creek fault may be underlain by a Precambrian fault that has a sense of displacement opposite to the displacement observed in the Phanerozoic strata. This is a characteristic of several faults in the Grand Canyon.

The northwest-trending Verde fault zone is irregular in fine detail. Paleozoic sedimentary strata, and Tertiary sedimentary and volcanic strata are nearly horizontal on the Black Hills. However, at places along the eastern flank of the Black Hills, these strata are sharply tilted northeastward across the Verde fault zone toward the Verde Valley. Tilting and faulting have occurred in apparent response to tensional separation subsidence, and formation of a basin in the area of the Verde Valley; subsidence perhaps reflected withdrawal of magma erupted as basaltic and dacitic flows in the region. In contrast to the Precambrian Shylock fault zone, the Verde fault zone is very difficult to identify in the orbital images (see Figs. II-B-3 and II-B-4). The Verde fault has the same general trend and lack of lateral continuity as northwest-trending Precambrian faults in the Grand Canyon. The "diffuseness" of the Verde fault zone in orbital images reflects its multiple character, at places near Jerome occurring on as many as thirteen strands (Anderson and Creasey, 1958, p. 80). The Verde fault

zone thus probably does not correspond to a single through-going fault in the basement but rather may follow a series of discontinuous breaks in the Precambrian rocks. At Jerome, about 450 m of Tertiary displacement (down on the east) occurs across the Verde fault zone. The sense of possible Precambrian displacement across the Verde fault zone is uncertain (Lindberg and Jacobson, 1974, p. 798), although about 300 m of down-to-the-east Precambrian displacement at Jerome has been reported by Anderson and Creasey (1958, p. 70, 145).

Northern Arizona

Faults in the Grand Canyon.--Maxson and Campbell (1934) recognized that two groups of faults predated deposition of the Grand Canyon Supergroup (Table 1):
1) faults that trend northeast and generally parallel the schistosity; and,
2) faults that trend northwest and generally parallel master joints.

Grand Canyon Supergroup.--The later Precambrian structural history of the Grand Canyon has been most recently investigated and discussed by Maxson (1961, ed. of 1968) and by Sears (1973; in part summarized in Huntoon and Sears, 1975). Each has recognized multiple periods of deformation and faulting. Sears (1973) recognized several northwest to southeast compressional events during deposition of the Unkar Group, which occurred on five northeast-trending, southeast-dipping reverse faults. Four of the faults have associated northwest-facing monoclines (Fig. II-B-2), and the faults and folds all strike in the azimuthal range 35-55°. Sears also recognized in Unkar Group strata a population of expansion faults related to the intrusion of diabase sills. Precambrian normal displacements (downthrown blocks on the west) also were recognized by Sears on the five northeast-trending reverse faults. The latest Precambrian faulting occurs on large normal faults that trend north to north-northwest, and northwest (the Butte

and adjacent Palisades faults) near the eastern limit of exposures of Precambrian rocks in the Grand Canyon (Fig. II-B-2). The events proposed by Sears for an interval of time that embraces much of structural deposition of the Unkar Group includes: 1) formation of northwest-facing monoclines accompanied by reverse faulting (along the Bright Angel fault, folding began at the time of deposition of the basal conglomeratic sandstone of the Shinumo Quartzite); 2) intrusion of diabase sills (which Sears assumed occurred after deposition of the Unkar Group); and 3) two or three interspersed periods of normal faulting. The compressional regime recorded by the reverse faults and associated monoclines apparently favored intrusion of the diabase sills. The stratigraphically highest sill in the Unkar Group occurs in the lower part of the Dox Sandstone, in a newly discovered exposure on the north side of the Palisades fault in the eastern Grand Canyon (Elston and Grommé, 197).

Northwest-trending Precambrian faults in the Grand Canyon are subordinate with respect to the northeast-trending faults (see Maxson, 1967, 1969; Sears, 1973). Although some of these faults have appreciable normal displacement (as much as 600 m; Sears, 1973), the northwest-trending system is marked by comparatively short exposed segments, and they are segments that cannot be traced or extended readily in the synoptic orbital images. This appears to be a general characteristic of the northwest-trending faults.

Phanerozoic strata.--East-west compressive stresses also apparently occurred during Paleozoic time. Sears (1973, p. 64) has observed reverse drag or contrary bending in the Redwall Limestone (Mississippian) on the Bright Angel fault that records minor reverse displacement; the folded beds, moreover, are truncated beneath the Supai Formation (Pennsylvanian and Permian). The northwest-facing monoclinal structure in the Mississippian strata thus formed at approximately

the time of the Antler orogeny in the Great Basin to the west (for a description of which, see Poole, 1974), and could reflect the compression that manifested itself in the Great Basin by overthrusting from the west along the Roberts Mountain thrust.

This structure in the Redwall Limestone mimics the northwest-facing monoclines in the underlying Unkar Group that formed prior to and during intrusion of the diabase sills. The northwest-facing fold in the Redwall subsequently was offset by Tertiary normal faulting (downthrown block on the southeast) on the Bright Angel fault.

Precambrian and Phanerozoic faults in and near the Grand Canyon have been compiled and mapped by Shoemaker and others (1974). They have mapped faults across the Coconino Plateau, south of the Grand Canyon, and have applied the names Bright Angel and Mesa Butte fault systems (Fig. II-B-2) to two prominent northeast-trending groups of faults that can be traced across the region in the orbital images. The Precambrian age of the Bright Angel fault system is unquestioned, whereas that of the Mesa Butte system is inferred. Several of the eruptive centers of the late Tertiary San Francisco volcanic field are localized along or near the Mesa Butte fault system (Fig. II-B-2), suggesting that this system is underlain by a through-going fracture system.

Shoemaker and others (1974) have discussed the possible relationships of the Bright Angel and Mesa Butte fault systems to the Chaparral and Shylock fault zones of north-central Arizona. In particular, they have called attention to the existence of linear aeromagnetic anomalies that coincide with parts of these systems, anomalies that can be interpreted to reflect large structural as well as compositional discontinuities in the basement.

3. ORTHOGONAL FRACTURES AND LINEAMENTS

Image Analysis

A new and revealing overview of the geology and the structural grain of north-central Arizona has been provided by LANDSAT-1 multispectral scanner images (originally called Earth Resources Technology Satellite No. 1), and by Skylab spacecraft multiband camera (S190A) color film images. A photogeologic map, and maps of the faults and lineaments of north-central Arizona were prepared at 1:200,000 scale from the spacecraft images. Mapping was guided by published geologic maps at scales of 1:48,000-1:375,000 (see index map, Figure II-B-3, for sources of geology). To allow for a correlation of the azimuthal distributions of fractures (joints and faults) and lineaments between the reconnaissance and detailed scales of mapping, a photogeologic and a fracture-lineament map of an area of about six 7-1/2" quadrangles that includes part of the Mogollon Rim near Sedona, were made at a scale of 1:24,000 from high-resolution, high-altitude RB-57 aircraft color film photographs. The results have been field checked, and a geologic map is in preparation. The detailed photo geology encompasses an area of 900 km^2, about one-tenth of the area of the 1:200,000 scale reconnaissance mapping (Fig. II-B-1). Parameters for the imaging systems and images, which affect resolution and concern illumination, are summarized in Table II-3.

Landsat images.--Lineaments revealed in the Landsat images (Fig. II-B-4) were mapped from stereoscopic and monoscopic analysis of electronically cleaned photographic prints at a scale of 1:200,000. Faults depicted on published and unpublished geologic maps were transferred, by inspection, to the Landsat photobase. The traces of some were readily identifiable in the synoptic image; others, in particular the Verde fault sysltem and several associated northwest-trending faults were not identifiable as lineaments. Resolution in Landsat

Table II-3. Parameters for analyzed LANDSAT, Skylab, and RB-57 aircraft images, and their imaging systems

LANDSAT-1 Fourband multispectral scanner (stereoscopic pair)

E-1014; 6 Aug. 1972, 1737:50 hours GMT

Sun elevation, 58°; sun azimuth 116°

E-1032; 24 Aug. 1972, 1737:50 hours GMT

Sun elevation 54°; sun azimuth 126°

Nominal flight height, 904 km

Nominal resolution, non-linear object, 100 m

Skylab 3; Frame 61, S190A, 70 mm multiband

Camera system (focal length, 152.44, ±0.015 mm)

Color and color infra-red monoscopic frames

5 Nov. 1973, 1529 hours GMT

Sun elevation 46.5°; sun azimuth 137°

Nominal flight height (above spherical earth), 438.5 k

Nominal resolution, non-linear object, 40 m

RB-57 aircraft; RC-8, 9" x 9" multiband camera

system (focal length, 152.0 mm)

Color and color infra-red stereoscopic pairs

3 May 1973, 1910-1940 hours GMT

Sun elevation 71°; sun azimuth 177°

Flight height, 19 km

Nominal resolution, non-linear object, ≳3 m

images employed is of the order of 100 m for non-linear features. Linear features of smaller width, which includes a few of the roads in the area, were observed in the LANDSAT images.

Skylab images.--The lineament map constructed from Skylab images (Fig. II-B-5) employed 70 mm multiband camera color and color infra-red (IR) film positives (image scale ∿1:3,000,000) photographed during a single pass of the Skylab 3 spacecraft over central Arizona. Although stereoscopic analysis was precluded because the image scenes are identical, this pair of images was analyzed in the Analytical Plotter Coordinatograph (AP/C), a magnifying high-resolution computer-driven photogrammetric plotter at Flagstaff, Arizona. The enlarged viewing and plotting scale of the photogrammetric model was ∿1:200,000. Contrasting information contents of the superimposed IR and color images produced a false stereoscopic effect that allowed useful photogeologic interpretations to be made. Resolution for non-linear features is about 40 m. As in the LANDSAT images, linear features of comparatively small width, which included several roads and an aircraft runway, could be discriminated.

RB-57 images.--A 900 km^2 control area that includes Sedona, Arizona (Fig. II-B-1), was studied in detail. High resolution ($\lesssim$3 m) aircraft color images obtained by the NASA RB-57 aircraft were analyzed stereoscopically in the AP/C plotter. The flight height was approximately 19 km, and the resolution of the 9" x 9" color film positives allowed individual bushes, automobiles, and light aircraft on the ground to be resolved. Vertical resolution in the AP/C plotter was adequate to allow the approximate height of the aircraft to be determined. Late Paleozoic strata crop out extensively in the Sedona area, and joint and fracture systems are, in many places, perfectly exposed. Where bedrock is exposed, individual joints or fractures, and swarms of fractures, were mapped in fine detail at 1:24,000 scale (Fig. II-B-6). Where alluvium conceals

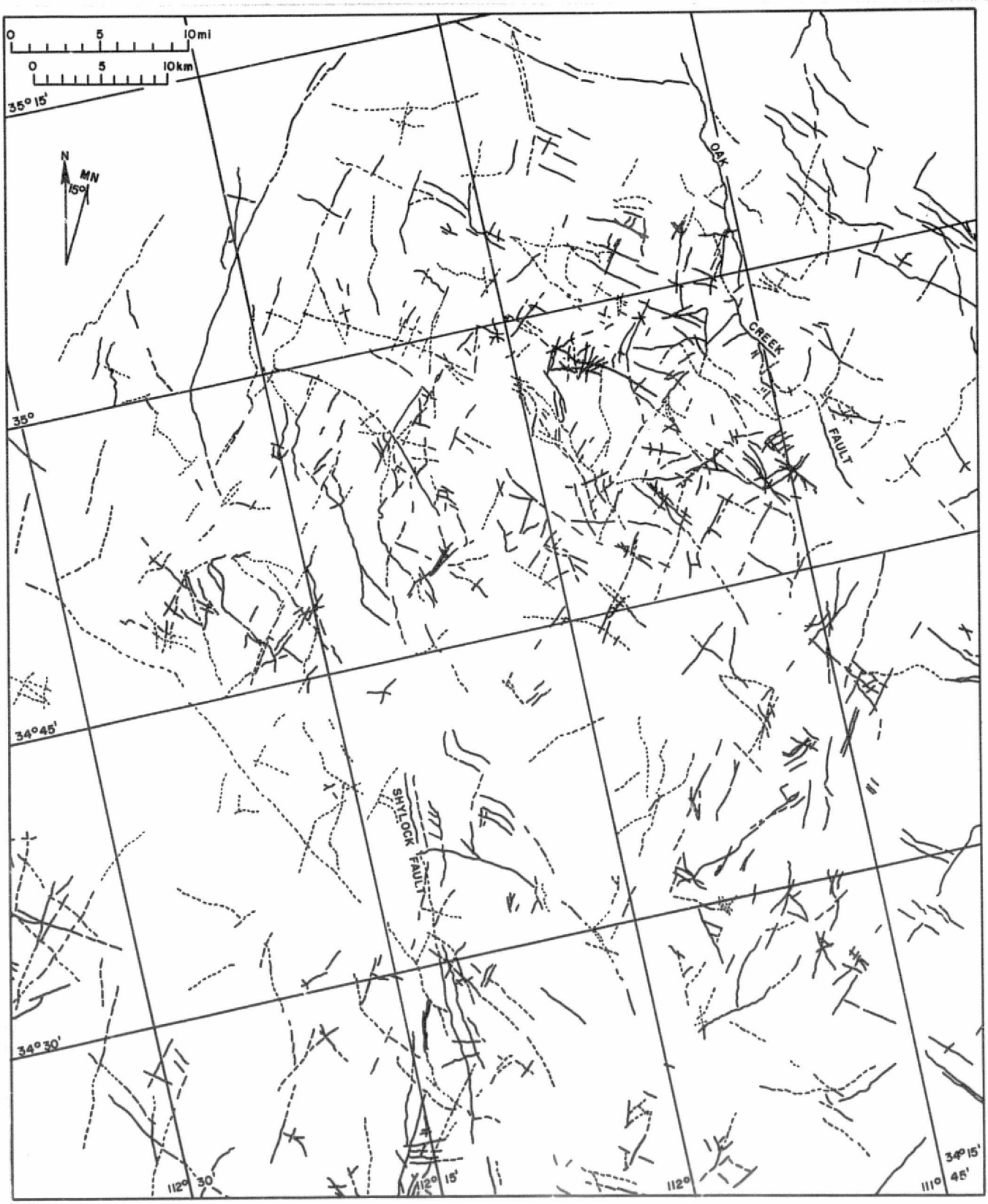

Fig. II-B-5. Lineaments of north-central Arizona mapped from Skylab color images.

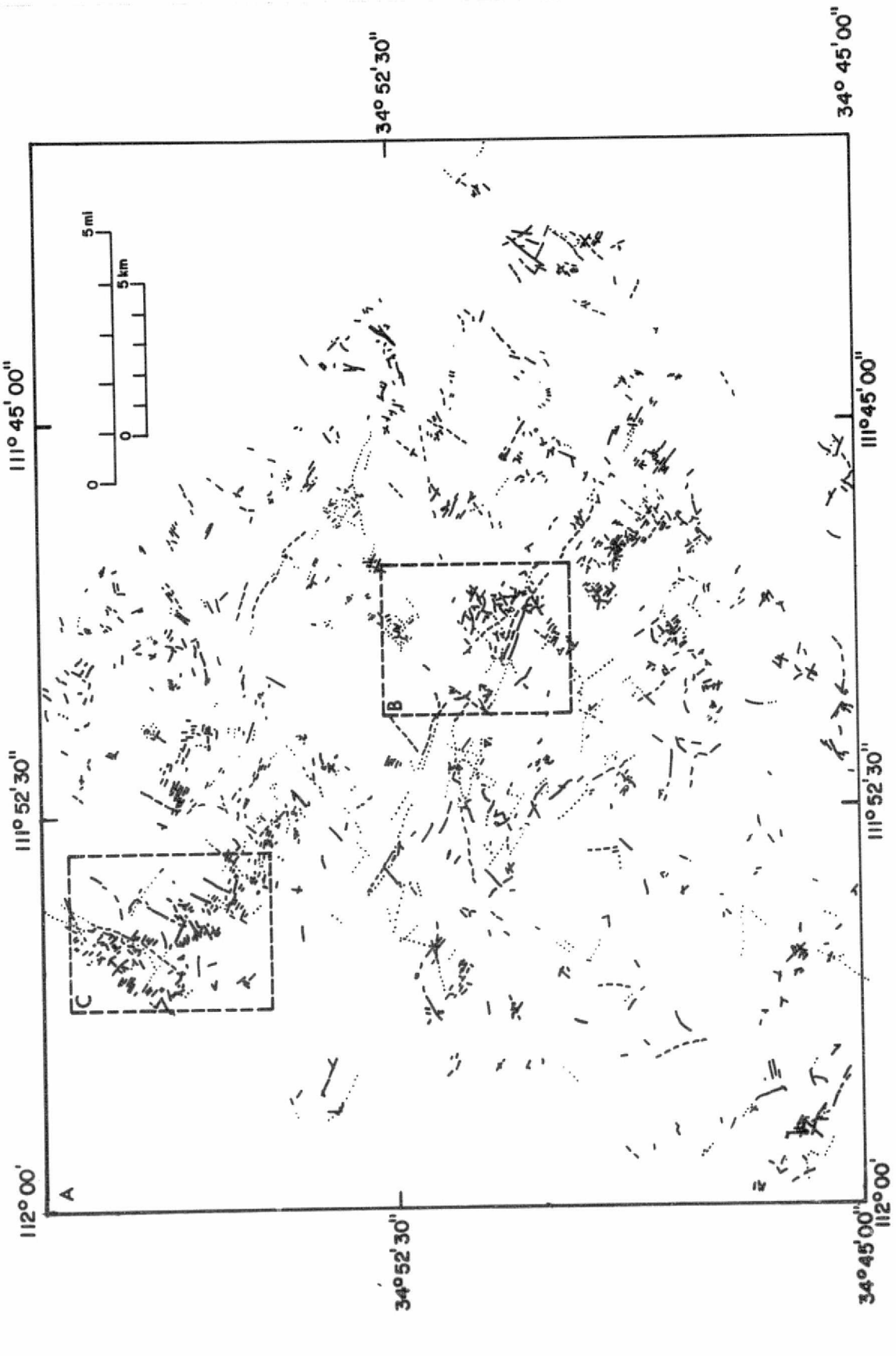

Fig. II-B-6a. Generalized map of fractures and lineaments of the Sedona area, north-central Arizona, mapped from high-altitude aircraft color images. (Details in areas B and C are shown in Figures 6b and 6c.)

the bedrock, extensions of fracture traces were revealed by means of aligned bushes in alluvium and straight-line segments of stream courses. Such elements are classed as lineaments and are shown by dotted lines on the maps (Fig. II-B-6b and II-B-6c); in contrast, the solid and dashed lines represent the discrete, observable (not inferred) traces of individual joints and faults in the bedrock. Details that are shown in Figures II-B-6b and II-B-6c are reproduced here to convey a visual impression as to the detailed, geometrically controlled, character of the mappiong, and the relative distribution of fractures observed in the bedrock and lineaments mapped in the alluvium. The use of the AP/C photogrammetric plotter has allowed the fractures and the lineaments mapped, respectively from RB-57 and Skylab images to be accurately plotted on planimetric bases that meet standards for map accuracy.

Fractures, Lineaments, and Pairsets

Pairsets, and Correlation of Fractures and Lineaments

Azimuthal and frequency data for lineaments and fractures in north-central Arizona derived from maps made from the orbital and aircraft images are summarized in Table II-4. They have been plotted in histogram form in a cartesian system in which the number of lineaments and fractures of a given azimuth are plotted on the vertical axis, and azimuthal directions are plotted for the northwest (270-360°) and northeast (0-90°) quadrants, and the quadrants are stacked so that orthogonal and near-orthogonal lineament pairs, and groupings of pairs, may be visually recognized and compared.

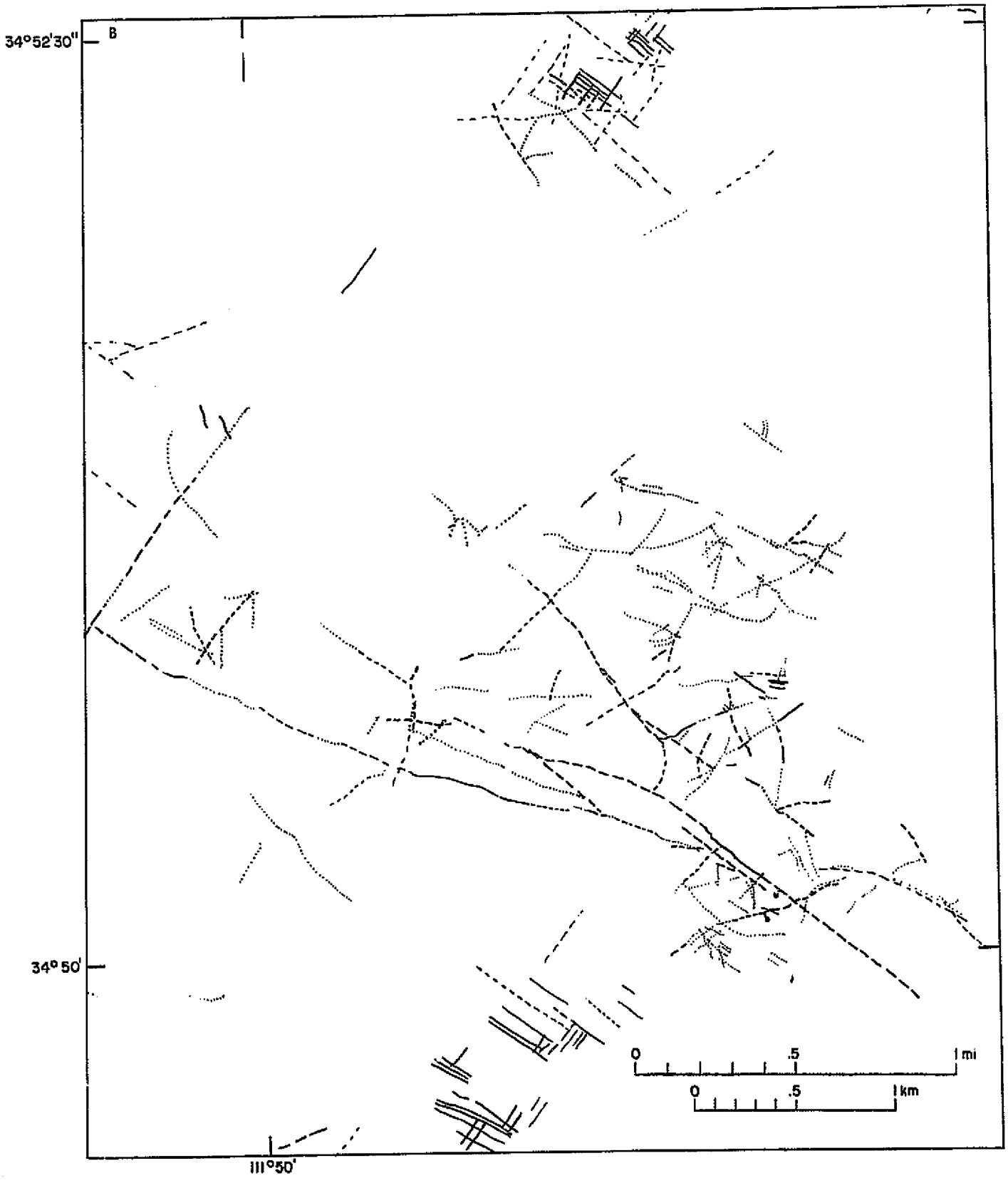

Fig. II-B-6b. Map of fractures and lineaments within the Sedona map area showing details at approximately the scale of mapping.

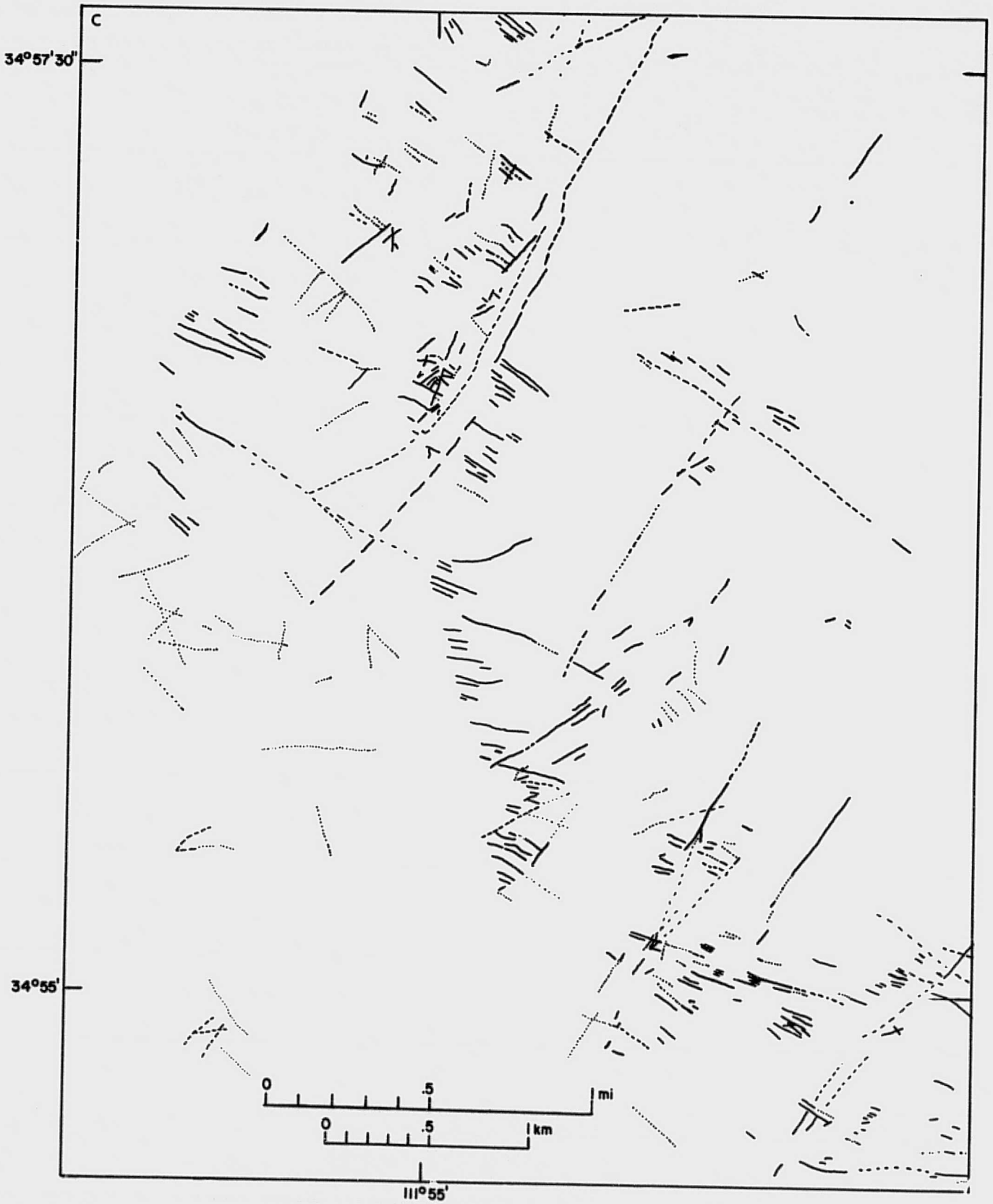

Fig. II-B-6c. Map of fractures and lineaments within the Sedona map area showing details at approximately the scale of mapping.

Table II-4. Azimuthal and frequency distributions of lineaments mapped from LANDSAT, Skylab, and RB-57 images, north-central Arizona

Northwest Quadrant				Northeast Quadrant			
Azimuth	LANDSAT	Skylab	RB-57	Azimuth	LANDSAT	Skylab	RB-57
271				01			
272				02			
273	1		1	03		1	
274				04	3	3	1
275			3	05	5	1	
276			1	06	2	4	1
277		2	7	07	2	5	3
278	2			08	1	4	4
279		4	28	09	6	8	5
280	3	2	18	10	4	8	
281	1	1		11	7	2	6
282	5	3	7	12	5	14	
283	1	1	9	13	7	8	6
284	2	3	13	14	7	6	8
285		3	30	15	5	8	
286	2	3	28	16	3	2	10
287	1	3	17	17	5	11	
288			13	18	2	3	10
289			37	19	5	3	
290		4	13	20	10	10	
291	2	2	28	21	5	7	15
292	2	1	9	22	9	7	1
293		1	3	23	4	13	6
294		2	36	24	11	7	22
295	1	7	47	25	14	12	
296	1	6		26	11	10	
297		6	57	27	9	10	17
298		2		28	10	10	6
299		3		29	1	3	4
300	1	8	79	30	12	15	33
301		2	4	31	10	5	
302	1	7		32	5	6	14
303	1	5	44	33	8	11	20
304	2	2	1	34	12	16	9
305	1	12	80	35	7	16	41
306		7		36	3	41	4
307	1	9	4	37	7	13	44
308		27	163	38	11	10	2
309		18		39	8	7	11
310	1	11	64	40	18	8	30
311		8	36	41	6	5	13
312	1	19	32	42	7	9	9
313	3	7		43	5	12	4
314	1	13	6	44	4	6	15
315	7	9	23	45	13	11	15
316		4	32	46	2	7	13

Table II-4. Continued

Northwest Quadrant				Northeast Quadrant			
Azimuth	LANDSAT	Skylab	RB-57	Azimuth	LANDSAT	Skylab	RB-57
317	1	4	13	47	9	8	12
318		8		48	6	5	17
319	1	11	13	49	4	3	
320	2	12	29	50	17	10	28
321	1	5		51	5	5	13
322	2	16	10	52	2	6	
323	5	8		53	5	8	
324	3	9		54	6	4	9
325	3	17	18	55	11	10	18
326	3	7	13	56	11	3	3
327	8	9	2	57	5	1	6
328	3	9	8	58	4	5	7
329	3	6		59	3	4	5
330	8	16	14	60	7	9	16
331	2	7		61	6	7	4
332	6	6	5	62	6	8	4
333	7	8		63	4	9	2
334	2	8		64	3	8	13
335	8	7	8	65	5	5	
336	9	8		66	8	1	2
337	10	6		67	8	2	17
338	8	5	10	68	3	3	
339	6	8		69	3	4	4
340	14	10		70	10	7	7
341	5	3		71	4	5	13
342	11	11	13	72	2	6	5
343	3	6		73	4	4	12
344	5	6	3	74	3	1	6
345	1	8		75	3	6	
346	3	9		76		6	15
347	3	5		77	1	4	
348	1	3	3	78	4		
349	2	4		79		4	8
350	5	8	5	80	1	2	9
351	2	7		81	1	3	12
352	1	4		82			4
353	3	1	1	83	3		
354		4		84	2		4
355	1	1	4	85	3		6
356		5		86			1
357	1	4		87			
358		3		88			
359				89			
360	67	101	54	90	20	36	102
Totals/quadrant	206	529	1216		475	721	786

Totals for both quadrants: LANDSAT - 681; Skylab - 1250; RB-57 - 2002.

The trend of individual lineaments and fractures for each of the maps were measured to the nearest degree, with mean directions recorded for curved lineaments. The azimuthal-frequency plots (Fig. II-B-7) reveal that a surprisingly large number of lineaments appear to have orthogonal or very nearly orthogonal equivalents. Particularly prominent are lineament-pairs that trend north-south and east-west, and northeast and northwest. Pairs of lineaments that are essentially orthogonal to one another are called pairsets, a term applied by Gay (1972, 1973) to orthogonal pairs of aeromagnetic lineaments. The reason for the orthogonality is not known, but it appears to be a fundamental characteristic of both the fracture and the lineament systems.

A total of 31 possible pairsets occur in the three lineament maps (Fig. II-B-7; Table II-5). Nineteen occur in the Landsat Map, 21 occur in the Skylab map, and 22 occur in the detailed map of the Sedona area. Of these, 19 moderately to very strongly developed pairsets, and two pairset groups, appear to be common to all three maps. The individual pairsets are orthogonal to 1° and the pairset groups are orthogonal within a range of 3-4°.

The existence of the seemingly closely correlated orthogonal pairsets derived from the three analyses may not be accidental. The orthogonal pairsets for the Sedona area are clearly defined (Fig. II-B-7), so much so that several pairsets containing comparatively large populations of fractures and lineaments are separated from other pairsets by virtual hiatuses in the frequency distributions. The orthogonal pairsets of the Sedona area reflect the existence of populations of orthogonal fractures in the bedrock. The occurrence of the same pairsets derived from orbital images of a larger area of north-central Arizona indicates that the principal fracture systems of a region can be obtained by mapping lineaments from synoptic images.

Fig. II-B-7. Histograms of lineaments and fractures mapped from orbital and aircraft images, arranged orthogonally to reveal pairsets.

Table II-5. Principal and subordinate lineament and fracture pairsets, and pairset groups, mapped from orbital and aircraft images, north-central Arizona

Pairset Identification No.[1]	Pairsets: Lineaments LANDSAT	Pairsets: Lineaments Skylab	Pairsets: Fractures and Lineaments RB-57	Correlated pairsets and pairset groups	Classification[2]	
1.*	270/360	270/360	270/360	270/360	p	G
2.*	- /4-7	277/7	277/6-7	277/7	s	(Shylock)
3.*	280/9	279-280/9-10	279-280/8-9	279/9	s	
4.	282/11	282/12	-			
5.*	284/13-14	285/15	285/13-14	284-286/14-16	g	g
	286-287/17	287/17	286/16		p	
			289/18(?)			
6.*	291-292/20	290/20	291/21	290-291/20-21		g
	291-292/22					
7.*	295-296/24-26	295/25	294-295/24	295/25	s	
8.*	- /28	296-297/26-28	297/27	297/27	s	
9.*	300/30	300/30	300/30	300/30	p	
10.*	304/34	302/-	302/32-33	303/33	s	
11.*		305/35-36	305/35	305/35	s	G
12.*	307/37-38	308/37-38?	308/37	308/38	s	(Mazatzal)
13.*	310/40	310?/40	310/40	310/40	p	
14.	312-313/42	312/42-43	312/-	-		
15.*	315/45	314-315/45	315-316/44-45	315/45	s	
16.	317/47	- /47	/48	-		
17.*	320/50	320/50	320/50	320/50	p	
18.	323/-	322/52-53	322/-	-		
19.*	- /55-56	325/55	325/55	325/55	p	G
20.*	327/-	327-328/58	328/58	328/58	s	(Chaparral)
21.*	330/60	330/60	330/60	330/60	p	
22.	332-333/61-62	333-334/63	332/-	-		

Table II-5. Continued

Pairset Identification No.[1]	Pairsets: Lineaments LANDSAT	Pairsets: Lineaments Skylab	Pairsets: Fractures and Lineaments RB-57	Correlated pairsets and pairset groups	Classification[2]	
23.†	336-337/66-67	336/-	335/64	335-338/64-67		g
24.†			338/67			
25.	340/70	340/70	342/71 ?	340-344/70-73	s	g
26.†	342/-	342/72				
27.†	344/73	-	344/73			
28.	346-347/-	345-346/75-76	- /76	-		
29.*	350/80-81	350-351/79-81	350/79-81	350/79-81	s	
30.	353/83	354?/-	353/-	-		
31.*	355/85	356?/-	355/85	355/85	s	

Totals:			
	19 pairsets	21 pairsets	22 pairsets
	19 orthogonal	19 orthogonal	13 orthogonal
		2 orthogonal to 1°	9 orthogonal to 1°

Of the 31 pairsets identified, 19 are correlated in the three images, and they are orthogonal or orthogonal to 1°. Two pairset groups that contain principal pairsets are included in the 19 correlated pairsets (Nos. 5 and 6). Two additional pairset groups, without principal pairsets, also are recognized (Nos. 23-24 and 25-27), bring to 21 the number of correlated pairsets and pairset groups.

In the overall population, three principal pairset groups (G) are recognized. They include the dominant lineaments and fractures of the region whose trends correspond with the trends of mapped Precambrian faults and fault systems, after which they are named.

Table II-5. Continued

[1/] See Figure 7. * - pairsets common to the three analyses. Includes pairsets not completely represented in northwest (down-sun) quadrant of Landsat images and presumed lost as a consequence of low-resolution and down-sun washing out of detail. Of 19 pairsets, 14 are completely represented in the three images.
† - pairset group that does not contain a principal pairset.

[2/] p - principal pairset; three complete pairsets in the three images.
s - subordinate pairset; 2.5, and in one case 2.0, pairsets from the three analyses.
g - subordinate pairset group; cluster of pairsets or nearly orthogonal pairsets whose azimuthal distributions form a population cluster.
G - principal pairset group; a grouping of principal and subordinate pairsets defined from frequency distributions (Figure 7) and from azimuthal relationships to early structural episodes.

Comparison of results from Landsat and Skylab images reveals, not unexpectedly, that the higher the resolution of the synoptic image, the better the map product. On the basis of the total number of lineaments and fractures mapped for each of the scenes (Table II-4), the Skylab images are about one-half as "efficient", and the Landsat images only one-third as "efficient" as the aircraft images. Nonetheless, the basic lineament-fracture pattern emerges in both types of orbital images, although much more clearly in the Skylab images. Subsequent to the foregoing study, we examined Skylab-4 images of the Sedona area that were taken with a long focal length camera (S190B; focal length 457 mm). These show greater resolution (10 m) than the S190A, short focal length Skylab-3 images used in this study. The mapping "efficiency" of the long focal length images approaches that of the RB-57 aircraft images.

Effects of illumination.--When viewed with the eye, an image scene that lies in a directly down-sun direction lacks strong contrast, presumably because of a subordination of shadows, and the scene is marked by a "bright-spot" and loss of information. Such a "bright-spot" effect is routinely expected when viewing terrane in a down-sun direction from an aircraft, and also should affect resolution in the down-sun directions of photographic image scenes. Such is suggested when frequency data for lineaments are compare for the Landsat, Skylab, and RB-57 maps (Table II-4, Figure II-B-7). (Particulars concerning the illumination are summarized in Table II-3.) The Landsat and Skylab images were acquired in the morning, some two to four hours before the RB-57 images, which were acquired just before noon. Sun elevations for the orbital images were 17-25° lower than in the aircraft images. The down-sun directions are shown on the histogram plots (Fig. II-B-7), as are the scan line directions for the Landsat images. A marked deficiency in resolved lineaments exists in the northwest quadrants of both the LANDSAT and Skylab images with respect to the RB-57 images, particularly near the

down-sun directions. The effect is so pronounced in the LANDSAT images that a substantial part of the northwest quadrant is of doubtful utility. LANDSAT images thus cannot be recommended for the unbiased discrimination of linear elements. The RB-57 data can be considered as baseline data because photographic resolution was adequate to resolve individual north-trending fractures that could exhibit only a minimum shadow development in the near-noon, high-sun conditions, yet the strong frequency peak for north-trending fractures exists for the detailed map of the Sedona area as well as for the regional maps.

Stratigraphic and synoptic image filtering.--The trends of the strongly developed north- and northeast-trending lineaments correlate with the trends of major faults in the basement. These lineaments occur even in areas where very young strata blanket the basement. In contrast, northwest-trending faults in the basement are comparatively discontinuous, as are individual northwest-trending faults in overlying Phanerozoic strata. Apparently, even small structural adjustments on through-going faults in the basement result in the development of long but subtle linear elements in overlying strata--elements which apparently consist of both joints and small faults. These subtle linears, seen best in synoptic images, reflect the existence of otherwise concealed structural discontinuities in the basement. Whereas through-going linear elements in the basement appear to be revealed in the synoptic images, non-through-going linear elements appear to be subordinated. Few long northwest-trending linears are recognized in the orbital images, even in Precambrian terrain, and the locations of known northwest-trending faults in Phanerozoic strata need to be located on the synoptic images principally by means of existing geologic maps rather than by the traces of linears. Such a relationship between through-going and non-through-going basement faults, and faults, joints, linears in overlying strata,

may serve to at least partly explain the different frequency distributions of northwest- and northeast-trending lineaments and fractures mapped from the orbital and the aircraft images. The northwest-trending fractures in Paleozoic strata mapped in the Sedona area from aircraft images are very abundant, whereas the northeast-trending fractures have frequencies similar to frequencies of lineaments mapped from the orbital images (see Table II-5 and Figure II-B-7). The marked abundance differences for the northwest quadrants cannot be adequately accounted for by a down-sun washing-out of linear elements in the orbital images. Rather, some other effect is required, one that might be called stratigraphic and synoptic image filtering. Stated simply, linear elements above through-going breaks in the basement are propagated in even very young strata presumably because the through-going breaks are susceptible to responding to and undergoing even minor structural adjustments, and such long linear elements are preferentially resolved in the synoptic images. In contrast, the abundant northwest-trending fractures mapped in detail in Paleozoic strata in the Sedona area, although they reflect comparatively recent Tertiary structural adjustments, are mostly of limited lateral extent, with the result that most are not detected in the orbital images. Our studies suggest that comparatively high resolution synoptic images provide an overview that allows the longer linear elements of the crust to be identified. It is an overview not duplicated by the mosaicking of low altitude, high resolution aerial photographs of variable illumination and contrast.

Faults, lineaments, and linear aeromagnetic discontinuities.--Faults of the region and lineament pairs common to the LANDSAT and Skylab images have been compiled, and they are shown superimposed on a part of the aeromagnetic map of Arizona (Sauck and Sumner, 1971; Fig. II-B-8). A map that shows only faults would have been adequate to reveal a correlation with the principal aeromagnetic

discontinuities. The Shylock, Pine Mountain, and part of the Oak Creek fault zones coincide in part with linear aeromagnetic discontinuities. In contrast, the Chaparral fault zone appears to transect the aeromagnetic structure. An arresting discontinuity is seen in the aeromagnetic low west of the Shylock fault zone, which coincides with Chino Valley, and an aeromagnetic low that lies well to the south on the east side of the Shylock. The discontinuity appears to mirror the right-lateral displacement of the Shylock. The southern margin of the aeromagnetic low is bounded by the inferred southwestward extension of the Pine Mountain fault zone, wouth of which is an aeromagnetic high. The high resembles the aeromagnetic high west of the Shylock in the Bradshaw Mountains to the north, and near the Chaparral fault zone still farther to the north. Except for this very large aeromagnetic feature, and for aeromagnetic discontinuities associated with the Oak Creek and Pine Mountain faults, detailed correlations between faults and aeromagnetic discontinuities appear ambiguous. The ambiguity extends to the principal lineaments of the region which do not appear to correlate in detail with linear elements that might be drawn from the aeromagnetic map (Fig. II-B-8).

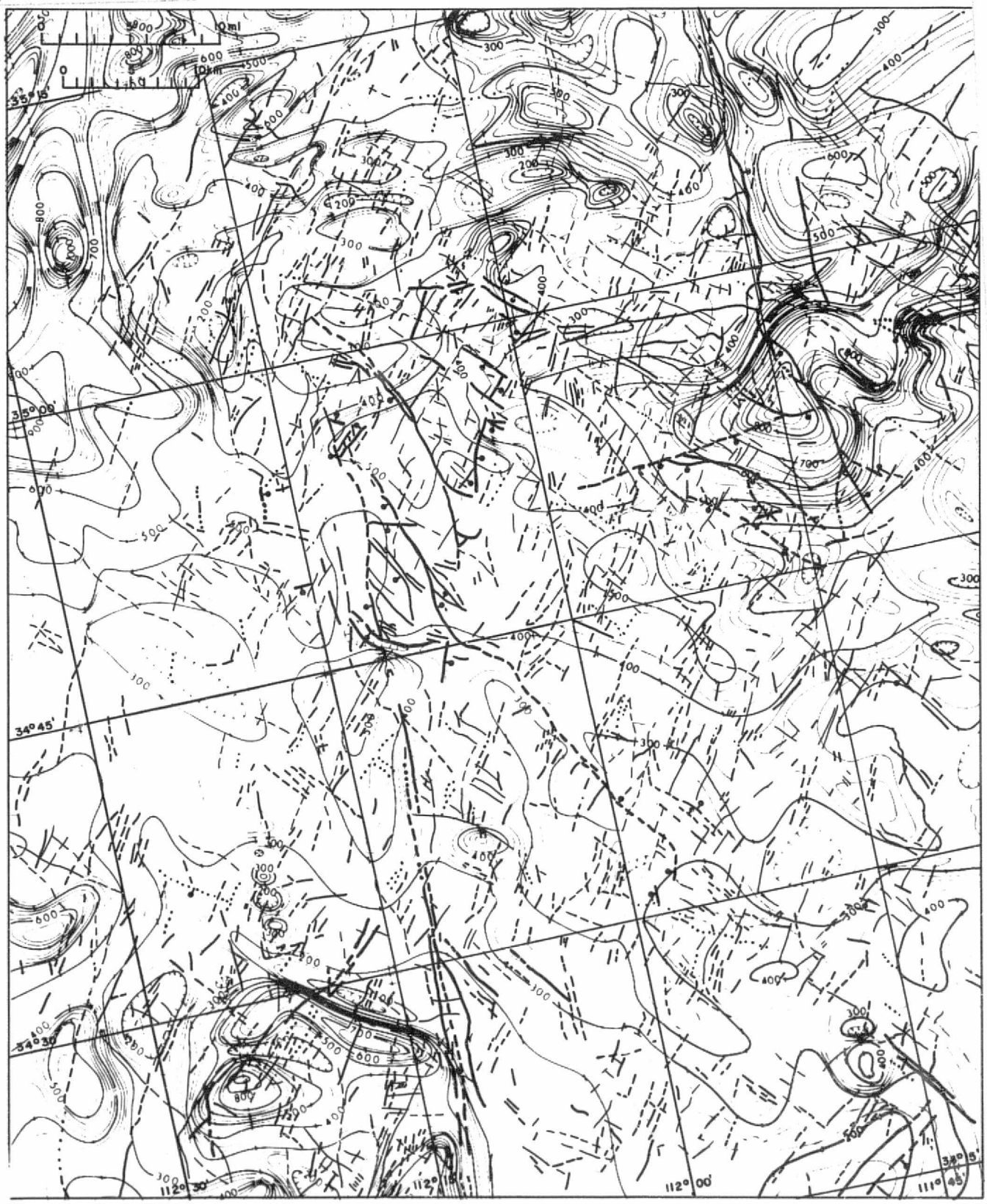

Fig. II-B-8. Principal faults and lineaments superimposed on aeromagnetic map of north-central Arizona.

4. SUMMARY

Several, perhaps as many as nineteen orthogonal pairsets of faults and lineaments are recognized in north-central Arizona. A number of the pairsets cluster in three major pairset groups (355-360° - 85-90°, "Shylock"; 30-40° = 300-310°, "Mazatzal"; and 50-60° - 320-330°, "Chaparral-Pine Mountain") whose trends coincide with the trends of major Precambrian faults in central and northern Arizona. Groups of lineament pairsets are named for the oldest fault zones in which their trends are identified.

Several structural episodes, perhaps as many as seven, have been responsible for the complex patterns of faults, joints, and lineaments that have been mapped from synoptic orbital and aircraft images in both Precambrian and Phanerozoic terrane of central Arizona. Detailed mapping of lineaments and fractures in north-central Arizona has revealed that the strongly developed lineaments accurately reflect important through-going fracture systems in the bedrock. Analysis of lineament maps has provided an azimuthal-frequency framework for evaluating fracture system trends that are related to different structural episodes. Identification of fracture and lineament trends for three early structural episodes suggests that discrete series of fractures were successively impressed on the Precambrian terrane, and that these breaks served to localize subsequent structural adjustment.

REFERENCES

Anderson, C. A., and Creasey, S. C., 1958, Geology and ore deposits of the Jerome area, Yavapai County, Arizona: U.S. Geol. Survey Prof. Paper 308, 185 p.

Anderson, C. A., 1967, Precambrian wrench fault in Central Arizona: U.S. Geol. Survey Prof. Paper 575C, p. C60-C65.

Anderson, C. A., and Creasey, S. C., 1967, Geologic map of the Mingus Mountain quadrangle, Yavapai County, Arizona: U.S. Geol. Survey Map GQ-715 (1:62,500 scale).

Anderson, C. A., Blacet, P. M., Silver, L. T., and Stern, T. W., 1971, Revision of Precambrian stratigraphy in the Prescott-Jerome area, Yavapai County, Arizona: U.S. Geol. Survey Bull. 1324-C, p. C1-C16.

Anderson, C. A., 1972, Precambrian rocks in the Cordes Area, Yavapai County, Arizona: U.S. Geol. Survey Bull. 1345, 36 p.

Anderson, C. A., and Blacet, P. M., 1972, Geologic map of the Mayer Quadrangle, Yavapai County, Arizona: U.S. Geol. Survey Map GQ-996. (1:62,500 scale).

Anderson, C. A., and Blacet, P. M., 1972a, Geologic map of the NE 1/4 Mount Union quadrangle, Yavapai County, Arizona; and 1972b, Precambrian geology of the Northern Bradshaw Mountains, Yavapai County, Arizona: U.S. Geol. Survey Bull. 1336, 82 p. (1:24,000 scale).

Canney, F. C., Lehmbeck, W. L., and Williams, Frank E., 1967, Mineral resources of the Pine Mountain Primitive Area, Arizona: U.S. Geol. Survey Bull. 1230-J, 45 p.

Cooley, M. E., and others, 1967, Arizona Highway Geologic Map: Geologic map, explanation, and geologic history of Arizona: Ariz. Geol. Soc. (1:1,000,000 scale).

Damon, P. E., Livingston, D. E., and Erickson, R. C., 1962, New K-Ar dates for the Precambrian of Pinal, Gila, Yavapai, and Coconino Counties, Arizona, in Guidebook of the Mogollon Rim region, east-central Arizona, New Mexico Geol. Soc., 13th Field Conf., Socorro, New Mexico, p. 56-57.

Damon, P. E., Shafigullah, M., and Leventhal, J. W., 1974, K-Ar chronology for the San Francisco volcanic field and rate of erosion of the Little Colorado River.

Elston, Donald P., McKee, E. H., Scott, G. Robert, and Gray, G. Dale, 1974, Miocene-Pliocene volcanism in the Hackberry Mountain area and evolution of the Verde Valley, north-central Arizona, in Geology of northern Arizona with Notes of Archaeology and Paleoclimate, Pt. II - Area Studies and Field Guides: Geol. Soc. of America Rocky Mountain Section Meeting, Flagstaff, Ariz., p. 602-610.

Elston, Donald P., and Grommé, C. Sherman, 197_, Precambrian polar wandering from Unkar Group and Nankoweap Formation of Grand Canyon Supergroup, Arizona: Correlation with central Arizona Precambrian and Laurentian polar wandering path (to be submitted to Precambrian Research for publication).

Elston, D. P., and Scott, G. R., 197_, Geologic and paleomagnetic evidence of a hiatus at the Cardenas-Nanioweap contact (Precambrian) Grand Canyon Supergroup, northern Arizona: (Submitted to Geol. Soc. America for bulletin publication).

Ford, T. D., and Breed, W. J., 1973, Late Precambrian Chuar Group, Grand Canyon, Arizona: Geol. Soc. America Bull., v. 84, p. 1243-1260.

Gay, S. Parker, Jr., 1972, Aeromagnetic lineaments, their geological significance and their significance to geology: The New Basement Tectonics, American Stereo Map Co., Salt Lake City, 94 p.

Gay, S. Parker, Jr., 1973, Pervasive Orthogonal fracturing in earth's continental crust: A closer look at "The New Basement Tectonics:" American Stereo Map Co., Salt Lake City, 121 p.

Glossary of Geology and Related Sciences, 1957, The American Geological Institute, Wash., D.C., p. 169, lineament: "These significant lines of landscapes which reveal the hidden architecture of the rock basement are described as lineaments." They are character lines of the earth's physiognomy." (Hobbs, W. H., Earth Features, etc., p. 227, 1912).

Glossary of Geology, 1972, Margaret Gary, Robert McAfee, Jr., and Carol L. Wolf, eds., American Geological Institute, Wash., D.S., p. 408.

Hamblin, W. K., 1965, Origin of "Reverse Drag" on the downthrown side of normal faults: Geol. Soc. America Bull., v. 76, no. 10, p. 1145-1164.

Helsley, Charles E., and Spall, Henry, 1972, Paleomagnetism of 1140 to 1150 million-year diabase sills from Gila County, Arizona: Jour. Geophys. Research, v. 77, no. 11, p. 2115-2128.

Hoppin, R. A., 1974, Lineaments: their role in tectonics of Central Rocky Mountains: AAPG Bull. (Part I of II), v. 58, no. 11, p. 2260-2273.

Huff, Lyman C., Santos, Elmer, Raabe, R. G., 1966, Mineral resources of the Sycamore Canyon Primitive area, Arizona: U.S. Geol. Survey Bull. 1230-F 19 p.

Huntoon, Peter W., and Sears, James W., 1975, Bright Angel and Eminence Faults, Eastern Grand Canyon, Arizona: Geol. Soc. Amer. Bull., v. 86, no. 4, p. 465-472.

Krieger, Medora H., 1965, Geology of the Prescott and Paulden Quadrangles, Arizona: U.S. Geol. Survey Prof. Paper 467, 127 p.

_____ 1967, Reconnaissance geologic map of the Ash Fork quadrangle. Yavapai and Coconino Counties, Arizona: U.S. Geol. Survey Map I-499 (1:62,500 scale).

Krieger, M. H., Creasey, S. C., and Marvin, R. F., 1971, Ages of some Tertiary andesitic and latitic volcanic rocks in the Prescott-Jerome area, north-central Arizona: U.S. Geol. Survey Prof. Paper 750-B, p. B157-B160.

Lehner, R. E., 1958, Geology of the Clarkdale Quadrangle, Arizona: U.S. Geol. Survey Bull. 1021-N, p. 511-592 (Pl. 45, geologic map, 1:48,000 scale).

Lindberg, Paul A., and Jacobson, H. S., 1974, Economic geology and field guide of the Jerome district, Arizona, in Geology of Northern Arizona with Notes on Archaeology and Paleoclimate, Pt. II - Area Studies and Field Guides: Geol. Soc. Amer. Rocky Mountain Section Meeting, Flagstaff, Ariz., p. 794-804.

Livingston, Donald E., and Damon, Paul E., 1968, The ages of stratified Precambrian rock sequences in central Arizona and northern Sonora: Canadian Jour. Earth Sciences, v. 5, no. 3, p. 763-772.

Lucchitta, Ivo, 1974, Structural evolution of northwest Arizona and its relation to adjacent Basin and Range Provice Structures, in Geology of Northern Arizona with Notes on Archaeology and Paleoclimate, Pt. I - Regional Studies: Geol. Soc. Amer. Rocky Mountain Section Meeting, Flagstaff, Ariz., p. 336-354.

Ludwig, Kenneth Raymond, 1974, Precambrian geology of the central Mazatzal Mountains, Arizona, Pt. I: Ph.D. thesis, California Institute of Technology, Pasadena, 218 p.

Maxson, J. H., and Campbell, Ian, 1934, Faulting in the Bright Angel quadrangle, Arizona (Abs.): Geol. Soc. America Proc., 1933, p. 301.

Maxson, J. H., 1961, Geologic history of the Bright Angel quadrangle in Geologic map of the Bright Angel quadrangle: Grand Canyon Natural History Assoc. (3rd ed., rev., 1968).

Maxson, J. H., 1967, Preliminary geologic map of the Grand Canyon and vicinity, Arizona, Eastern section: Grand Canyon Natural History Assoc. (62:500 scale).

Maxson, John H., 1969, Preliminary geologic map of the Grand Canyon and vicinity, Arizona, western and central sections: Grand Canyon Natural History Assoc. (62,500 scale).

McKee, E. H., and Anderson, C. A., 1971, Age and chemistry of Tertiary volcanic rocks in north-central Arizona and relation of the rocks to the Colorado Plateau: Geol. Soc. America Bull., v. 82, p. 2767-2782.

McKee, E. D., and McKee, E. H., 1972, Pliocene uplift of the Grand Canyon region Time of drainage adjustment: Geol. Soc. America Bull., v. 83, no. 7, p. 1923-1932.

McKee, Edwin H., and Noble, Donald C., 1974, Rb-Sr age of the Cardenas Lavas, Grand Canyon, Arizona, in Geology of northern Arizona with Notes on Archaeology and Paleoclimate, Pt. I - Regional Studies: Geol. Soc. America Rocky Mountain Section Meeting, Flagstaff, Ariz., p. 87-96. (Submitted for publication in Precambrian Research.)

Mears, Brainerd, Jr., 1948, Cenozoic faults, gravels, and volcanics of Oak Creek Canyon, Arizona: Ph.D. thesis submitted to Dept. of Geology, Colombia University, New York, 84 p.

Mears, Brainerd, Jr., 1950, Faulting in Oak Creek Canyon and a discussion of contrary bending: Plateau, v. 23, no. 2, p. 26-31.

Moore, Richard T., Wilson, Eldred D., and O'Haire, Robert T., 1960, Geologic map of Coconino County, Arizona: Ariz. Bureau of Mines and Univ. of Ariz., Tucson (1:375,000 scale).

Noble, L. F., 1914, The Sinumo Quadrangle: Grand Canyon District, Arizona: U.S. Geol. Survey Bull. 549, 100 p.

Pasteels, Paul, and Silver, Leon T., 1965, Geochronologic investigations in the crystalline rocks of the Grand Canyon, Arizona (Abs.): Geol. Soc. America Special Paper 87, Abstracts for 1965, p. 124.

Poole, F. G., 1974, Flysch deposits of Antler Foreland Basin, western United States, in Dickinson, William R., ed., Tectonics and Sedimentation, Soc. of Economic Paleontologists and Mineralogists Special Pub. No. 22, p. 58-82.

Ragan, Donal M., 1968, Structural geology: An introduction to Geometrical Techniques: John Wiley & Sons, Inc., 166 p.

_____ 1973, Structural geology: An introduction to Geometrical Techniques: John Wiley & Sons, 208 p. (2nd ed.).

Ransome, F. L., 1903, Geology of the Globe copper district, Arizona: U.S. Geol. Survey Prof. Paper 12.

Sauck, W. A., and Sumner, J. S., 1971, Residual aeromagnetic map of Arizona: Univ. of Arizona, Tucson.

Scott, G. Robert, and Elston, Donald P., 1974, Generalized geologic map of Hackberry Mountain area, central Arizona, in Scott, Gary Robert, 1974, Geology, Petrology, SR-isotopes and paleomagnetism of the Thirteenmile Rock volcanics, central Arizona: M.S. thesis, University of Texas as Dallas.

Sears, J. W., 1973, Structural geology of the Precambrian Grand Canyon Series, Arizona: Univ. of Wyoming M.S. thesis, 100 p.

Shoemaker, E. M., Squires, R. L., and Abrams, M. J., 1974, The Bright Angel and Mesa Butte Fault Systems of northern Arizona, in Geology of Northern Arizona with Notes on Archaeology and Paleoclimate, Pt. I - Regional Studies: Geol. Soc. America Rocky Mountain Section Meeting, Flagstaff, Arizona, p. 355-391.

Silver, Leon T., 1963, The use of Cogenetic uranium-lead isotope systems in zircons in geochronology, in Proceedings of the Symposium on Radioactive dating, Athens, 1962: International Atomic Energy Agency, Vienna, p. 279-287.

Silver, L. T., 1964, Mazatzal orogeny and tectonic episodicity (abs.): Geol. Soc. America Spec. Paper 82, p. 185.

in Guidebook of the Black Mesa basin, northeastern Arizona: New Mexico Geol. Soc., 9th Field Conf., p. 186-190.

Stewart, John H., 1974, Correlation of uppermost Precambrian and lower Cambrian strata from southern to east-central Nevada: U.S. Geol. Survey Jour. Research, v. 2, no. 5, p. 609-618.

Stewart, J. H., and Poole, F. G., 1974, Lower Paleozoic and uppermost Precambrian Cordilleran Miogeocline, Great Basin, Western United States, in Dickinson, William R., ed., Tectonics and Sedimentation, Soc. of Economic Paleontologists and Mineralogists Spec. Pub. No. 22, Tulsa, Okla., p. 28-57.

Twenter, F. R., and Metzger, D. G., 1963, Geology and groundwater in Verde Valley--The Mogollon Rim region, Arizona: U.S. Geol. Survey Bull. 1177, 132 p.

Van Gundy, C. E., 1951, Nankoweap Group of the Grand Canyon Algonkian, of Arizona: Bull Geol. Soc. America, v. 62, no. 8, p. 953-959.

Wilson, E. D., 1939, Pre-Cambrian Mazatzal Revolution in Central Arizona: Bull. Geol. Soc. Am., v. 50, p. 1113-1164.

Wilson, E. D., and Moore, R. T., 1958, Geologic map of the Yavapai County, Arizona: Ariz. Bureau of Mines and Univ. of Ariz., Tucson (1:375,000 scale).

Wilson, Eldred D., Moore, Richard T., and Cooper, John R., 1969, Geologic map of Arizona: Ariz. Bureau of Mines and U.S. Geol. Survey (1:500,000 scale).

II-C. Coconino Plateau

M. J. Abrams and B. S. Siegal

1. INTRODUCTION

Within the past few years, considerable interest has developed in determining the feasibility of using satellite data for geologic mapping. Satellites not only provide synoptic, large-scale, planimetric views, but also provide spectral information about the earth's surface. Now, with the ready availability of various types of satellite data, it has become necessary to determine which type of satellite data and what spectral regions are best suited for geologic mapping in various terrains.

This section compares the usefulness of both SKYLAB and LANDSAT digital data and SKYLAB photographs for geologic mapping in the Coconino Plateau, Arizona.

2. REGIONAL DESCRIPTION

The Coconino Plateau (Fig. II-C-1) lies in north-central Arizona, within the southwestern part of the Colorado Plateau province. The regional slope of the land surface on the Coconino Plateau is to the south. Extensive grasslands form the central plains of the Coconino Plateau. These plains have an average elevation of about 1900 m. Cataract Creek, the principal drainage of the Coconino Plateau, is the major physiographic feature in the plains. The Mt. Floyd volcanic field lies to the south of the plains; it is covered primarily by juniper and pinon pine forests. The average elevation of the northern escarpment of the Mt. Floyd volcanic field is about 1850 m.

A semi-arid climate characterizes the plains area, with an average annual precipitation of about 25 cm. Half of this precipitation falls in summer thunderstorms, and the other half falls as snow during regional storms in the winter.

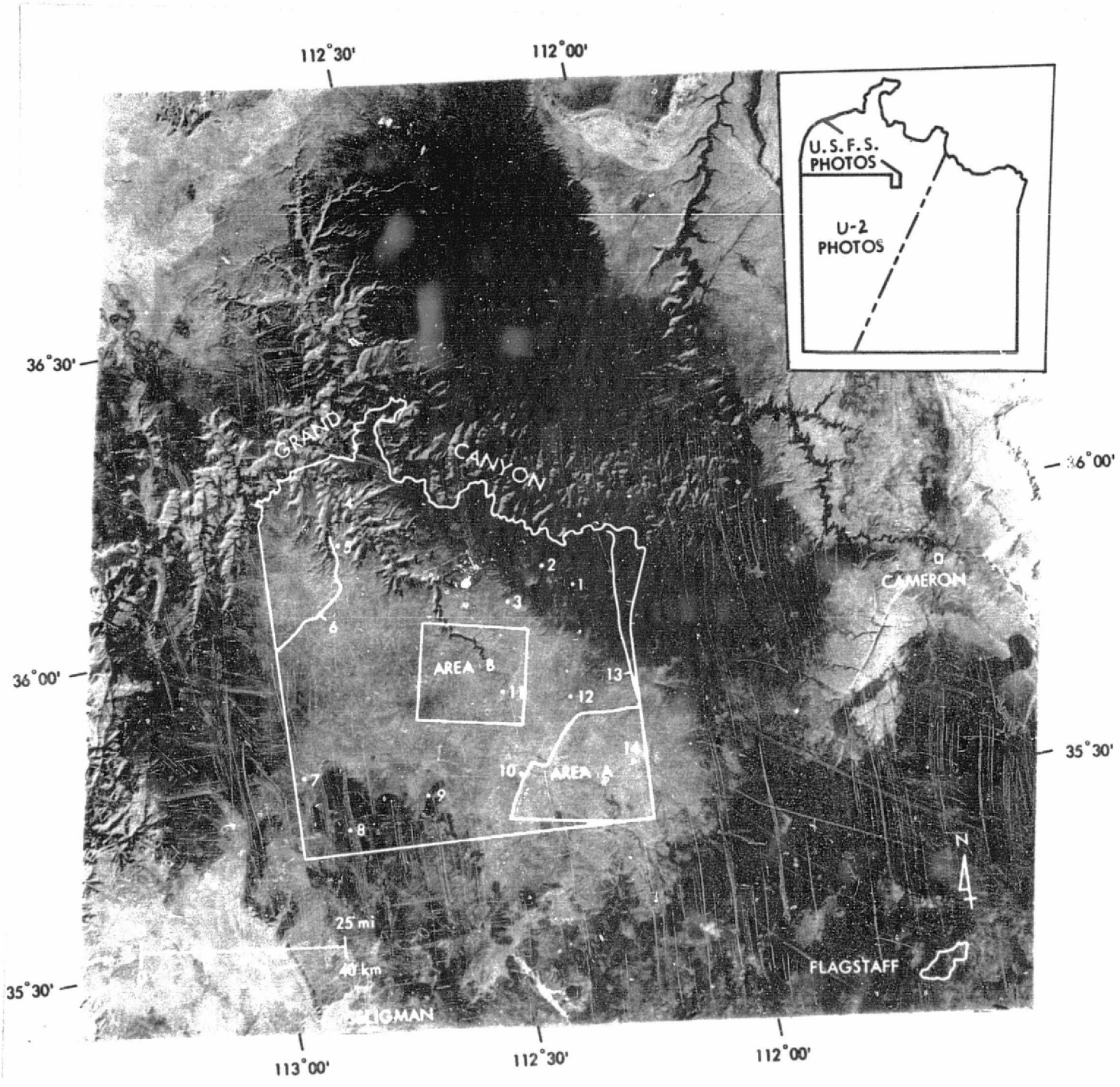

Fig. II-C-1. LANDSAT picture of Coconino Plateau, showing outline of study areas A and B and high altitude U.S. Forest Service photo coverage.

a. Stratigraphy

The Coconino Plateau is underlain primarily by flat-lying to gently dipping sedimentary rocks of Paleozoic age. These rocks, about 1200 m thick, consist of an alternating sequence of sandstone, shale, and limestone. The older Palezoic rocks are exposed chiefly in the Grand Canyon and in side canyons tributary to the Grand Canyon.

Most of the Coconino Plateau is a stripped surface formed on the Kaibab Formation of middle Permain age. Locally, the Kaibab Formation is overlain by the Moenkopi Formation of Triassic age. At the southern edge of the Plateau, sediments and volcanic rocks of Tertiary and Quaternary age overlie the Kaibab and Moenkopi Formations. A generalized stratigraphic section of the rock units on the Coconino Plateau is shown in Fig. II-C-2.

The Kaibab Formation is subdivided into the Beta Member at the base and the Alpha Member at the top. The contact between the Alpha and Beta Members, as shown in Fig. II-C-2, is at the base of the lowermost redbed in the Kaibab Formation. This contact differs slightly from that of McKee (1936) and is about 15 m above his contact.

Within the Coconino Plateau, the Alpha Member contains six mappable units: three red claystone, siltstone, and sandstone units (units 1, 3, and 5), which alternate with three relatively unfossiliferous dolomite (see Fig. II-C-2) units (2, 4, and 6). Unit 1 is the basal unit of the Alpha Member. Locally, gypsum deposits occur within the clastic units, and nodular chert generally occurs within carbonate units 4 and 6. The upper parts of the Alpha Member (units 5 and 6) have been eroded away in places. Where the complete section is present, the Alpha Member typically ranges in thickness from 33 to 40 m. Locally, however, the total thickness may be 50 m where gypsum deposits thicken within one or more of the clastic units.

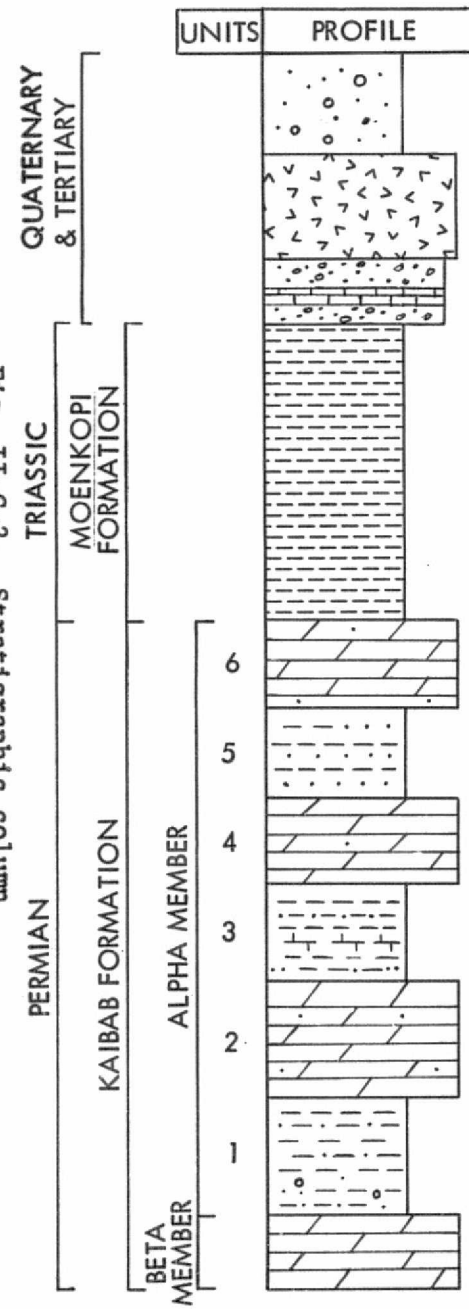

UNITS	GENERAL LITHOLOGY & THICKNESS	WEATHERED COLOR
	STREAM ALLUVIUM, GRAVELS, LOESS. VARIABLE THICKNESS	RED TO TAN DEPENDING UPON SOURCE
	BASALT FLOWS, ASSOCIATED PYROCLASTICS, RHYOLITE AND OBSIDIAN FLOWS, TALUS AND LANDSLIDES. 5 TO 100 m	BLACK
	SANDSTONE, CONGLOMERATE, AND LACUSTRINE LIMESTONE. MAXIMUM 50 m.	RED AND WHITE SANDSTONE; GRAY LIMESTONE
	SILTSTONES AND CLAYSTONES WITH INTERBEDDED FINE-GRAINED MASSIVE SANDSTONES; CHERT AND LIMESTONE PEBBLE CONGLOMERATE AT BASE. MAXIMUM 130 m.	REDDISH SILTSTONES; GREEN AND RED BROWN CLAYSTONES; REDDISH SANDSTONES AND CONGLOMERATES; ENTIRE UNIT: 10R5/2
6	DOLOMITE, NODULAR WHITE AND PINK CHERT, SANDY AT TOP AND BASE, LOCALLY FOSSILIFEROUS. MAXIMUM 8 m.	GRAY TO BUFF
5	SANDSTONES, SHALES AND GYPSUM; VERY FINE TO MEDIUM GRAIN LIMEY QUARTZ SANDSTONES, LOCALLY CONGLOMERATIC. MAXIMUM 25 m.	YELLOW BROWN AND PINKISH SANDSTONES; REDDISH SHALES WHITE GYPSUM
4	DOLOMITE, ABUNDANT WHITE CHERT AT TOP, SOME BEDDED CHERT, SANDY LAYERS, LOCALLY OSTRACODES. MAXIMUM 8 m.	GRAYISH WHITE TO BUFF: 5YR8/1
3	SHALES, SILTSTONE, AND GYPSUM, INTERBEDDED LIMESTONES AND FINE GRAIN CALCAREOUS SANDSTONES. MAXIMUM 15 m	RED AND GREEN SHALES AND SILTSTONES, WHITE GYPSUM
2	DOLOMITE WITH SANDY INTERBEDS, IRON NODULES COMMON AT TOP, LOCALLY PYRITIC AT BASE, LOCALLY GASTROPODS AND BIVALVES. MAXIMUM 8 m.	YELLOW BROWN: 10YR6/4
1	CALCAREOUS SILTSTONES AND SHALES INTERBEDDED DOLOMITES, LOCALLY FINE GRAIN SANDSTONES AND CONGLOMERATIC SANDSTONES. MAXIMUM 9 m.	RED TO BUFF SILTSTONES AND SHALES; BUFF TO YELLOW SANDSTONES
	DOLOMITE, CHERTY AND FOSSILIFEROUS, LOCALLY ABUNDANT PRODUCTIDS, SPONGES, GASTROPODS, AND CRINOIDS. MAXIMUM 100 m.	GRAYISH WHITE

Fig. II-C-2. Stratigraphic column of rock units on the Coconino Plateau.

b. Structure

The regional dip of the sedimentary rocks that underlie the Coconino Plateau is about 2° to the south. Normal faults and monoclines, structures typical of this part of the Colorado Plateau province, offset these strata to a maximum of about 70 m, and in general trend northwest. Most of the faults occur in the Cataract Creek system (Shoemaker et al., 1974).

In addition to the Cataract Creek system, there are two major northeast-trending fault system, termed by Shoemaker et al. (1974) the "Bright Angel and Sinyala systems", which may be related to fault zones in the crystalline Precambrian basement.

Most of the northwest-tending faults have displacements down to the southwest, and most of the northeast-trending faults have displacements down to the southeast.

c. Geologic Map

The Coconino Plateau was mapped in detail by M. Abrams and R. Squires from June 1973 to May 1974. Fourteen mappable units were recognized in the field. High-altitude color photographs were available for the western half of the study area, and low-altitude U.S. Forest Service color photographs also were used for the field mapping of the western part of the Kaibab National Forest adjacent to the southern rim of the Grand Canyon (see Fig. II-C-1). The geology was mapped on black and white 1:60,000 scale U.S.G.S. aerial photographs, then compiled on a 1:125,000 blow-up of a LANDSAT photograph.

From inspection of unenhanced and enhanced LANDSAT images it was readily apparent that all 14 geologic units were not distinguishable because of the limited resolution of the photography. Consequently, for the purposes of comparing LANDSAT and SKYLAB imagery, some of the lithologic units were

combined. A modified geologic map showing the distribution of combined lithologic units is shown in Fig. II-C-3. Seven units are depicted:

(1) Alluvium, reworked Tertiary gravel, and Tertiary gravel;

(2) Basalt flows, landslides, and talus;

(3) Moenkopi Formation;

(4) Unit 6 of the Alpha Member of the Kaibab Formation

(5) Units 4-5 of the Alpha Member of the Kaibab Formation;

(6) Units β-1-2-3 of the Kaibab Formation;

(7) Older Paleozoic rocks.

3. AVAILABILITY, SELECTION, AND PROCESSING OF IMAGERY

a. S190A Data

SKYLAB data from the S190A camera were acquired on September 15, 1973 on the SKYLAB 3 mission (Pass 43, Frame 334). The photo products available for analysis in the present study were 2-1/4 x 2-1/4" (1:2,850,000) and 9" x 9" (1:845,000) transparencies. The images were acquired by camera with filters separating the wavelength of recorded light into the 6 spectral bands:

Number	Wavelength	"Name"
1	0.7 - 0.8	infrared 1
2	0.8 - 0.9	infrared 2
3	0.5 - 8.8	color infrared
4	0.4 - 0.7	color
5	0.6 - 0.7	red
6	0.5 - 0.6	green

Both processed and unprocessed photo products were analyzed for geologic information.

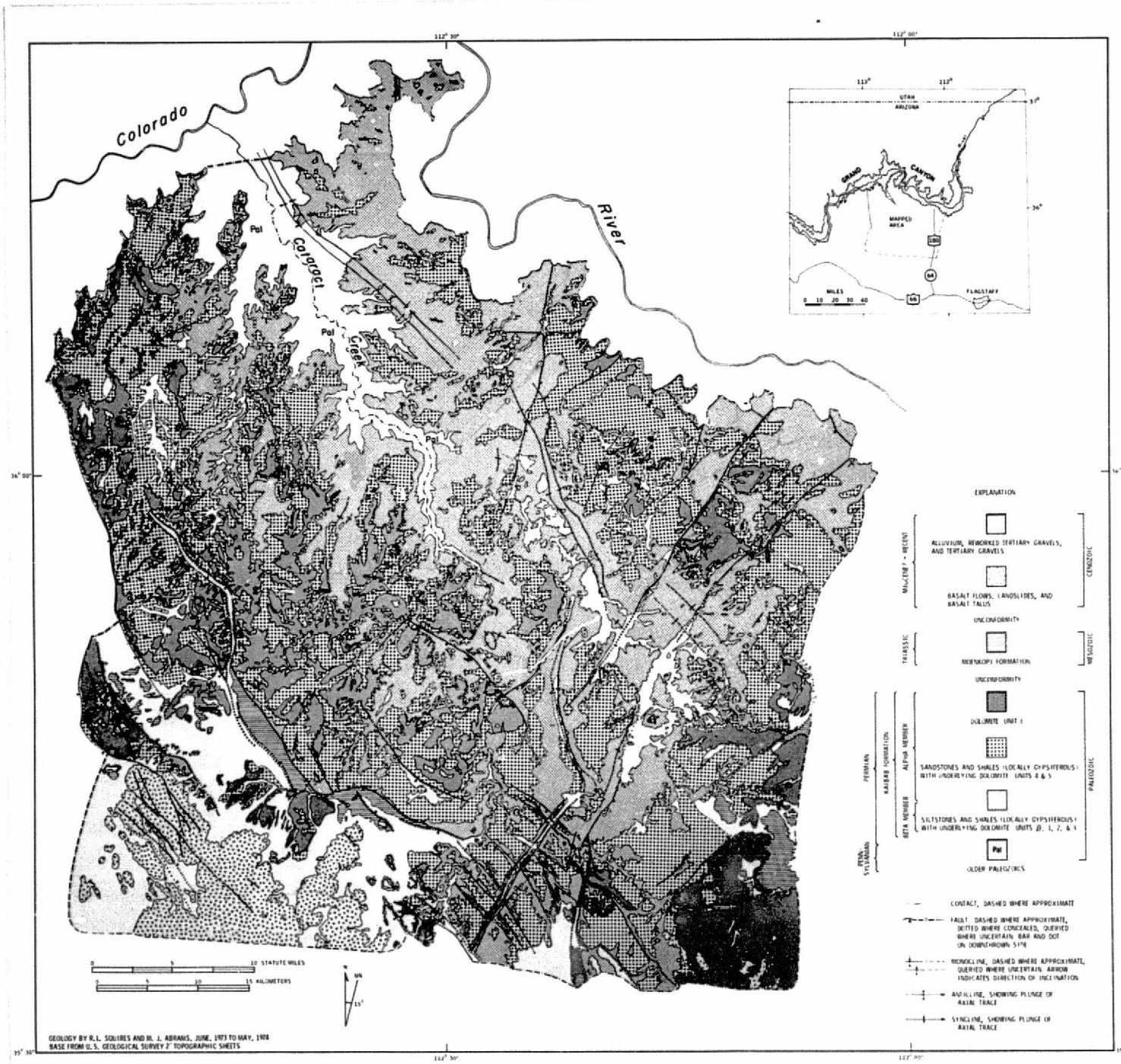

Fig. II-C-3. Simplified geologic map of the Coconino Plateau showing distribution of geologic units.

Unprocessed positive transparencies (2-1/4" x 2-1/4") were photo-interpreted singly on a Bausch and Lomb Zoom Transfer Scope. A false color composite photograph (Fig. II-C-4) was made on an additive color viewer by projecting the green band in blue light, the red band in green light, and the second infrared band in red light. Photo interpretation was also performed on this composite image. The results of analyses of the four positive transparencies and the false color composite photograph were combined to produce a single photo-interpretation map of structures and inferred lithologies.

The same four black-and-white transparencies of the four wavelength bands were scanned on a Perkin-Elmer microdensitometer, and the photographs were converted to digital form onto magnetic tape. The format of the data was then changed to make it compatible with the JPL-IPL IBM 360/44 computer system.

Each of the four bands was individually contrast stretched in JPL's Image Processing Laboratory using techniques described in Section III, then analyzed similarly to the original photos. A false color composite photograph was also created, and photo-interpreted for geologic information.

The four digital images were then registered to each other, pixel for pixel, using the programs described in the section on Processing (III). After registration, the 12 possible band-to-band ratios were created (green/red, green/infrared 1, green/infrared 2, red/infrared 1, red/infrared 2, infrared 1/infrared 2, and their six inverses). The value of ratioed images is that they remove, to the first order, the effect of topography in introducing artificial brightness differences in an image (Goetz & Billingsley, 1973), and give a truer picture of a material's spectral characteristics. False color composite pictures were produced from various combinations of three ratio images and they were also analyzed for lithologic information.

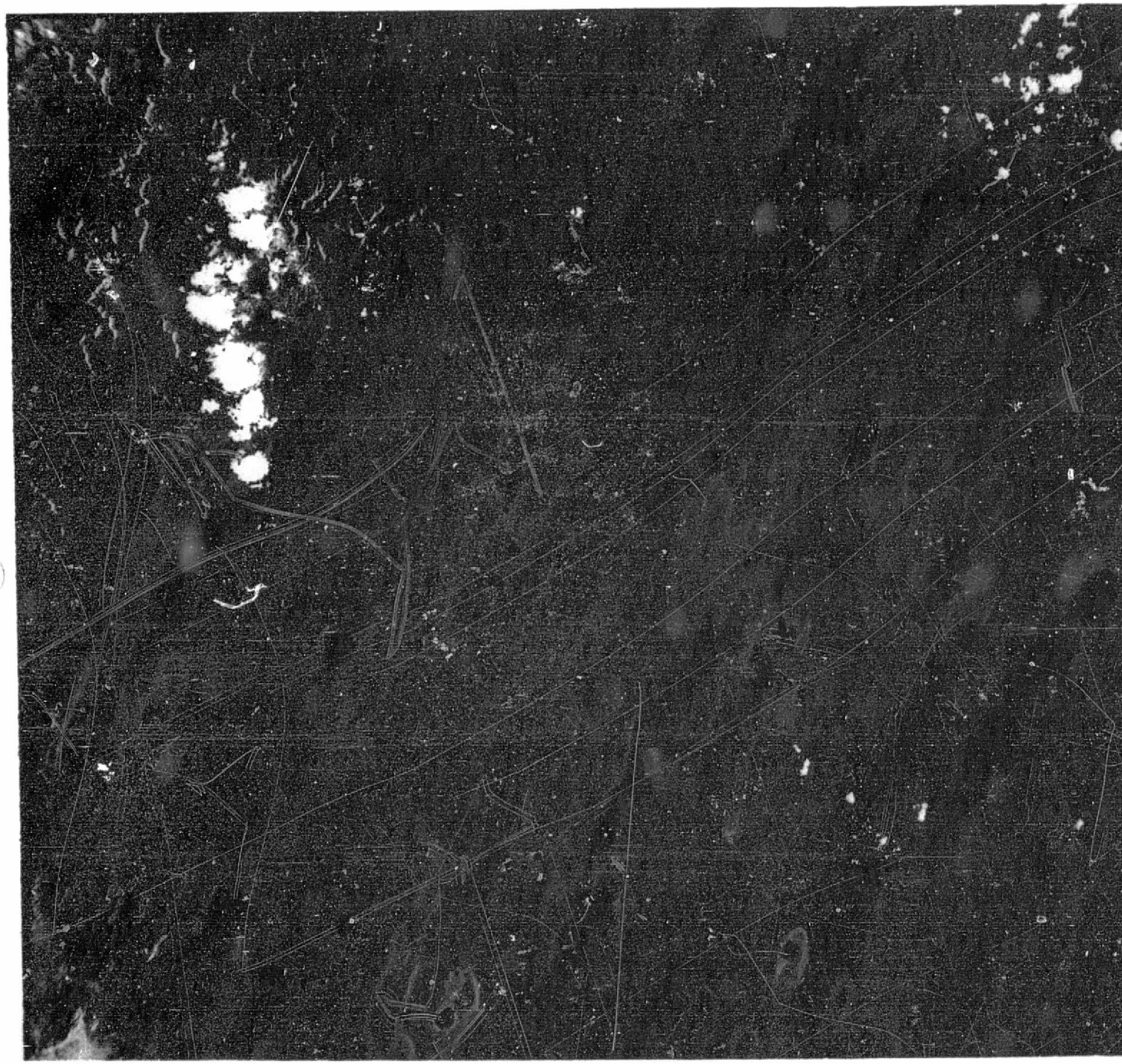

Fig. II-C-4. S190A false color infrared composite picture.
Green band displayed as blue, red band as green, infrared band as red.

b. S192 Data

Multispectral digital data for thirteen wavelength bands from the SKYLAB S192 scanner were obtained on magnetic tapes from JSC.

Band	Range (μm)	"Name"
1	0.41-0.46	Violet
2	0.46-0.51	Violet-blue
3	0.52-0.56	Blue-green
4	0.56-0.61	Green-yellow
5	0.62-0.67	Orange-red
6	0.68-0.76	Red
7	0.78-0.88	Infrared 1
8	0.98-1.08	Infrared 2
9	1.09-1.19	Infrared 3
10	1.20-1.30	Infrared 4
11	1.55-1.75	Infrared 5
12	2.10-2.35	Infrared 6
13	10.2-12.5	Thermal infrared

Preliminary computer processing of the data to rectify the geometry and remove the conical scan was performed using the methods described in Section III. Paper prints (9" x 9") and transparencies (70 μm) were produced of the different wavelengths bands. Because of the large number of possible combinations which could be generated from the data, only the optimal combinations were used for analysis.

The selection of the optimal wavelength bands was based upon discriminant analysis of the spectral reflectivity of the 6 major lithologic units (units 6, 4-5, 3, 2, β, Trm) exposed in the study area. The spectral reflectivity in the region of 0.4 to 2.5 mm of 83 representative samples of the various

units was measured in the field in May, 1974 by use of the JPL portable field reflectance spectrometer (PFRS). The spectra were then digitized at 0.5 m intervals in the wavelength region of 0.4 to 1.0 μm and 0.1 μm intervals thereafter. A stepwise linear discriminant analysis (see III) was used to determine the three optimum wavelength bands for separability of the lithologic units. They are in order of separability: 1.3 μm, 1.0 μm, and 0.5 μm. The S192 wavelength bands which were the most similar to the optimal wavelength regions, as measured by the PFRS, were then used to make a false-color composite image (Fig. II-C-5). A true color composite image was also produced by registering and projecting bands 2, 4, 6 on the I^2S in blue, green and red, respectively.

Ratio images were made from the S192 data. Figure II-C-6 shows the ratio of wavelengths 0.52 μm and 0.62 μm. Due to the poor quality of the ratio images caused by the high noise level, ratio pictures were not used for analysis of geologic information.

c. LANDSAT Data

LANDSAT frames 1032-17373 and 1032-17375 acquired on August 24, 1972 were used for analysis and comparison with SKYLAB data. The LANDSAT data were acquired digitally, and available on computer compatible magnetic tapes. Data were acquired in four wavelength bands:

Band	Wavelength (μm)	"Name"
4	0.5 - 0.6	Green
5	0.6 - 0.7	Red
6	0.7 - 0.8	Infrared 1
7	0.8 - 1.1	Infrared 2

Preliminary processing consisted of unleaving the multispectral data, removing synthetic data, correcting the geometry, and removing the effects

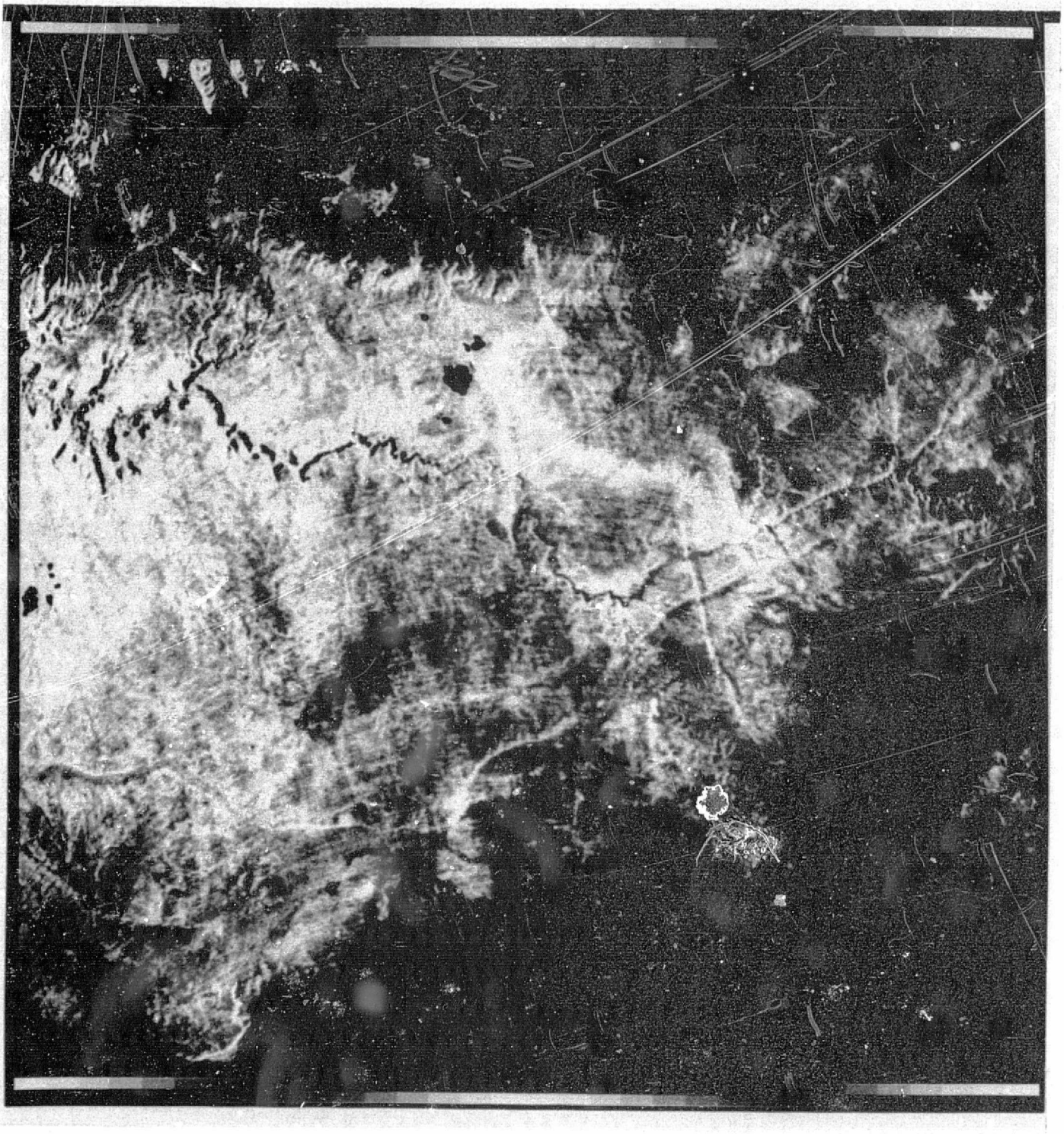

Fig. II-C-5. S192 false color composite made from bands 2, 8, and 10.

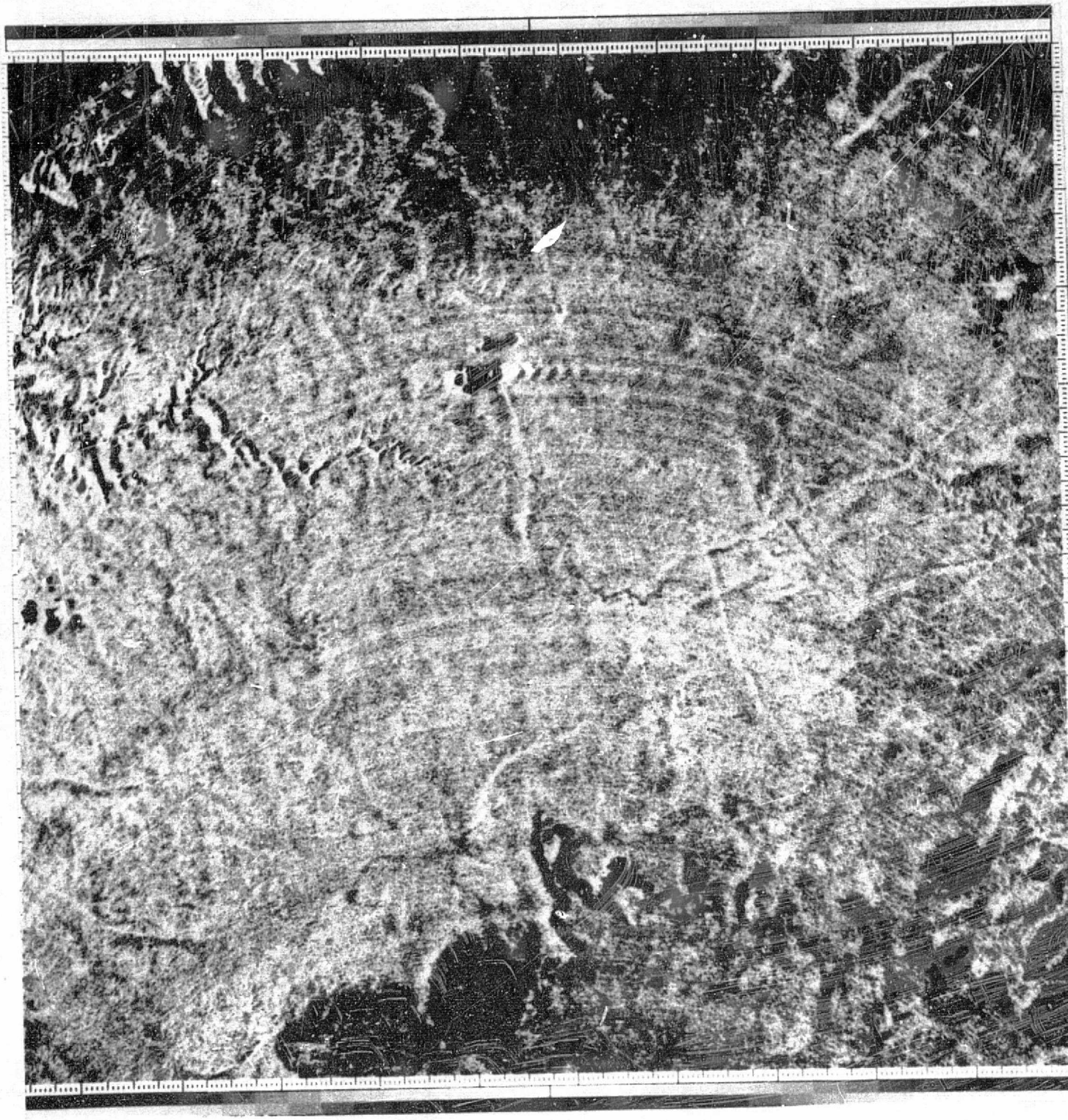

Fig. II-C-6. S192 ratio picture made from ratio of bands 3 to 5.

of the spacecraft motion. (A detailed description of the techniques used can be found in Section III.) The two frames were then concatenated into one image, since neither included the entire study area.

Computer enhancement of the LANDSAT data was necessary to extract a subset of the 200 million bits of information contained in each frame which is useful to the investigator. Only about one-tenth of the full information content of a LANDSAT image can be usefully displayed at one time on film for interpretation.

The simplest, and one of the most useful forms of image enhancement, is a contrast stretch in which the brightness data distribution is expanded or stretched to fill the dynamic range of the display medium, in this case film. Figure II-C-7 is an example of this technique applied to one of the LANDSAT bands. There is a significant enhancement of the details discernible in the originally flat, gray area. A thorough treatment of this enhancement technique can be found in Goetz et al., 1975.

For the study area, a color composite of contrast-stretched black-and-white transparencies of bands 4, 5 and 7 was produced and used for photo-interpretation of lithologic and structural information (Fig. II-C-8a).

Several different combinations of color ratio composite images were produced and analyzed for the study area. Overlays were produced on prints of the color composites, showing photo-interpretation of lithologic information discernible. One of the ratio composite used, (4/7, 4/5, and 7/4), is shown in Fig. II-C-8b.

4. MAPPING COMPARISON

Study area A was analyzed in the southeast part of the Coconino Plateau. This area, 60 by 40 kilometers (Fig. II-C-1) was selected because:

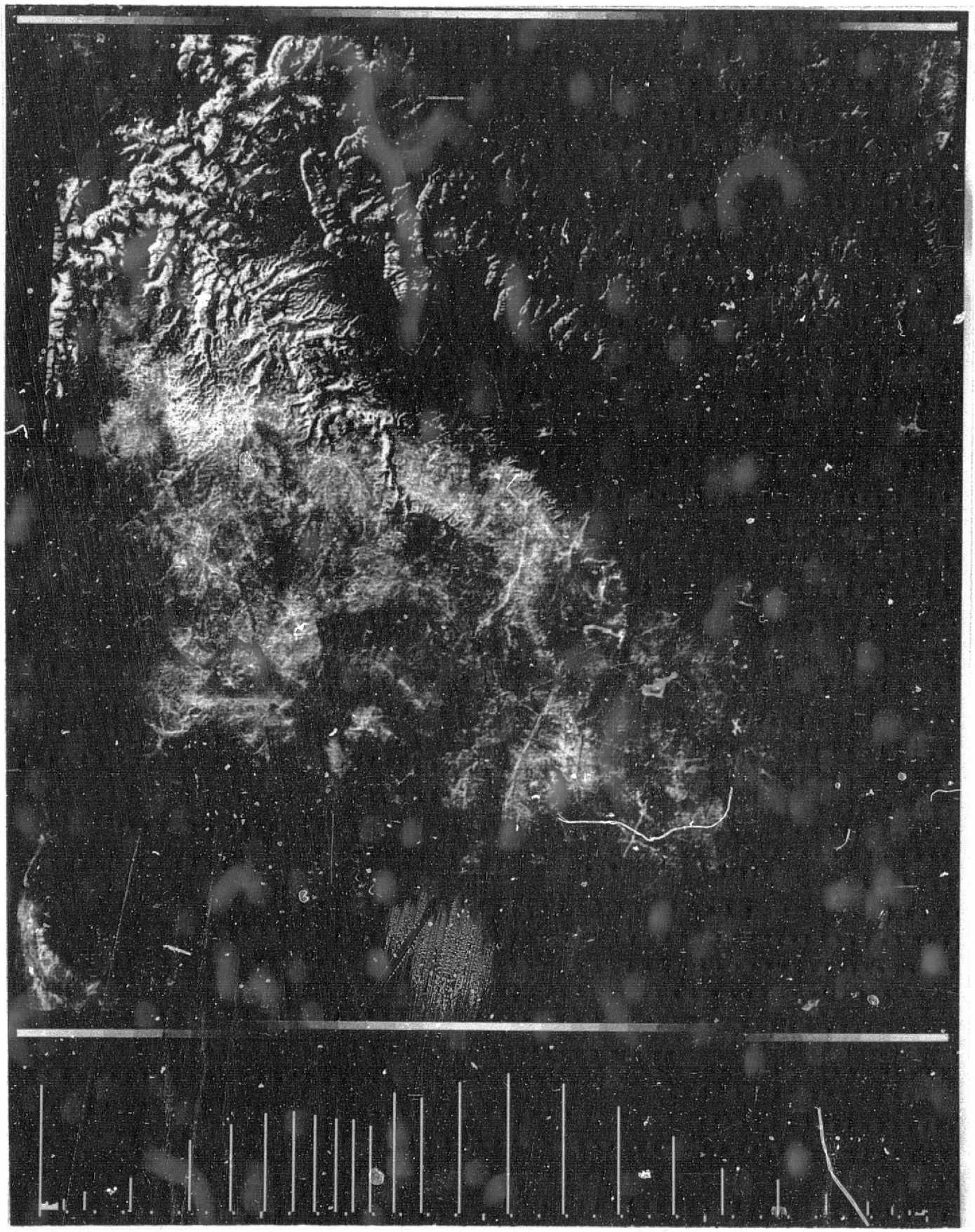

Fig. II-C-7. Gaussian contrast stretch print of LANDSAT band 7.

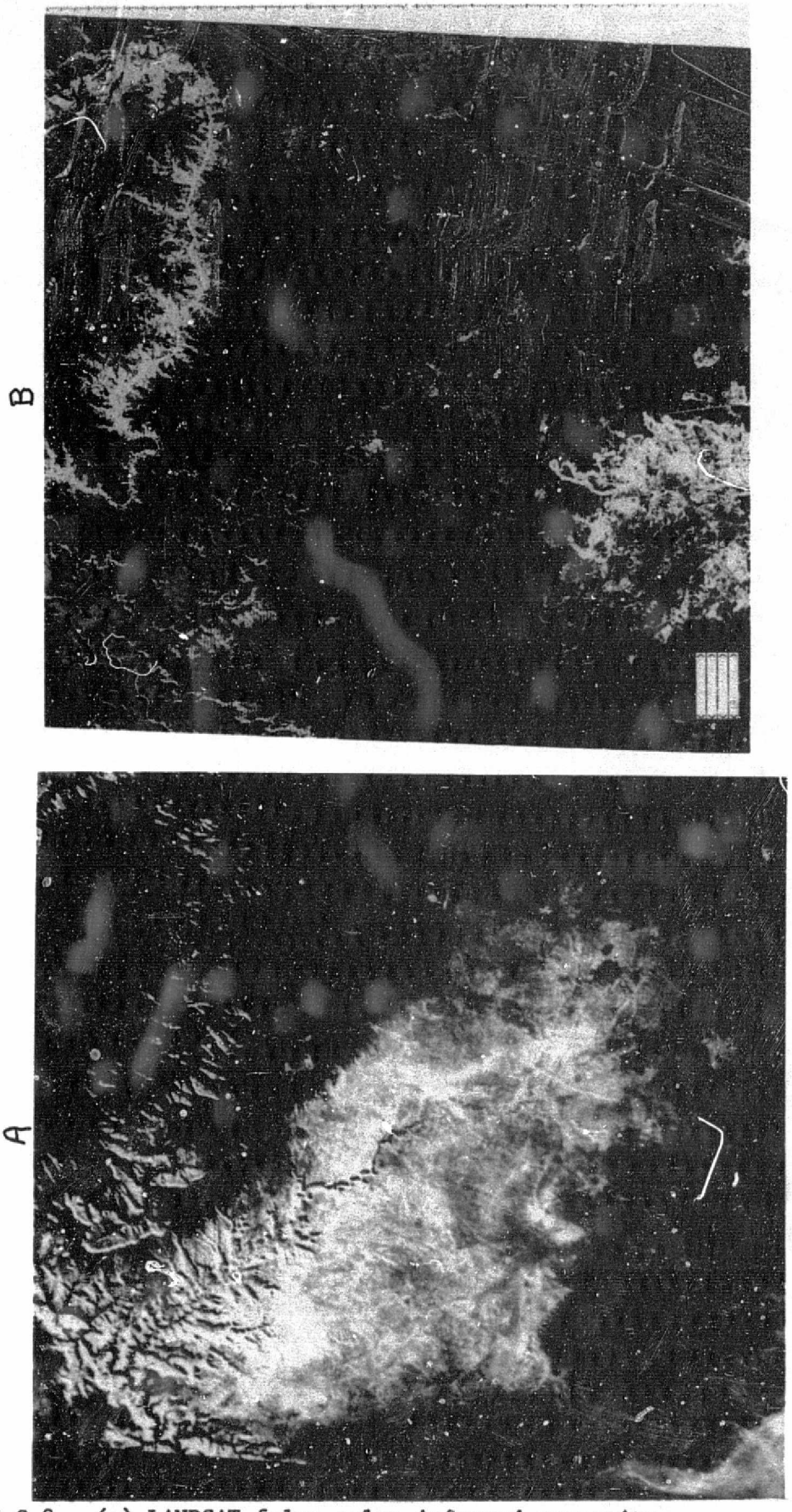

Fig. II-C-8. (a) LANDSAT false color infrared composite.
(b) LANDSAT false color ratio composite; ratio 4/5, 4/7, and 7/4 printed as green, red, and white respectively.

1. It was well known geologically;

2. All lithologies found on the Coconino Plateau outcrop in the area;

3. It has a good representation of regional structural features.

A comparison was made of the amount of geological information discernible through photo interpretation of the image products described in the previous section.

The following products were analyzed:

1. S190A, photo products from JSC, and color composites made from digitized and enhanced photos;

2. Digitized S190A ratio composites;

3. S192 color composite (SDO's 17, 18, and 19, see Section IV);

4. LANDSAT stretched images and color ratio composites.

a. Structure Analysis

The test area is characterized by two near-orthogonal sets of normal faults, one trending north-northeast, the other northwest. Faults identified from field mapping are shown in Fig. II-C-9b. (The solid black feature is a basalt outcrop, for reference.) Field observations indicate that some, but not all, of the faults have clearly recognizable topographic expression.

Photo interpretation of fault structures for S190A photos, S192 composite, and LANDSAT images is shown in Fig. II-C-9c, Fig. II-C-9d, and Fig. II-C-9a, respectively. The photo interpretation maps were produced from transparent overlays on the enhanced photos, or by use of a Bausch and Lomb Zoom Transfer Scope.

All three photo-interpretation maps are in excellent agreement with the field-derived map. The most accurate is that derived from S190A photos, though it is not significantly better than the other two maps.

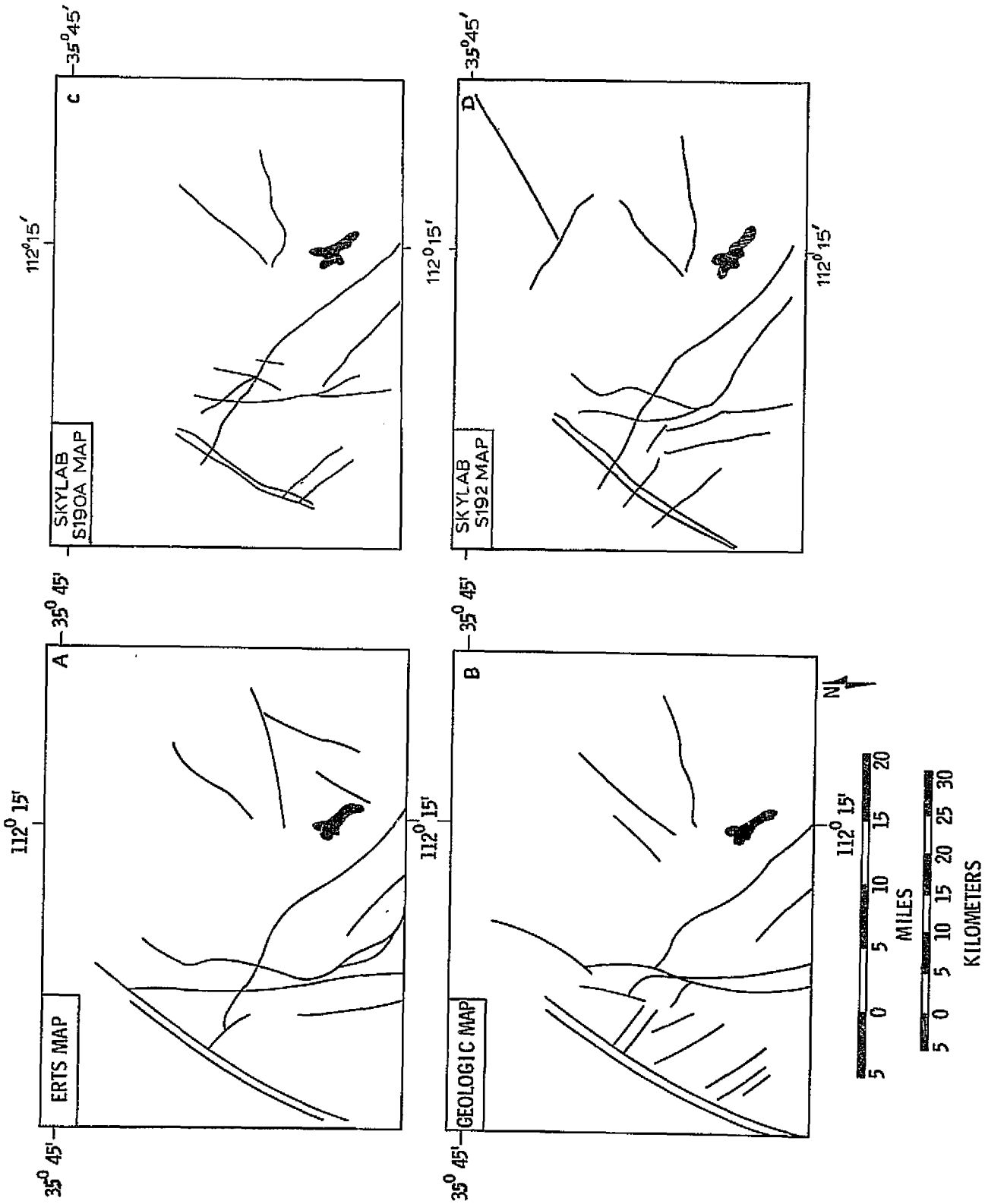

Fig. II-C-9. (a) Fault map derived from LANDSAT images.
(b) Fault map derived from field observations.
(c) Fault map derived from SKYLAB S190A photos.
(d) Fault map derived from SKYLAB S192 images.
Black feature is basalt outcrop.

b. Lithologic Mapping Analysis

Photo-interpretation maps of lithologic information were made from use of both direct transparent overlays and transfer of contacts using the Bausch and Lomb Zoom Transfer Scope. In the analysis of the LANDSAT images, several different enhancements were interpreted; then a compilation was made of all the data, eliminating discrepancies and ambiguities.

Figure II-C-10 shows the three photo-interpretation maps (A is the LANDSAT map, B is the S190A map, D is the S192 map) and the modified geologic map (C) for the study area. In addition to the units of the Kaibab Formation, both basalt and Moenkopi outcrops are present.

Owing to the great difference in contrast, basalt outcrops and associated talus deposits were easily identified. However, on the S190A and S192 images, an area identified as basalt in the southwest part of the area is in reality a large, densely tree-covered hill. Because most of the basalt outcrops are also tree-covered, this area was misidentified.

The most accurate identification of Moenkopi outcrops was possible from the S192 composite photograph. All outcrops were correctly and accurately recognized. Next in accuracy were the LANDSAT images; and finally the S190A imagery.

Excellent detail was recognizable in the LANDSAT images among units of the Kaibab Formation. The eastern third of the area was mapped from LANDSAT images as unit 6, which corresponds well to the actual field-mapped area of this unit; the other area of unit 6 in the center of the area corresponds fairly well to the actual area of unit 6. All areas mapped from LANDSAT images as unit 4-5 are generally correctly identified. The small areas at the western edge of the map along the southern edge are reasonably accurate, with somewhat less accuracy in the larger areas. Unit β-1-2-3 was correctly mapped, except

Fig. II-C-10. (a) Lithologic map compiled from LANDSAT images.
(b) Lithologic map compiled from SKYLAB S190A images.
(c) Geologic map.
(d) Lithologic map compiled from SKYLAB S192 false color composite.

for the south-central part of the area, which consists primarily of unit 4-5. The two areas mapped as alluvium from the images correspond to actual field-mapped occurrences of alluvium.

The map compiled from S190A sources is comparable in accuracy to the LANDSAT-derived map. Unit 6 was correctly mapped for the eastern third of the study area, though outcrops in the central part were not identified. Outcrops of unit 4-5 in the northern part of the study area were correctly identified, as were two small outcrops on the western edge. All other actual outcrops, especially the large region in the south-central part of the area, were not identified. Unit β-1-2-3 was accurately identified except for the south-central area, where it was misidentified as unit 4-5. The large region of alluvium was correctly identified in the southwest corner.

The map produced from the S192 composite showed the greatest accuracy in identification and delineation of the Kaibab Formation units, with the possible exception of unit 6. Outcrops of unit 6 were correctly identified in the central part of the area, and in the northern part. The regions mapped as unit 6 in the southeast portion of the area are accurate, but not extensive enough. Unit 4-5 was very accurately mapped throughout the study area. The small outcrops on the western edge were recognized; and the large swath of unit 4-5 crossing the study area in a northeast-southwest direction was accurately delineated. The only misidentification occurred in the southeast corner of the study area. Unit β-1-2-3 was accurately identified throughout the study area, with little misidentification. The large outcrop of alluvium was correctly mapped in the southwest corner of the area.

Analysis of the "true color" S192 color composite image indicated that there was very little lithologic information discernible. This is not surprising in view of previous work which showed that lithologic units are not separable in the visible wavelength region.

5. LITHOLOGIC MAPPING BY CLASSIFICATION

Lithologic mapping of the central portion of the study region was attempted by classification, using both supervised and unsupervised approaches. Classification was performed for the LANDSAT image only, because of the excessive noise in the SKYLAB S192 data.

The supervised classification techniques employed were: (1) a stepwise linear discriminant analysis algorithm, and (2) a hybrid algorithm (see III for technical details). The discriminant analysis algorithm determines the optimum input variables for separability of the lithologic units and computes a transform using these variables to minimize the ratio of the difference between group multivariate means to the group multivariate variances. The hybrid approach incorporates a parallelepiped algorithm and the Bayesian maximum likelihood function. The former is used in a table-lookup fashion to assign unambiguous individual pixels to specific groups or classes (lithologic units); whereas, the latter resolves ambiguities or assigns "unknown" pixels to specific groups through claculation and analysis of normal multivariate probability density functions.

The unsupervised classification algorithm employed, CLUS (see III for technical details) is an iterative technique in which the optimum grouping and number of groups is determined from evaluation of variance and covariance matrices. The "best" classification is one which maximizes the between-group and minimizes the within-group variation.

a. Study Area and Preclassification Analytical Techniques

A 20 by 20 km area of study (Area B, Fig. II-C-1) located in the center of the mapped area was chosen for analysis. The units exposed are ß, 2, 3, 4, 5, and 6 of the Kaibab Formation, and the Moenkopi Formation (TRM).

Units 4 and 5 were combined in the analysis because of the limited areal extent and outcrop of unit 5.

Training areas for the supervised classification of the LANDSAT data were chosen from within the study area. For each of the five subdivisions of the Kaibab Formation, two training areas were used; only one area was used for the Moenkopi Formation because of its limited outcrop area in the study region. Each training area covered 25 pixels and its size and location were selected on the basis of: large areal extent of the unit; homogeneity as determined from examination of LANDSAT imagery; and minimal, but not insignificant soil covering. The spectral reflectivity of the individual pixels in the LANDSAT MSS bands was extracted for each training area. Ratios of spectral bands (4/5, 4/6, 4/7, 5/6, 5/7, 6/7) were computed and used with the raw spectral values as initial input variables.

The 10 possible input variables were compared pairwise for separability (see III) for the hybrid classifier and MSS bands 4, 5, 7, and ratios 4/5, 4/6, and 4/7 were used in the classification. Only 3 input variables, MSS bands 4, 5 and ratio 4/5 were required, as per analysis, for the linear discriminant classifier.

For the unsupervised classification, a 19 line by 19 sample grid was overlaid on the study area and the DN values (MSS bands 4, 5, 6, 7) were extracted from the digital data for 361 pixels. The DN values were ratioed, thus producing a 361 x 10 data matrix. Principal component analysis in the R-Mode was performed, and on the basis of the analysis (see Siegal and Abrams, 1975, for details) MSS bands 4, 5, and ratios 4/6, 5/6, 6/7, were used as input variables for the classification. Classification of the 361 pixels for two through seven groups was performed. An optimum number of three groups was indicated and the entire study area was classified according to the multiple

discriminant functions computed by the CLUS program for separability of the 361 pixels.

b. Classification Results

The thematic maps (see Fig. II-C-11) produced by the unsupervised classification algorithm (CLUS) and the two supervised classification schemes, the hybrid algorithm, and the linear discriminant analysis algorithm, were overlaid on the geologic map (see Fig. 11a) and areas correctly and incorrectly classified were identified.

Both supervised classification schemes correctly classified approximately half of the study region. Using the discriminant classification algorithm, all outcrops of the Moenkopi Formation were correctly identified; however, an equal area was incorrectly assigned to this unit. Using the hybrid classifier, all outcrops of Moenkopi were also correctly identified; misclassification was minor.

Unit 6 was more accurately mapped by the discriminant analysis classifier, and approximately one-third of the outcrop areas was correctly classified; however, about one-tenth of the remaining study area was incorrectly classified as unit 6. Approximately 5% of this unit was correctly classified by the hybrid algorithm, with only minor misclassifications.

Units 3 and 4-5 taken together were equally well mapped by both classification programs; approximately half of the outcrop area was correctly mapped. The hybrid classifier misidentified a greater percent of the study area than the discriminant algorithm.

Approximately 40% of unit 2 outcrop was correctly classified by the hybrid scheme and an equal area was misclassified. The discriminant analysis algorithm correctly recognized only half as much area as the hybrid classifier.

Fig. II-C-11. (a) Geologic map
(b) Classification map using unsupervised (CLUS) algorithm
(c) Classification map using hybrid supervised algorithm
(d) Classification map using linear discriminant analysis algorithm

The hybrid classifier correctly identified about half of the Beta unit; only a third of the unit was correctly identified by the other algorithm. Both misclassified an insignificant portion of the study area.

Using the unsupervised three-group classification (see Fig. II-C-11b), many lithologic boundaries were correctly delineated, though identification of units 3 and 4-5. Red areas include all outcrops of the Moenkopi Formation, some of the Beta outcrops along Cataract Creek and miscellaneous areas of the other geologic units. The green areas are, in general, outcrops of units 3 and 4-5. It is not possible to determine the percent of the area correctly classified, when classifying 6 geologic units into three groups.

c. Analysis of Results

In terms of accuracy, both the supervised classification schemes were comparable though they correctly classified only 50 percent of the study area. The unsupervised algorithm delineated the major lithologic boundaries and, in a very general way, delineated each of the lithologic units.

The Beta unit and the Moenkopi Formation were most accurately mapped by all three algorithms. Identification of the other units was not as successful. There appears to be several reasons for this lack of success. Facies changes of geologic units are prevalent but not generally recognized in delineating mapable units for regional mapping. This was not a serious problem in the study region, as changes were slight and consisted of an increase or decrease in the siltstone/sandstone composition of the clastic units. Vegetation cover can pose a real problem in lithologic identification. In the study area, vegetation cover was minimal. Vegetation communities were constant for any one lithologic unit, and the only significant change observed was associated with the change from one lithology to another. Problems of alluvial outwash masking or covering

the bedrock are a significant factor affecting comparison of LANDSAT-derived maps with geologic maps. Because a geologic map represents bedrock geology without soil cover, it is an idealization of the true physical setting. LANDSAT senses only the surface of the ground, it does not penetrate through the soil mantle. In some instances, transported surface material may be derived from different lithology, unrelated to the underlying bedrock. Another effect of this transport phenomenon is to smooth out sharp lithologic boundaries and produce gradational boundaries.

The above factors contribute to producing inhomogeneity in the spectral signatures of the training areas. To assess the significance of this effect, the spectral homogeneity of the training areas was examined by use of the CLUS algorithm. Using four principal components for the ten variable data set of the training areas tekan together, classification was performed for two through seven groups. Various options were used to improve the initial grouping. The results are tabulated in Table II-6. As indicated, the geologic themes are not spectrally homogeneous for the range of groups tested, i.e., the variation within groups is greater than the variation between groups.

A second major reason for the inability of the classification schemes to discriminate the geologic themes is the similarity of the spectral signatures in the four LANDSAT bands. (See Fig. II-C-12.)

There are two possible solutions to this problem. First, increase the sample size for each theme - this is difficult to do unless the study area is very well known (in which case there is no need for classification). Second, examine the spectral reflectivity in wavelength bands different than LANDSAT to determine if greater lithologic separation is possible.

To evaluate the second solution, reflectance spectra of representative samples of the five geologic themes were acquired in the field by use of a

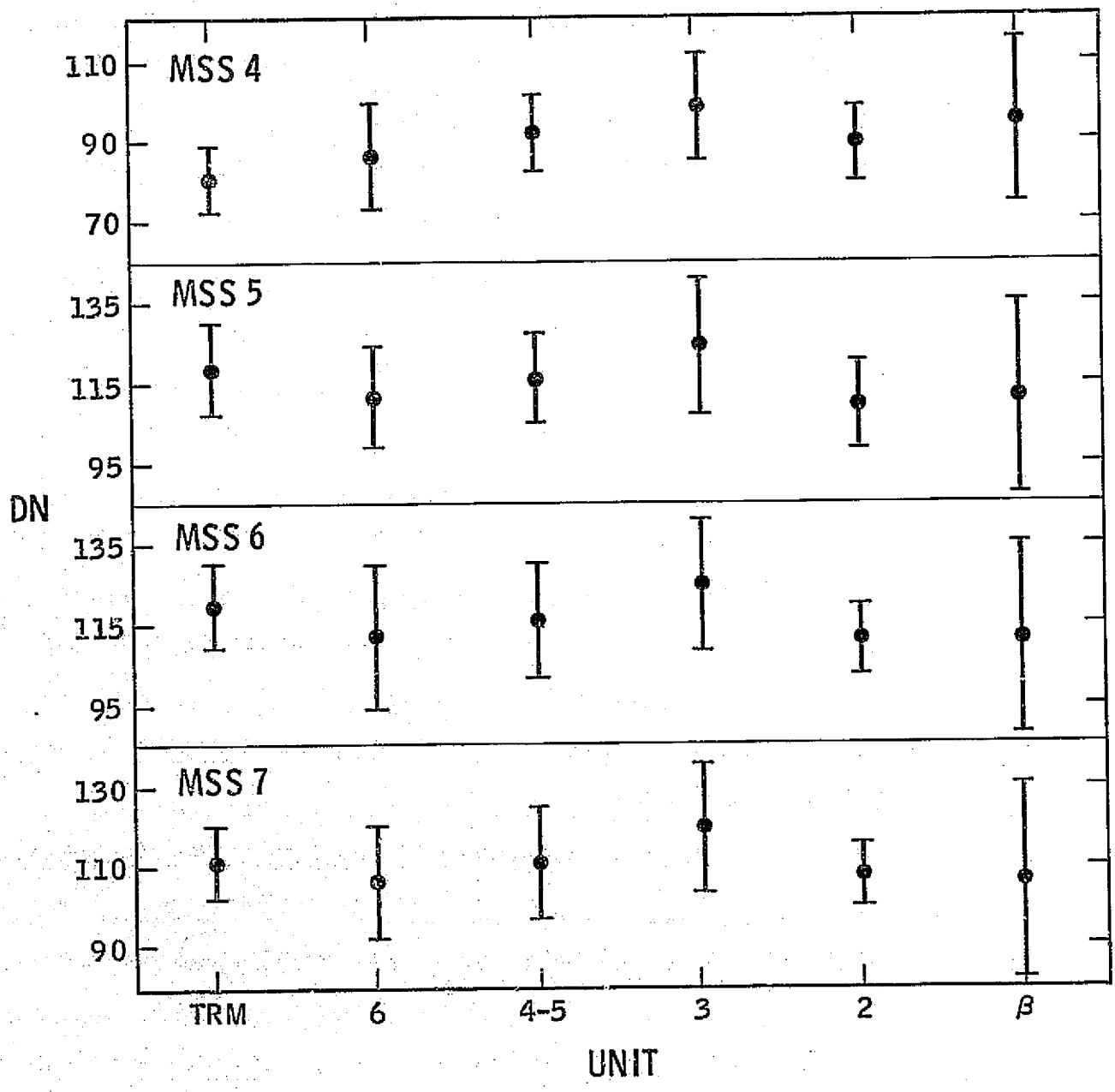

Fig. II-C-12. Mean and two standard deviation plots of the spectral reflectivity of geologic units from LANDSAT data.

Table II-6. Unsupervised Classification of Themes

(A = TRM; B = UNIT 6; C = UNIT 4-5; D = UNIT 3; E = UNIT 2; F = UNIT 8)

	1	2	3	4	5	6	7
	25A						
	31B	19B					
2	23C	27C					
	3D	47D					
	27E	23E					
	21F	49F					
	7A		18A				
	17B	5B	23B				
3	23C	9C	18C				
	22D	26D	2D				
	22E	9E	19E				
	14F	23F	13F				
	2A			23A			
	16B	6B		23B			
4	22C	10C		18C			
	25D	25D					
	21E	12E		17E			
	10F	25E	9F	6F			
		10A	3A	12A			
		16B	14B	17B	3B		
5	4C	10C	13C	16C	11C		
	12D	9D	8D	8D	25D		
	3E	14E	13E	13E	7E		
	20F	3F	16F	6F	5F		
		11A	2A	11A	1A		
		17B	14B	16B	3B		
6		10C	12C	18C	6C	4C	
		9D	9D	8D	12D	12D	
		14E	12E	14E	7E	3E	
	9F	3F	16F	6F	4F	12F	
		7A	4A	8A	2A		4A
	3B	16B	10B	10B	5B	2B	7B
7	6C	6C	3C	14C	14C	1C	6C
	5D	7D	5D	1D	17D	10D	5D
	12E	12E	7E	7E	5E		7E
	1F	6F	11F	5F	5F	12F	10F

GROUP NUMBER

portable reflectance spectrometer. Reflectance was measured continuously over the range of 0.4 to 2.4 μm, which includes the 0.5 to 1.1 μm region scanned by LANDSAT. The spectra were digitized at 0.05 μm intervals in the region of 0.4 to 1.0 μm and at 0.1 μm intervals thereafter. A total of 83 spectra were analyzed. Using the stepwise linear discriminant analysis algorithm, the four best wavelengths for separability of themes were determined. They are, in order of separability, 1.3 μm, 1.0 μm, and 1.2 μm. On the basis of the optimum linear combination of these bands, the probability of each sample coming from each of the themes was computed, and the samples were assigned to the theme for which their probability was the greatest. The classification matrix is presented in Table II-7. The classification is much better than that obtained using the LANDSAT bands, and only unit 3 is not, in general, classified correctly. If the spectral reflectivity of the samples measured in the field is representative of the geologic units, then greater discrimination of rock type could be obtained by use of wavelength bands outside the region of LANDSAT.

A far more useful selection oi bands is available from S192 data. Although the random noise encountered in S192 data in this data prohibited classification, a false color composite image was produced from the three optimal wavelength band images. Lithologic information contained in the false color composite exceeded that available from the LANDSAT image and the "true color" S192 image.

Table II-7. Classification Matrix

Number of Cases Classified into Group

GROUP	Trm	Unit 6	Unit 4-5	Unit 3	Unit 2
Trm	19	0	0	1	0
Unit 6	0	14	0	1	0
Unit 4-5	0	0	14	3	3
Unit 3	0	4	3	5	0
Unit 2	0	0	5	0	13

6. CONCLUSIONS

The feasibility of using satellite data for geologic mapping on the Coconino Plateau was examined by use of both enhancement and classification techniques. The specific data analyzed were SKYLAB S190A multispectral photographs, SKYLAB S192 multispectral scanner digital data, and LANDSAT multispectral digital data. The following conclusions are a result of this analysis:

(1) Structural information is equally well seen on all three types of imagery. The photo-interpretation maps produced each accurately identify the major faults in the test area.

(2) Photo-interpretation maps of lithologic information were compiled for each of the data sources, using several enhancement images. For LANDSAT data, false color ratio composites proved to be the most useful. For SKYLAB S192 data, a false color composite created from wavelength bands indicated by use of a linear discriminant algorithm proved to be the most useful. A "true color" composite S192 image did not contain as much lithologic information. And for SKYLAB S190A data, a false color infrared composite was the most useful.

All three photo-interpretation maps are accurate enough to serve as geologic reconnaissance maps. The S192 map is the most accurate.

(3) Separation of different lithologic units can best be accomplished with imagery in wavelength regions other than those availabel for the LANDSAT MSS. In this study, the wavelength bands 0.46 to 0.51 μm, 0.98 to 1.08 μm, and 1.20 to 1.30 μm were selected, based on analysis of actual field spectral reflectance measurements, and an enhanced color composite was produced from SKYLAB S192 data covering those bands. The resulting image allowed the most accurate separation and identification of lithologic units in test area A.

(4) The thematic maps produced by the three classification algorithms anlayzed were not as accurate as the photo-interpretation maps produced from the computer enhanced imagery. However, in general, the linear discriminant algorithm appeared to be the most accurate of the three, and was more efficient than the others.

(5) From the preceding study, it is strongly recommended that additional investigations be undertaken to determine the optimal wavelength bands for lithologic mapping. The results of this study strongly suggest that they will be in the far reflective infrared portion of the spectrum, which is presently not sensed by any of the orbiting satellites.

7. REFERENCES

1. Goetz, A. F. H. and F. C. Billingsly, "Digital Image Enhancement Techniques Used in Some ERTS Application Problems, Contributions to Geology", 12, 2, University of Wyoming, 1975.

2. Goetz, A. F. H., Billingsly, F. C., Gillespie, A. R., Abrams, M. J., Squires, R. L., Shoemaker, E. M., Lucchitta, I., and Elsten, D. P., "Application of ERTS Images and Image Processing to Regional Geologic Problems and Geologic Mapping in Northern Arizona", NASA-Jet Propulsion Laboratory, Technical Report 32-1597, 188 pp., Pasadena, California, 1975.

3. McKee, E. A., The Environment and History of the Toroweap and Kaibab Formations of Northern Arizona and Southern Utah, Carnegie Institute Publication, 492, 268 pp., 1938.

4. Shoemaker, E. M., Squires, R. L., and Abrams, M. J., "The Bright Angel and Mesa Butte Fault Systems of Northern Arizona", in Geology of Northern Arizona with Notes on Archaeology and Paleoclimate, Part I, p. 355, for Geological Society of America, Rocky Mountain Section Meeting, Flagstaff, Arizona, 1974.

5. Siegal, B. S., and Abrams, M. J., "Geologic Mapping Using LANDSAT Data", in press Journal of Photogrammetric Engineering and Remote Sensing, 1975.

II-D. RED LAKE, ARIZONA

M. J. Abrams and B. S. Siegal

1. INTRODUCTION

To assess the feasibility of using various types of imagery and different wavelength bands, multispectral data of Red Lake, Arizona, as acquired by a Bendix 24-channel MSS, was analyzed and compared with LANDSAT images and Skylab S190A imagery. The dates of data acquisition are tabulated in Table II-9.

Table II-8. Imagery Analyzed

Type	Date Acquired
S190A	June 12, 1973
LANDSAT	June 9, 1973
24-Channel MSS	June 12, 1973

The Bendix scanner was flown aboard a C-130 aircraft at the same time as the Skylab overflight. Data were acquired in digital form for thirteen wavelength bands (Table II- 9). The digital data were processed by JPL's Image Processing Laboratory. Geometric distortions resulting from mirror scan effects and variations in the aircraft flight path were removed. The data were contrast stretched for display on photographic medium.

Table II-9. 24-Channel MSS Wavelength Bands

Channel	Wavelength Band	"Color"
2	0.41 - 0.45 μm	Violet
4	0.54 - 0.58 μm	Orange
5	0.59 - 0.64 μm	Red
6	0.65 - 0.69 μm	Red
7	0.71 - 0.76 μm	Infrared
8	0.77 - 0.81 μm	Infrared
9	0.83 - 0.88 μm	Infrared
10	0.98 - 1.04 μm	Infrared
24	1.06 - 1.05 μm	Infrared
23	1.33 - 1.20 μm	Infrared
11	1.20 - 1.30 μm	Infrared
12	2.30 - 2.43 μm	Infrared

The wavelength bands of the S190A and LANDSAT imagery have been described previously.

In situ reflectance measurements of Red Lake, in the wavelength region of 0.4 - 2.5 μm were attempted with the JPL Portable Field Reflectance Spectrometer at the time of the overflights. Due to technical difficulties, no usable spectra were obtained.

2. DESCRIPTION OF TEST SITE

Red Lake is an 8 km diameter dry, inter-mountain lake bed, located south of Lake Mead at the north end of Hualapai Valley (See Figure II-E-1). The lake is dry except for brief periods during summer and winter storms, when there is often several cm of standing surface water on the low-lying parts of the lake. The surface of Red Lake consists of mud-cracked, vegetation-free, silty clay of high albedo.

The areas immediately surrounding Red Lake consist of alluvial fans covered with coarse debris shed from the neighboring mountains. These fans support a flora of sparse grass and small bushes. The closest bedrock is found adjoining the northwest corner of the lake, and is made up of Pre-Cambrian gneiss overlain by Quaternary-Tertiary basalt.

3. ANALYSIS

From preliminary examination of the imagery, eight features were selected on Red Lake for detailed analysis. These features were chosen because of pronounced albedo differences in different wavelength bands. A field reconnaissance was undertaken in August, 1975. The features were identified and are described in Table II-10.

Table II-10. Selected Features for Analysis on Red Lake

Feature	Description
A	Wash area, barren, 2 - 5% dry brush; surface clay-silt; partially disturbed by cows; small (< 2 m wide) drainages have green shrubs with occasional small trees.
B	Alluvium; 10-30% cover of grass and small shrubs; about 1% basalt cobbles.
C	Same as B with addition of 15-20% and cover of 1 m mesquite bushes.
D	Basalt hills; weathered talus covers slopes.
E	Alluvium; 30% cover of .5 m bushes.
F	Playa surface; small mud cracks; no vegetation.
G	Playa surface; deeper mud cracks; denser distribution; no vegetation.
H	Playa surface; inferred standing water or moist ground[a]

[a]Climatological records from Truxton Canyon, 25 km southeast of Red Lake show precipitation on June 12, 1973.

A comparison was made of the Skylab S190A photos, LANDSAT images, and 24-channel MSS images of Red Lake. For illustrative purposes, Figure II-D-1 presents the green wavelength pictures of the S190A (A), LANDSAT (B), and 24-channel (C) images.

Examination of the four Skylab S190A photographs revealed that only four of the eight features were discriminable. The identifiable features were B, C, D and H. It was not possible to separate F and G, the two different playa surfaces, due to photographic saturation of the playa on the S190A film. Although the wet area, feature H, is discernible, variations in it cannot be seen. In general, more information was extractable from the green and red photographs due to the graininess and poor resolution of the latter.

Standard EROS paper prints of the four LANDSAT MSS bands (Frame 1321-17440) were analyzed at a scale of 1:1,000,000. The same features discernible on the S190A photographs were seen, except for feature H, whose absence may only reflect the different acquisition dates of the imagery. No major differences in discrimination of the selected features are evident between the LANDSAT images. Frames from several other dates were examined for the test area to insure that photographic quality was not a significant variable; and little variation was found.

The thirteen different wavelength bands of the 24-channel MSS data were examined for the distinctness of the eight features of interest. Black and white paper prints at a scale of about 1:100,000 were used in the analysis. The results of visual inspection of the photos are tabulated in Table II-11.

From inspection of Table II-11, it is apparent that many of the features are more distinct in the longer wavelength bands. The change in the texture in the playa surface (features F and G) is most pronounced in the infrared region beyond 0.81 μm, and in the violet region of the spectrum. Also of interest is

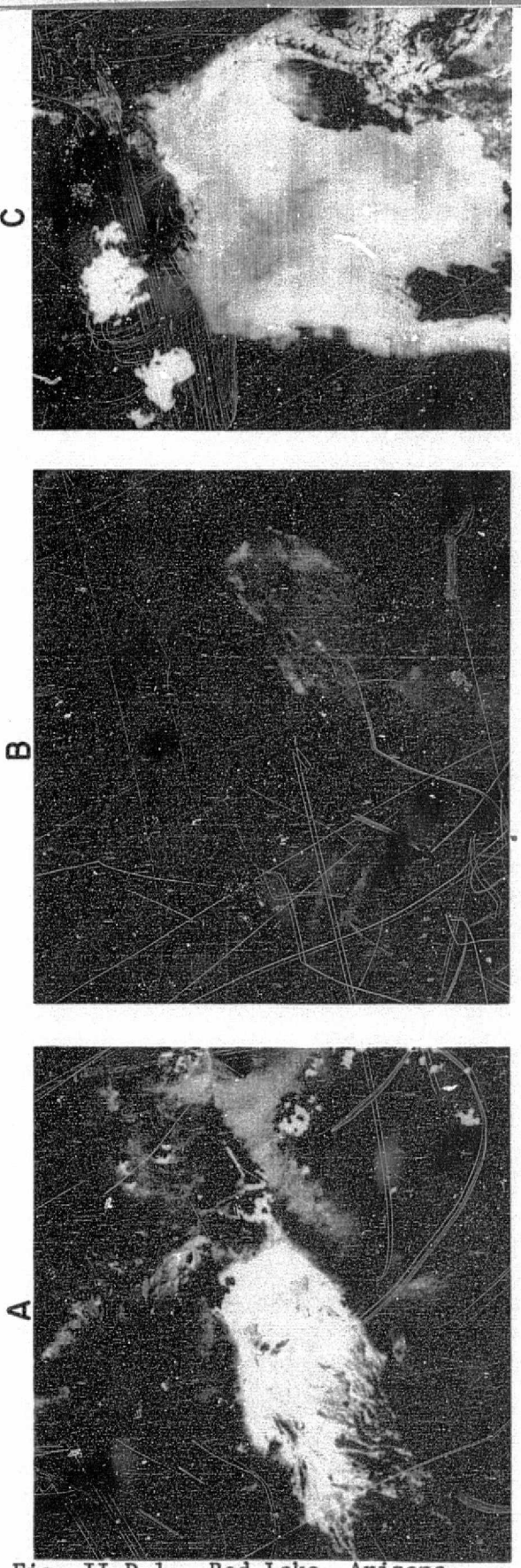

Fig. II-D-1. Red Lake, Arizona.
(a) S190A greenband.
(b) Landsat greenband.
(c) 24 channel scanner greenband.

the distinctive appearance of variation in moisture of the playa surface, which can only be seen in the wavelength bands beyond 0.98 μm. Feature E is only visible in the longest infrared wavelength bands.

Table II-11. Relative Discriminability of Selected Features on 24-Channel Images

	Feature							
	A	B	C	D	E	F	G	H
Band								
2	+	+	+	o	o	+	+	o
4	+	+	+	+	o	+	+	o
5	+	+	+	+	o	o	o	o
6	+	+	+	+	o	o	o	o
7	+	o	+	+	o	o	o	o
8	+	o	+	+	o	o	o	o
9	+	o	+	+	o	+	+	o
10	+	o	o	+	o	+	+	+
24	+	o	o	+	o	+	+	o
23	+	o	o	+	o	o	o	+
11	+	+	+	+	+	+	+	+
12	+	+	+	+	o	+	+	+
13	+	+	+	+	+	+	+	+

+ = discriminable

o = not discriminable

4. CONCLUSIONS

Although this is a very preliminary analysis of different kinds of multispectral data available, certain conclusions and recommendations can be made:

1) The selected features on Red Lake are in general very subtle on the LANDSAT images, and there is little variation between bands.

2) The photographs acquired with the S190A camera with green and red filters are similar and are comparable to the LANDSAT images. The S190A photographs acquired with infrared filters contain much less usable information.

3) The best discrimination of vegetation features, playa texture, and moisture variation can be achieved from use of images acquired in longer wavelength bands (further in the reflected infrared region). This information is available from use of an instrument such as the Bendix 24-channel scanner.

II-E. NW Arizona - Comparison of S190A and LANDSAT Photographic Images

M. J. Abrams

1. INTRODUCTION

Most users of Skylab and LANDSAT data do not have image processing facilities (such as IPL-JPL) at their disposal. Consequently, they must rely only on the standard photo products available from EROS. In order to better assess the usefulness of photo imagery for photogeologic mapping, a comparison was made between the standard Skylab S190A images and LANDSAT images for an area in northwest Arizona.

There is little doubt that many factors influence the quality of imagery obtained from EROS. These include:

(1) Sun angle and elevation

(2) season of the year that the imagery is acquired

(3) variation in quality of photo reproduction.

These problems confront all users of EROS imagery. In this section, their effect on the usability of the various images is considered in the comparison of Skylab and LANDSAT imagery.

2. STUDY AREA

The study area is located in northwest Arizona (Figure II-E-1). It is well suited for a remote sensing study, as vegetation is minimal and the rock lithologies are diverse and well exposed.

The study area is bounded on the north and west by the Colorado River, on the east by the Grand Wash Cliffs, and on the south by latitude 34°45' north.

Physiographically the area is on the eastern margin of the Basin and Range province, and hence is characterized by north-trending fault-bounded mountain ranges, alternating with long, narrow alluviated valleys. The Grand Wash Cliffs on the east mark the beginning of the Colorado Plateau province.

Fig. II-E-1. Location map with features.

Prominent physiographic features, as shown in Fig. II-E-1, include the Black Mtns., Cerbat Mtns., Hualapai Mtns., Peacock Mtns. and the Grand Wash Cliffs. Between these ranges are alluviated valleys: Detrital, Sacramento, Hualapai, and Big Sandy Valleys. The only flowing river in the area is the Colorado River, which has been dammed to form Lake Mead and Lake Mohave; and at the northern end of Hualapai Valley is Red Lake, a dry inter-mountain lake bed.

The climate is arid, with scant precipitation falling as occasional summer thundershowers and winter rain, with snow in the highest elevations. Vegetation is sparse: cactus, scrub brush and grasses are found in the lowlands, with transition to conifer trees at higher elevations.

Lithologically the mountains and hills are mainly composed of igneous and metamorphic rocks. About half of the outcrop exposures consist of Precambrian schists, gneisses, and granites. These are overlain and intruded by Cretaceous, Tertiary, and Quaternary extrusive and intrusive rocks. Their composition ranges from andesites and tuffs to basalts and granites. Sedimentary rocks are restricted to the Paleozoic limestones, sandstones and shales exposed along the Grand Wash Cliffs, and Tertiary and Quaternary alluvial units. These are made up of Colorado River gravels and sediments, and moderately to weakly consolidated valley fill of local origin.

Structures are restricted to north and northwest trending normal faults, which bound and cut the mountain blocks. A geologic map of the area is shown in Figure II-E-2, compiled from Longwell (1963), Gillespie and Bently (1971), Wilson and Moore (1959), and Wilson, Moore, and Cooper (1969).

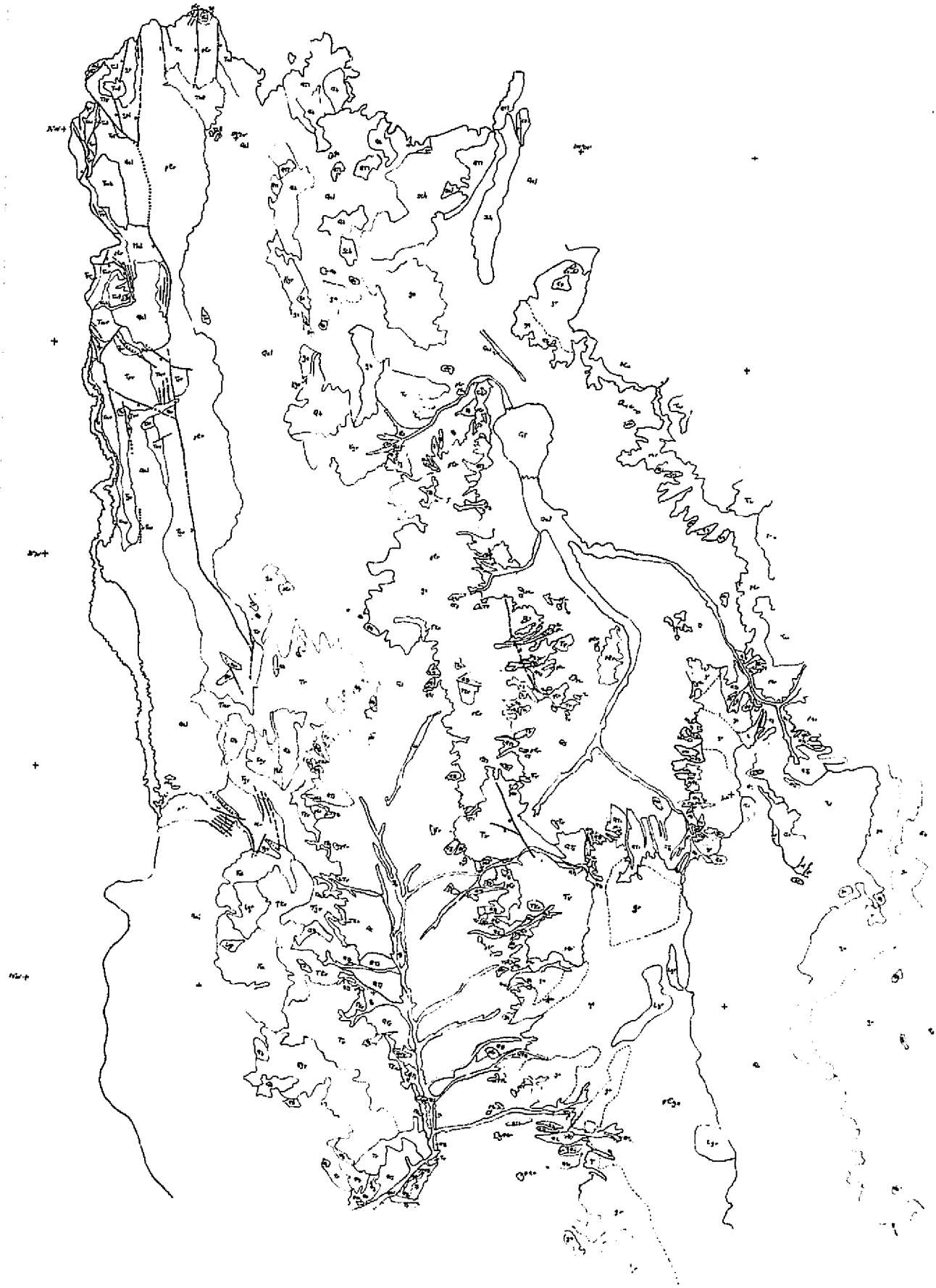

Fig. II-E-2. Geologic map of study area.

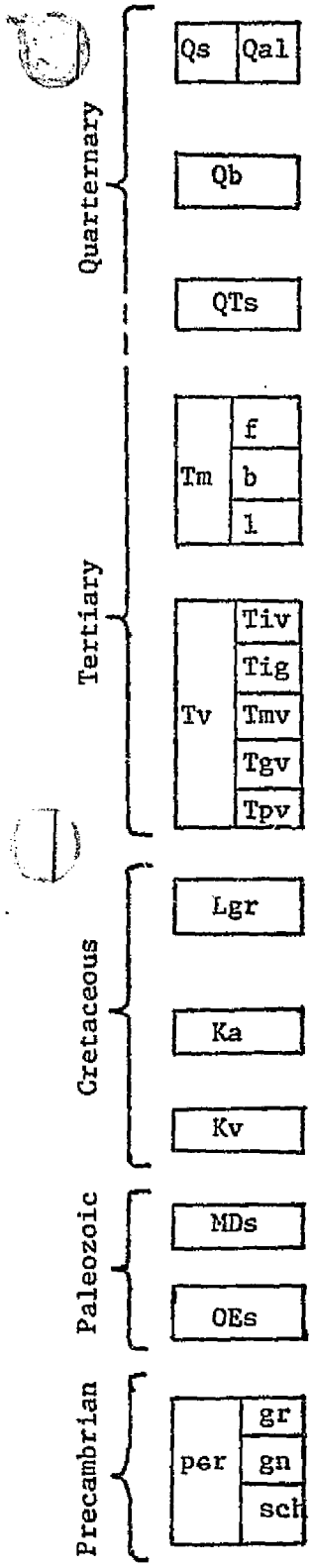

Alluvium
- Qs - alluvial deposits: sand, gravel, and conglomerate
- Qal - stream deposits

Basalt

Intermediate Alluvium
- Weakly to moderately consolidated

Muddy Creek Fm.
- Tm - undifferentiated Muddy Creek Fm.
- Tmf - Fortification basalt
- Tmb - breccia of landslide origin
- Tml - sandstone, silt, clay

Volcanic and Intrusive Rocks
- Tv - undifferentiated volcanic and intrusive rocks
- Tiv - undifferentiated, range in age from Patsy Mine to Mt. Davis
- Tig - Intrusive rocks, cut Mt. Davis or older volcanics
- Tmv - Mt. Davis volcanics; basalt and dark andesite
- Tgv - Golden Door volcanics; latite, rhyolite
- Tpv - Patsy Mine volcanics; andesite, basalt

Granite

Andesite
- Flows, tuffs, and agglomerate

Volcanic Rocks
- Rhyolite to andesite

Limestone
- Redwall and Temple Butte Fms.

Tonto Group
- Muav limestone, Bright Angel shale, Tapeats sandstone

Igneous and Metamorphic Rocks
- per - undifferentiated
- gr - granite
- gn - gneiss
- sch - schist

Figure II-E-2b. Description of Units

3. COMPARISON OF IMAGERY

The LANDSAT image analyzed is 1051-17432, which was acquired on September 12, 1972. The Skylab images were acquired on June 3, 1973 (Track 3, Pass 6) during the second Skylab mission.

Characteristics of each imaging system are spectral range of the cameras or sensors and resolution. The LANDSAT multispectral scanner (MSS) recorded reflected light in four wavelength bands. Skylab S190A cameras photographed the ground in 6 wavelength bands (Table II-12).

TABLE II-12

Wavelength	"Color"	LANDSAT Band	SL Band
5000-6000 Å	Green	4	6
6000-7000 Å	Red	5	5
7000-8000 Å	IR	6	1
8000-9000 Å	IR	-	2
8000-11000 Å	IR	7	-
4000-7000 Å	Color		4
5000-8800 Å	Color infrared	-	3

LANDSAT bands 4, 5, and 6 are equivalent to Skylab bands 6, 5, and 1. And, infrared band 7 of LANDSAT includes band 2 of Skylab. Therefore, differences in wavelength region are not a factor affecting the comparison of Skylab and LANDSAT imagery.

A comparison was made of resolution of Skylab S190A transparencies and LANDSAT transparencies. Skylab transparencies were obtained as copies of the original film: 70 mm second generation products, and 9" x 9" third generation products. ERTS transparencies are third generation products made from the original data which was acquired on magnetic tape.

Measurements were made on the positive transparencies using a Zeiss microscope. Reference points measured were inlets along the shore of Lake Mohave, and distances determined from the Spirit Mt. 7-1/2' topographic map. The closest two inlets resolvable through the microscope determined the resolution limit of the the transparencies (Table II-13).

TABLE II-13

	Band	Resolution (± 50 ft.)	
Skylab S190A	1	70 mm	9" x 9"
	2	450'	500'
	5	450'	450'
	6	200'	200'
	4	-	400'
		450'	450'
LANDSAT	4,5,6,7	650'	

From the measurements it is concluded that the resolution of Skylab 70 mm and 9" x 9" transparencies is the same, and both have better resolution than LANDSAT transparencies.

In order to compare LANDSAT and Skylab images, positive paper prints were made of all bands shown in Table II-12 at a scale of 1:500,000. Then, fifteen stratigraphic units were chosen. Overlays were produced of structural and lithologic features discernible by photointerpretation on each image. Each data set was rated according to the ability to discriminate the fifteen stratigraphic units and mapped faults, on a scale of 0 = poor, 1 = fair, 2 = good, and 3 = excellent.

The rating of the four LANDSAT bands is tabulated in Table II-14. Band 7 (infrared) proved to have the most lithologic information. The boundaries between all fifteen units were distinguishable. While it was not always possible to uniquely identify a unit strictly from the photo, with the aid of some ground truth (the geologic map) this was possible. Bands 5 and 6 were almost identical as to the amount of information discernible. All units but one, QTS, were delineated. And, band 4 had the least information, i.e., many lithologic units had similar reflectivities.

TABLE II-14. COMPARISON OF LANDSAT IMAGES

Band:	4	5	6	7
Unit				
Qal	1	1	1	1
Qs	1	1	1	1
Qb	2	2	2	2
QTs	0	0	0	1
Tm	2	2	2	3
Tv	1	2	2	2
Tmv	1	1	1	2
Tgv	1	2	2	2
Tpv	0	1	1	2
Ka	0	1	1	1
Kv	1	1	2	1
OEs	2	2	2	2
gn	1	2	2	2
gr	1	1	1	1
sch	2	2	2	2
TOTALS	17	22	23	28
FAULTS	1	1	1	2

A similar rating of the Skylab images is tabulated in Table II-15. Band 4, color, had the most lithologic information. All units except Cretaceous andesite, Paleozoic sediments, and Precambrian granite could be distinguished. Bands 5 and 6 were almost as good as the color picture for delineating lithologic units. Cretaceous andesite and volcanic rocks could not be recognized, nor could Precambrian granite. There was very good discrimination of Quaternary and Teriary alluvial and sedimentary roc . Bands 1 and 2 had the least amount of usable informatin, with six and seven indistinguishable units respectively.

TABLE II-15. COMPARISON OF SKYLAB IMAGES

Band:	1	2	4	5	6
Unit					
Qal	2	2	3	3	3
Qs	0	0	3	2	3
Qb	3	3	3	3	2
QTs	0	0	2	2	3
Tm	3	3	3	3	2
Tv	2	2	2	2	2
Tmv	2	0	1	1	1
Tgv	3	2	2	2	2
Tpv	0	0	1	1	1
Ka	2	2	0	0	0
Kv	0	2	1	0	0
OEs	0	0	0	1	1

Table II-15. Comparison of Skylab Images (contd)

Unit	Band:	1	2	4	5	6
gn		0	0	2	1	1
gr		2	0	0	0	0
Sch		2	2	2	2	2
	TOTALS:	21	18	25	23	23
	FAULTS:	0	1	1	1	1

A band-by-band comparison of the same LANDSAT and Skylab images is presented in Table II-16. Skylab green and LANDSAT infrared 2 are much better than their counterparts. For the red and infrared 1 images, there is little distinction.

Combining all four bands for each, the best discriminability for each lithologic unit is tabulated in Table II-17, without regard to which band was used. Skylab images were equal or better for 12 of the fifteen units. LANDSAT images were equal or better for 9 units. For structural discrimination, LANDSAT images were better.

TABLE II-16. COMPARISON OF SKYLAB AND LANDSAT IMAGES

	BAND							
Unit	L-4	SL-6	L-5	SL-5	L-6	SL-1	L-7	SL-2
Qal	1	3	1	3	1	2	1	2
Qs	1	3	1	2	1	0	1	0
Qb	2	2	2	3	2	3	3	3
QTs	0	3	0	2	0	0	1	0
Tm	2	2	2	3	2	3	3	3

Table II-16. Comparison of Skylab and Landsat Images (contd)

	BAND							
Unit	L-4	SL-6	L-5	SL-5	L-6	SL-1	L-7	SL-2
Tv	1	2	2	2	2	2	2	2
Tmv	1	1	1	1	1	2	2	0
Tgv	1	2	2	2	2	3	2	2
Tpv	0	1	1	1	1	0	2	0
Ka	0	0	1	0	1	2	1	2
Kv	1	0	1	0	2	0	1	2
OEs	2	1	2	1	2	0	2	0
gn	1	1	2	1	2	0	2	0
gr	1	0	1	0	1	2	1	0
sch	2	2	2	2	2	2	2	2
TOTALS:	16	23	21	23	22	21	26	18
FAULTS	1	1	1	1	1	0	2	1

TABLE II-17. COMPARISON OF OPTIMUM DISCRIMINABILITY

Best of Both

	LANDSAT	Skylab
Qal	1	3
Qs	1	3
Qb	3	3
QTs	1	3
Tm	3	3

Table II-17. Comparison of Optimum Discriminability (contd)

	LANDSAT	Skylab
Tv	2	2
Tmv	2	3
Tgv	2	3
Tpv	2	1
Ka	1	2
Kv	2	2
OEs	2	1
gn	2	1
gr	1	2
sch	2	2
TOTALS	27	33
FAULTS	2	1

4. DISCUSSION OF DIFFERENCES

One of the major differences between the LANDSAT and Skylab images is the position of the sun. (Table II-18)

TABLE II-18. SOLAR POSITION

	Azimuth	Elevation
LANDSAT	136.3°	49.6°
Skylab	189.0°	76.5°

Because the LANDSAT images were acquired when the sun was lower and more oblique to the structural fabric of the area, there is a relative enhancement of topographic features. This is seen in several ways. For example, the

ability to distinguish gneiss in the northeast part of the area is better, because the low relief of the gneissic hills is brought out by shadowing. On the Skylab pictures it is virtually impossible to separate these low hills from surrounding alluvium. Faults are also seen better on LANDSAT pictures due to enhancement of north-trending linear topographic features, which are expressions of normal faults. In the Skylab pictures, topographic detail relating to faults is suppressed, as the sun is shining from almost due south, parallel to fault trends.

Thus, the effect of sun position on usefulness of imagery is concluded to be significant. There is less detrimental effect in the LANDSAT scene because the sun was in a more advantageous position for enhancing topographic and structural details.

The effect of seasonal variation on the images is slight. Even though the Skylab and LANDSAT data were acquired almost a year apart, both times were excessively dry periods. Therefore vegetation was minimal.

5. CONCLUSION

A comparison was made between Skylab S190A images and LANDSAT images for lithologic identification. The following conclusions were made based on the preceding analysis:

(1) Resolution of S190A images is better than LANDSAT photo products, and is about 110 meters compared to 210 meters.

(2) Comparing equivalent spectral bands, Skylab images were more useful for lithologic discriminability in the green band; the LANDSAT infrared 2 band was better than the Skylab band; and red and infrared-1 bands were comparable.

(3) LANDSAT images were better for identifying faults. This is primarily due to the more advantageous position of the sun in enhancing topographic information.

6. REFERENCES

Longwell, C., 1963, "Reconnaissance Geology Between Lake Mead and Davis Dam, Arizona-Nevada", USGS Prof. Paper 374-E.

Gillespie, J. and Bently, C., 1971, "Geohydrogology of Hualapai and Sacramento Valleys, Mohave County, Arizona, USGS Water Supply Paper 1899-H.

Wilson, D. and Moore, R., 1959, "Geologic Map of Mohave County, Arizona", Arizona Bureau of Mines and Univ. of Arizona, Tucson.

Wilson, D., Moore, R., and Cooper, J., 1969, "Geologic Map of Arizona", Arizona Bureau of Mines and USGS, Tucson.

II-F. Photogrammetric Evaluation of Skylab Imagery, Central Arizona

S. S. C. Wu, F. J. Schafer, R. Jordan

1. INTRODUCTION

Skylab was the largest manned space station ever to be put in orbit. After 3900 orbits over a period of 171 days, the four Skylab missions have increased our knowledge of the Sun, and our knowledge of living organisms in an orbital environment. However, a primary experiment was the Earth resources experiments package (EREP), which gathered natural and cultural resource data for studying the Earth. (1)

EREP was another step forward in the application of equipment and techniques for the aerial survey of the Earth's surface. It was designed to provide a synoptic survey of the Earth's surface in the visible, infrared (IR), and microwave spectral wavelengths. The multispectral photographic array consisted of high precision multispectral cameras, and the Earth Terrain Camera, multispectral scanners, and other sensor information having application to Earth resource management surveys. The multispectral cameras are six identical mapping cameras having focal lengths of 6 inches and were equipped with a combination of filters and films to take photographs simultaneously at various wavelength bands in the visible and near-infrared portions of the spectrum. An area of 163 square km was photographed from a nominal altitude of 435 km. The Earth Terrain Camera (Hycon) is a single-lens camera having an 18 inch focal length. It complements the multispectral camera imagery by providing comparatively high-resolution photographs, allowing more detailed interpretation of the images. The angular field of view is 14.24°, providing a ground coverage of 109 km^2 from a nominal altitude of 435 km. The ground resolution ranges from 17 to 30 meters depending on the type of film used. (2)

The object of this work was to evaluate the precision and repeatability of photogrammetric measurements made from stereoscopic models established from

Earth Terrain Camera and multispectral camera images of central Arizona. A stereo model of color photographs taken with the Skylab 4-S190B Earth Terrain Camera and two stereo models from the multispectral camera (band 4) were established photogrammetrically with respect to ground control shown on 1:24,000 and 1:62,500 scales (7½) U. S. Geological Survey topographic maps, on an AP/C analytical plotter. A contour map was compiled at 1:100,000 scale with a contour interval of 500 feet using the ETC images, and spot measurements were made to evaluate the general accuracy of the compilation and the precision of photogrammetric measurements that could be made from the model. Results of this evaluation have demonstrated that it is possible to compile topographic maps having accuracies comparable to standard 1:250,000 scale maps (2^{o} sheets), as well as to revise existing maps from the Earth Terrain Camera photography. This is a significant step forward in our ability to survey the Earth's features.

2. EXPERIMENTAL CONDITIONS AND METHODS

A model of Skylab 4-S190B Earth Terrain Camera color photography (90-305 and -306) covering a part of central Arizona in the vicinity of Prescott, Jerome, Camp Verde, Clarkdale, Cottonwood and the Verde River, was set up on the AP/C analytical plotter. These photographs were taken at about 10:00 a.m. local time on April 12, 1973, when the sun angle was approximately 42^{o}, which is optimal for aerial photography. The photo scale is about 1:950,000. With the SO-242 high-resolution type of color film and 0.4 to 0.7 micrometer filter band, these photographs have an estimated ground resolution of 21 m (70 feet). As shown in Figure II-F-1 the image format is 11.43 x 11.43 cm^2. Contact positive transparencies were directly used on the plotter. For model orientation, control points were scaled from existing USGS 1:24,000 and 1:62,500 scale topographic maps. Both of these photographs are vertical and have a base-to-height ratio

Figure II-F-1. Skylab 4 Earth Terrain Camera color photograph 90-305 used in compiling the topographic map shown in Figure II-F-2. The outline in the photograph indicates the area mapped.

of 0.26. For evaluating the precision of elevation measurements, on the AP/C analytical plotter, 18 image points of different ground objects distributed throughout the model were measured with 5 readings being taken at each point. The standard errors of elevation readings range from 15 to 72 feet with an average standard error of elevation measurement of 30 feet. From these results, theoretically, it should be possible to compile a map with a contour interval of 100 feet. However, there appears to have been a problem with the model because the horizontal and vertical measurements were inconsistent. The AP/C plotter has the capability of automatically correcting for Earth curvature and atmospheric refraction, and because of this the only unknown factor is the camera. No precise camera calibration data were available for the study and a nominal focal length was used. The use of an incorrect camera focal length can result in a model scale that varies according to elevation; additionally, unknown camera lens distortions can cause significant inconsistencies in the photogrammetric measurements.

Ground coordinates of 76 points were measured from the model for evaluating horizontal measurements, and referred to points identified on the USGS topographic maps. To avoid errors due to different projections (orthographic projection for the model and transverse Mercator projection for the map), ground distances were computed from each of these points to a point near the center of the model. Each computed distance was then compared with the corresponding map distance. Differences are positives if the ground distance measured from the model is greater than the distance measured from the map. Ratios then formed by dividing the distance difference by the respective distance, are used to evaluate the accuracy of horizontal measurements. The ratios thus derived ranged from $\frac{1}{46}$ to $\frac{1}{141,000}$, with an average ratio of $\frac{1}{3,800}$. Distances measured from the

control point ranged from 15,400 feet to 215,500 feet. The numbers of positive and negative ratios are 44 and 32 respectively. The average value of absolute distance differences is 134 feet.

The differences of elevations of the same 76 points range from -680 feet to +660 feet, with an average of 156 feet for the absolute value of elevation differences. There are 42 positive elevation differences and 32 negative.

A contour map, shown in Figure II-F-2, with a contour interval of 500 feet was compiled from a part of this model as shown in Figure II-F-1. A contour interval as small as 200 feet could have been obtained for the compilation of topographic maps from this space photography taken with the Earth Terrain Camera if all the correct parameters required for model orientation had been available.

One of the objectives of this study was to explore the possibilities of topographic mapping from very small scale (1:3,000,000) photography. To do this, two stereo models of the 6" focal length multispectral camera (MSS, band 4) photography were analyzed in the AP/C analytical plotter. This camera with the FF filter has the same bandpass (0.4-0.7 m) as the Earth Terrain Camera. Using the SO-356 film, at low contrast, the ground resolution was estimated to be between 73 to 79 meters. With an image format of 5.72 cm^2 on 70 mm film, the cameras have a 21.2° field of view and thus cover 163 square kms of the ground from a nominal altitude of 435 km. The photographs used for these two models are 4B-035 and -036, and 4B-035 and -037 (Skylab 4). One-to-one contact size positive transparencies were used. These photographs were taken at about 10:00 a.m. local time on January 2, 1974 when the sun angle was approximately 24°. They are vertical photographs of central Arizona in the vicinity of Oak Creek Canyon, Prescott, the Verde River, Jerome, Sedona and part of Phoenix.

The model, using photographs 4B-035 and -036, has an overlap of about 75%. The base-to-height ratio is only 0.098, which is very poor for elevation

measurements. Even if every other photograph is used to increase the base-to-height ratio, such as photographs 4B-035 and -037, the base-to-height ratio is still as low as 0.19 with 50% overlap. From model 4B-035 and -36, 10 points with five elevation readings at each point were measured. The standard errors of elevation reading ranged from 40 to 330 feet, with an average of 157 feet. From model, 4B-035 and -037, which has twice the base-to-height ratio as the -035 -036 model, 13 points scattered across the model were measured. Standard errors of elevation readings ranged from 50 to 133 feet with an average of 87 feet which is about twice the accuracy of the elevation measurements from 4B-035 and 036 which has about one-half the base-to-height ratio.

3. SUMMARY

Even though camera calibration data required for model orientation were not available at the time of this study, and therefore the probable cause of inconsistencies in measurements in the stereo models on the AP/C analytical plotter, we have found that the image quality (resolution) of the multispectral and Earth Terrain Camera photographs is adequate for the preparation of some special purpose of topographic and planimetric maps, and revisions to existing regional map can be directly compiled from the EREP data. The Earth Terrain Camera provides the highest spatial resolution and image definition of any non-classified camera system yet flown in space. The photographs can be particularly useful for regional landform analysis for land use planning, and for the preparation of planimetric cartographic products.

The Earth Terrain Camera photography taken from orbital altitude has large coverage and photographic detail equivalent to that of 60,000 feet aerial photography. Considering both ground resolution and photo scale, the Earth Terrain Camera imagery has adequate detail for the compilation of 1:1,000,000 and possibly 1:50,000 scale maps.

4. REFERENCES

Skylab Program, EREP Investigator's Information Book, 1973, NASA MSC-07874.

Skylab Earth Resources Data Catalog, 1974, NASA JSC 09016.

III. PROCESSING

III-A. Processing of S192 Data

M. J. Abrams

1. PRELIMINARY PROCESSING

Raw, unline-straightened S192 data was obtained from JSC on computer-compatible magnetic tape. Computer processing of the tapes was performed at JPL's Image Processing Laboratory on an IBM 360/44 computer which uses VICAR, an image processing supervisor. VICAR is characterized by simple, standardized input/output and usage rules and by an extensive library of applications programs and procedures.

Each tape was first processed using VICAR program VSKY192. This program unleaves the multispectral data and creates a separate file for each SDO. A VICAR label is applied to each SDO and a check is made for synchrony between SDO's. If there is a lack of continuity between lines and SDO's, an appropriate number of lines are inserted or dropped. Next, VICAR program ERTSFIX is applied to the data to correct bad lines. The program operates by removing a bad line, and inserting a new one which is the average of neighboring lines.

At this point, the high data rate channels (SDO's 1-16) were merged into a single channel equivalent to the low data rate channels (SDO's 17-22). This was done using VICAR program SKYMRG which operates on two adjacent odd and even numbered channels. The DN at each pixel in the output picture is found by resampling data from the two input SDO's using a cubic convolution (spline) function, the resultant value occupying a position between the odd and even pixels.

The preliminary processing step is geometric rectification of the data. VICAR program SKYRECT is applied to the data, and compensates for the 5-1/2° cone

angle and 110° scan arc motion of the sensors. In addition a correction is made for spacecraft motion and earth rotation during the acquisition of the frame. In the process, SKYRECT reduces the acquired 1240 samples/line to 1056 samples/line.

2. ENHANCEMENTS

To produce the pictures used for geologic analysis, the images were contrast-stretched by methods fully described in Geotz et al., 1975.

3. RATIONING AND NOISE REMOVAL

Band-to-band ratios were made from the S192 channels. This was done using VICAR program RATIO, which compares two input pictures and produces an output picture according to the algorithm:

$$DN_o = a \frac{DN_1}{DN_2} + b$$

o = output

1, 2 = input pictures

The two constants a and b are determined by the program so that the output picture histogram will fill the dynamic range of the playback medium; thus a and b are dependent upon the scene being processed.

Fig. III-A-1d is the ratio of SDO3 and SDO7. (Fig. III-A-1a and III-A-1b are SDO's 3 and 7, respectively.) This rationing was done after the SDO's were line-straightened. Examination of Fig. III-A-1d reveals a very high noise level in the picture. This shows up as herring bone patterns, random noise, etc.

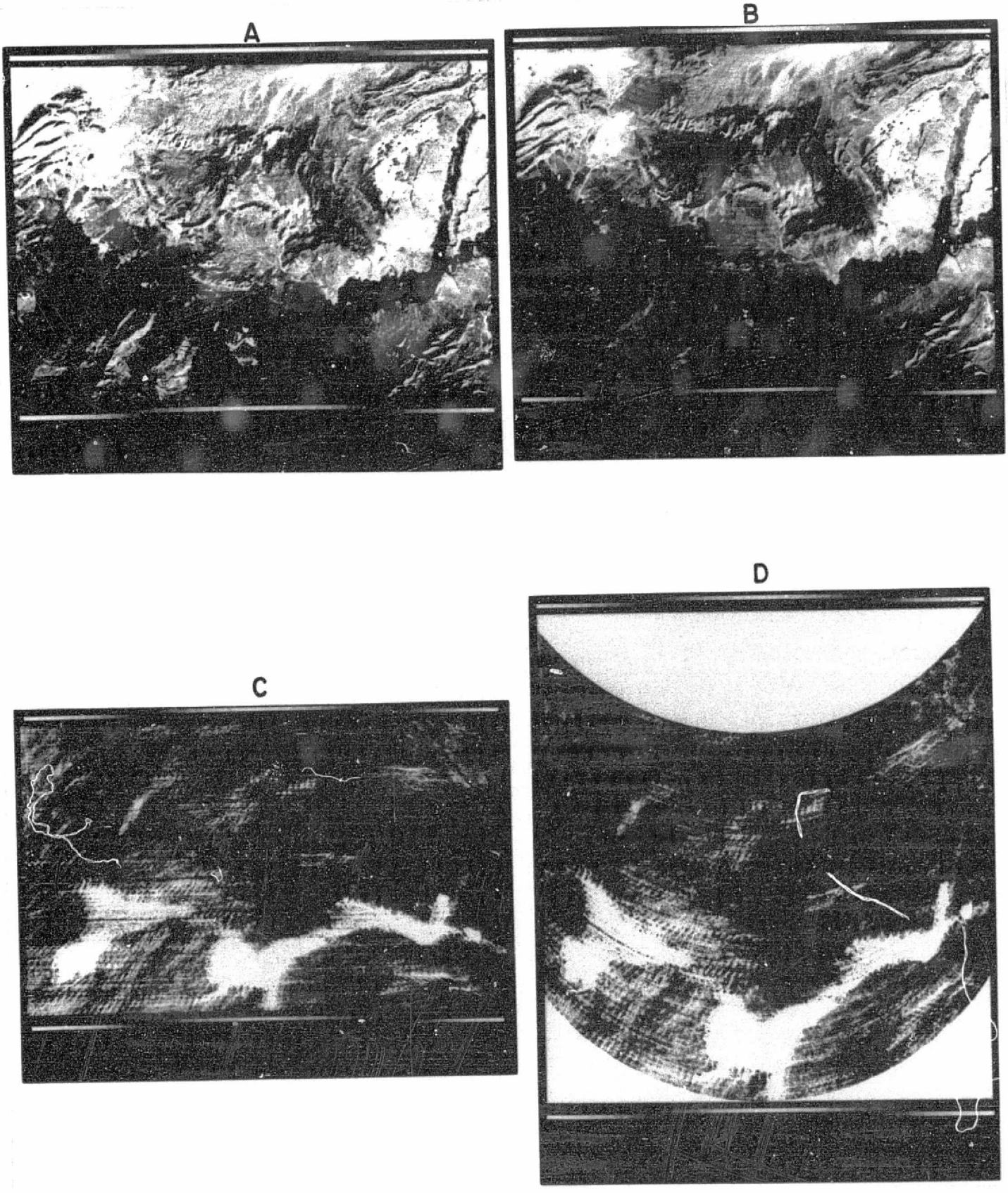

(a) SDO 3
(b) SDO 7
(c) Ratio of SDO3 and SDO7 before line straightening.
(d) Ratio of SDO3 and SDO7 after line straightening.

Fig. III-A-1. Skylab S192 images.

In order to try and identify the source of the noise, a one-dimensional power spectrum was made of the picture using VICAR program POWER. This program uses a fast Fourier Transform to acquire the power spectrum of each line, and produces a single spectrum by averaging together the individual spectra for each line. (See Fig. III-A-2a, for example.) Examination of the power spectrum identified anomalies corresponding approximately to a frequency of 16 cps and to its associated harmonics.

It was assumed that this noise was due to mirrophonic noise induced by the detector cooling system. However, other possible sources were investigated. A possible source for this noise was the geometrical corrections applied to the original data. To test this possibility, a ratio picture was produced from the unstraightened data (Fig. III-A-1c) and the same power spectra were acquired. No change was observed in the anomalous noise notches. Therefore, geometrical rectification was ruled out as a source of the noise.

Another possible source for the noise was misregistration between the channels due to physical misalignments of the detectors. VICAR program CROSS was used to check the correlation between the channels. Nine rectangles within the picture were used for comparison between channels; the correlation was excellent. It was concluded, therefore, that misregistration between channels was not the source of the noise.

In order to attempt to remove the noise, a convolution notch filter (Fig. III-A-2b) was designed to compensate for the anomolies in the power spectra. This filter was a one-line subractive box filter having a convolution Barnel consisting of 301 weights. The weights were found using VICAR program FILTER 2, which calculates rectangular filter weights using the Fourier transformation of a notch filter, which fits the power spectrum of the image. The notches were

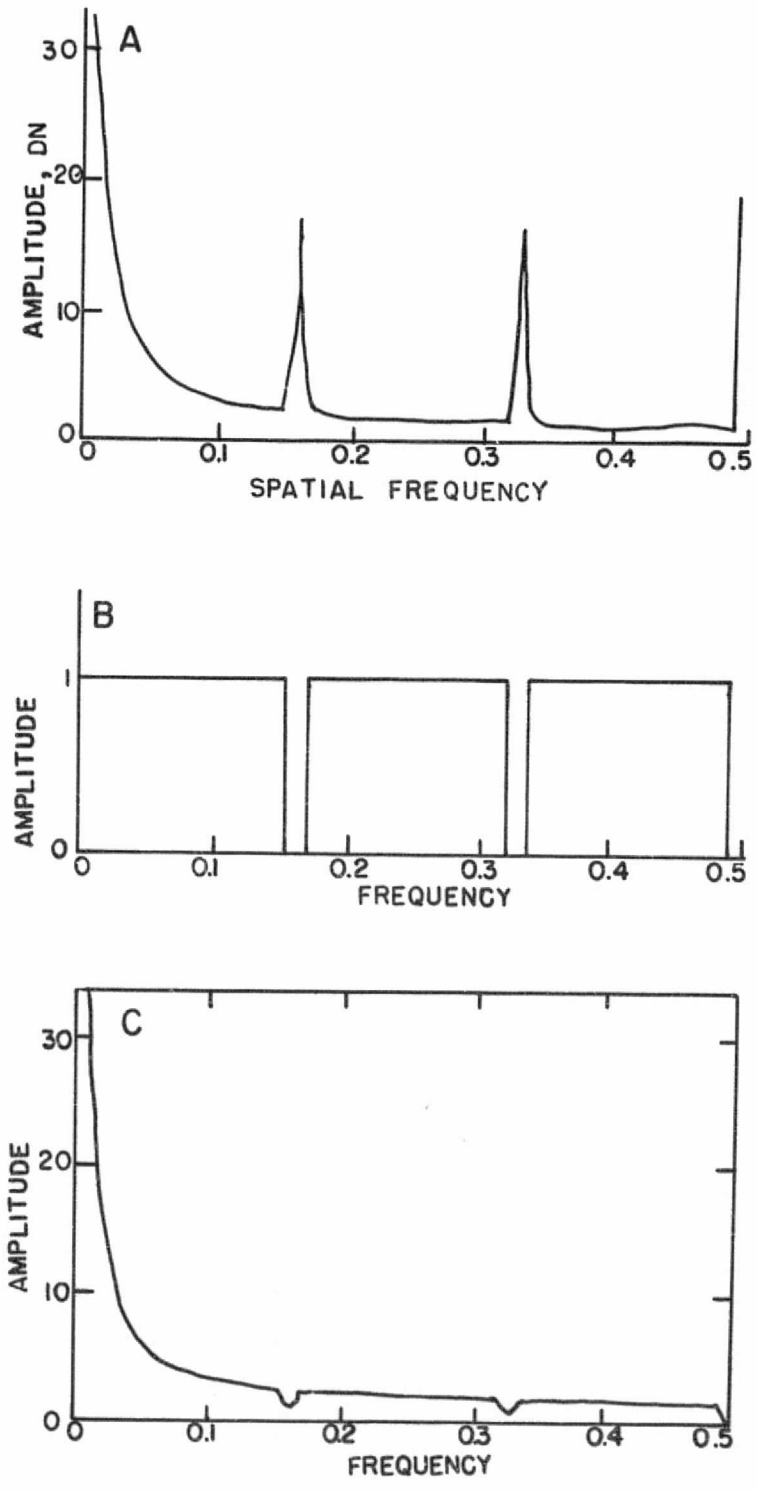

(a) Power spectrum of Skylab ratio picture.
(b) Convolution notch filter.
(c) Product of filter spectrum and image spectrum

Fig. III-A-2.

centered at the frequencies at which the noise was observed, and the shape of the notches specified to try to insure that the product of the filter spectrum and image spectrum show no noise spikes (Fig. III-A-2c).

After filtering the picture, a different picture was made by subtracting the "after" picture from the "before" picture using VICAR program DIFFPIC. Despite the fact that the difference picture showed the removal of considerable noise, the filtered picture still contained too much noise to be usable.

III-B. Computer Program Descriptions

AFILTER — Performs two-dimensional asymmetrical convolution filtering.

ASPECT — Performs one-dimensional resampling (bilinear interpolation).

ASPECT2 — Performs two-dimensional resampling (using bilinear interpolation, lagrangian centered function, or spline function).

ASTRTCH2 — Performs an automatic linear, ramp cumulative-distribution function (CDF), or gaussian contrast stretch on an image. The percentage of the input picture allowed to saturate black or white is controllable. A ramp CDF contrast stretch redistributes input digital numbers (DN) to enforce the condition that all gray levels in the output picture have the same frequency of occurrence. A gaussian contrast stretch modifies the input histogram to resemble a gaussian distribution.

BOXFLT — Applies a two-dimensional low-pass "box" convolution filter (with all weights = 1) to an image.

CROSS — Determines the translation necessary to register scene information between rectangular areas in two images. Calculates the sum of the squares of the differences between corresponding DN levels of a rectangle in image 1 and a rectangle in image 2. This process is repeated, moving the rectangle in image 2 by 1 pixel each time, until a matrix of registration coefficients is constructed. The minimum value yields the best registration.

DIFFPIC — Arithmetically computes the DN difference between two input pictures, scales the difference, and creates from it an output image. The input images can be displaced from each other.

ERTSFIX — Removes "striping" in ERTS MSS imagery by forcing agreement of means and standard deviations for each of the six sensor histograms per spectral band. Replaces spectral bands by interpolation as an option.

F — Fast and flexible byte arithmetic program accepting one or two input pictures. Utilizes a 256- by 256-byte lookup table to apply a chosen function. The table may be generated under parameter control or may be read from a disk or tape storage.

FASTFIL1
FASTFIL2 — Convolve an image with a high-pass filter in one (sample only) or two dimensions. Filter used is a subtractive equal-weight filter with dimensions n by m. As an option, FASTFIL2 creates the low-pass picture and/or histograms of the output.

FFT1
FFT2 — Compute the one- or two-dimensional complex Fourier transform. An option exists for the computation of the inverse transform. Transforms must have horizontal and vertical dimensions equal to power of 2.

FFTIL — Performs one-dimensional frequency space filtering of harmonic noise using the fast Fourier transformation algorithm. Noise spikes are removed one line at a time by either amplitude notching or by linear interpolation of the complex spectrum of each line across the harmonic noise spectral spikes. The output picture is the retransformed image including spectral corrections. POWER can be used to determine frequencies to be filtered.

FFTPICL — Process VICAR format complex Fourier transforms or complex pictures extracting, reorganizing, and automatically scaling various functions of the complex data for image display. Available functions of the complex input include amplitude, intensity (squared amplitude), phase (with or without sign), real part, and imaginary part. Linear or logarithmic scaling before output can be performed for all functions except phase.

FILTER — Performs two-dimensional convolution filtering followed by a linear transformation to scale the output. FILTER differs from AFILTER in that the filter weights must be symmetrical about the vertical and horizontal lines passing through the filter center.

FOTO — Creates a polaroid picture of an image.

GEOM
LGEOM — Effects geometric transformation of images using bilinear interpolation resampling algorithms. Geometric control is input via a rectilinear grid of control points over the output picture, describing the location of the same points in the input picture. LGEOM is a multipass version of GEOM and is more efficient if large vertical translations are required.

HISTO — Creates histogram data set in VICAR format for use in display programs and contrast modification programs such as ASTRTCH2.

LIST — Produces decimal printouts of a picture or portions of a picture. Optionally displays histograms of the examined regions.

MASK — Prepares digital image in VICAR format for display as a film picture. Pixel grids, gray scales, wall clock date and time, and the VICAR processing history label are shown along with the picture.

POLYFLTR Applies convolution filter to a picture. Filter weights used may belong to one of five different filters; the appropriate filter can be varied during processing, based on some parameter of the image being filtered (e.g., local brightness or variance of brightness).

POWER Computes one-dimensional power spectrum of a specified portion of a picture. The square root of the power spectrum is displayed on the line printer, and a file is written on an output tape suitable for plotting on a stand-along Calcomp plotter.

RATIO Computes parameters for F, causing F to apply

$$DN' = a \frac{DN_1 - \text{constant}_1}{DN_2 - \text{constant}_2} - b \qquad (1)$$

$$DN' = \log \; a \frac{DN_1 - \text{constant}_1}{DN_2 - \text{constant}_2} - b \qquad (2)$$

$$DN' = a\,(DN_1 - DN_2) - b \qquad (3)$$

or

$$DN' = \log\,[a(DN_1 - DN_2) - b] \qquad (4)$$

to produce a digital image comparing two input pictures. Determines coefficients a and b so that the resulting probability-density function (PDF) optionally occupies a 256-level dynamic range, and the distribution is centered on DN' = 128.

REGISTER	Aligns two images depicting the same scene, based on correlation of selected regions within the input pictures. Parameters are generated that allow GEOM or GEOMA to effect the desired geometric transformation.
SAR	Copies picutres from one data set to another. Replaced specified rectangular areas with data interpreted from the perimeter.
SKYMRG	Merges two adjacent odd and even numbered Skylab S192 SDO's, recorded at the high data rate, into a single channel equivalent to a low data rate channel.
SKYRECT	Line-straightness Skylab S192 conical data; computes parameters for LGEOM to perform geometrical corrections for satellite and earth motion.
TAPE2	Manipulates data stored on tape.
VSKY192	Converts Skylab S192 images from JSC tapes to VICAR format. Specifically, data are segregated by spectral channel (SDO); each individual channel image is assigned a standard 360-byte VICAR label.
WTGEN WTSIN WTGNI	Generate convolution filter weights if a filter modulation-transfer function (MTF) is defined by the user. WTGEN generates symmetrical two-dimensional filters. WTSIN allows the MTF to differ vertically and horizontally. WTGNI computes a one-dimensional filter only.

III-C. Skylab S192 Image Processing Sequence

M. J. Abrams

The computer programs described in III-B are used in the following sequence:

1. DATA PREPARATION

TAPE2. Checks for tape errors, missing data.

VSKY192. Converts to VICAR format.

SKYMRG. Merges high data channels.

SKYRECT. Removes conical scan.

ASTRTCH2. Performs linear contrast stretch and picture display.

2. GEOMETRIC RECTIFICATION

INSERT. Replaces missing data lines with interpolated data.

GEOM, LGEOM, GEOMA, EGEOM. Compensate for aspect ratio, roll and pitch of satellite, foreshortening caused by viewing geometry, and nonlinearities in the scan velocity of the multi-spectral scanner (MSS) mirror.

SKEW. Compensates for the Earth's rotation during picture acquisition.

ASPECT. Resamples to set the aspect ratio to unity.

WTGEN, WTSIN. Define convolution filter to restore uniform spatial-frequency response.

FILTER. Applies filter to restore uniform spatial-frequency response.

CROSS, REGISTER. Register images taken at different times, or register images to maps.

3. RADIOMETRIC RECTIFICATION

ERTSFIX. Removes stripping by matching means and standard deviations in the sensor histograms (probability-distribution or probability-density functions, PDF).

STRETCH. Performs nonlinear "table" stretch to cause radiometry to agree with ground observations.

4. COSMETICS

ERTSFIX. Replaces lines with severe stripping by interpolated values.

SAR. Interpolates across large blemishes.

FFT2, FFT1. Perform Fourier transformation of an image to identify and remove coherent noise.

5. ANALYSIS

a. Extractive routines

LIST. Displays on a line printer pixel listing, histograms, means, and standard deviations of rectangular areas within a picture.

FFT1, FFT2. Perform one-and two-dimensional Fourier transformation.

POWER. Creates one-dimensional power spectrum.

HISTO. Creates histograms and stores them in a VICAR format data set.

b. Dimension modification: image comparison

REGISTER. Registers automatically two images of the same scene.

CROSS. Prints out correlogram that indicates translation providing best registration for a small region in an image pair.

DIFFPIC. Differences two images arithmetically.

F. Performs fast, flexible byte arithmetic (using lookup table) for one or two input pictures.

RATIO. Predicts best linear transformations (stretch) to scale ratio or difference pictures into 8-bit output, then fetches F to perform the required operation. Useful for temporal or spectral comparisons.

6. DISPLAY

STRETCH. Performs linear and nonlinear contrast modifications.

ASTRTCH2. Performs automatic linear and limited nonlinear contrast modifications.

MASK. Annotates an image for display.

TEXTAD. Adds annotation within the image.

FILTER. Emphasizes different spatial spectral features. Enhances local contrast.

III-D. Classification Algorithms

B. S. Siegal

This section provides a general description of classifications, and outlines the classification algorithms and preclassification analytical procedures which were used in the geologic investigations described in Section II-D. These classification procedures are applicable for all multispectral data.

1. PROCESS OF CLASSIFICATION

Classification is the process of recognizing classes or groups whose members have certain characteristics in common. Ideally, the classes should be mutually exclusive and exhaustive; that is, there should be one and only one class to which an element is assigned, and all elements in the domain of interest may be so assigned. In practice, these requirements are difficult to fulfill and are not often achieved (Griffiths, 1968).

The classes or groups are based on properties possessed by the elements of a population, and classes are formed by grouping together those elements of a population that are alike, where likeness is defined by certain selected properties or criteria (Griffiths, 1968, Block, 1972). An optimum classification will group elements together into classes which are separated from one another by discontinuities in the ranges of their observed properties (Imbrie and Purdy, 1962).

Classifications can either be natural or artificial. In a natural classification, not only are the classes mutually exclusive and exhaustive, but they are based on the essential characteristics of the elements under investigation, and those elements are grouped together which possess fundamental similarities. In an artificial classification, the grouping is determined by superficial

resemblances or external criteria. The boundaries between the groups are artificial even though they may have been objectively determined (Hempel, 1952; Imbrie and Purdy, 1962).

In general, most classification schemes used for MSS data are artificial. Analysts are concerned with classifying MSS images into various subsets, each corresponding to features or themes of specific interest, such as geologic units, soils, cultural features or vegetation. Two different approaches to classification of MSS imagery are generally used. The classification can be supervised, in which training areas are established by the analyst, or unsupervised in which the boundaries are objectively determined from a computer algorithm to delineate natural clusters. In supervised classification, each training area, which supposedly is representative of a specific feature of interest, is determined from a priori knowledge, i.e., "ground truth". Statistics are computed for each theme and are used in various automated techniques to identify other areas within the MSS image which have similar characteristics. In unsupervised classification, no a priori knowledge is assumed, and the classes are based on the actual relations among the variables. In such classification schemes the number of classes can be established by an analyst or, more objectively, through the use of an algorithm in which the data itself is used to suggest the number of natural categories: that is, to find the number of clusters.

2. SUPERVISED CLASSIFICATION TECHNIQUES ANALYZED

a. Stepwise Linear Discriminant Analysis

Discriminant function analysis consists of finding a transform which minimizes the ratio of the difference between group multivariate means to the group multivariate variances.

The algorithm used here (after UCLA BMD07M Program) computes a classification function for each of the themes by choosing and inputting the independent variables in a stepwise manner. The variable entered at each step is selected on the basis of its F statistic. At each step of the analysis a classification function is computed for each theme. The equation of the classification function D_{ki} for the k^{th} theme for the i^{th} variable is given by

$$D_{ki} = d_{ko} + \sum_{i=1}^{r} e_{ki} \, z_{lki}$$

where

c_{ko} = constant term for the k^{th} theme

r = number of input variables (spectral bands or ratios)

e_{ki} = discriminant coefficient for the k^{th} theme and the i^{th} variable

z_{lki} = measured spectral parameter of the l^{th} case of the k^{th} theme for the i^{th} variable

The constant term c_{ko} is computed from $-1/2 \sum_{i=1}^{r} e_{ki} \, \bar{X}_{ki}$, where $\bar{X}_{ki}$ is the mean of variable i for theme k. The coefficient e_{ki} is computed from $(n-g) \sum_{J=1}^{r} \bar{X}_{kj} \, a_{ij}$. At each step of the procedure the variables are divided into two dispoint sets: those included in the discriminant functions (r) and those not included. The within-group matrix of cross products of deviations (W) and the matrix of cross products of deviations for the total sample (T) are computed. The elements of these matrices are:

$$w_{ij} = \sum_{k=1}^{g} \sum_{n=1}^{n_g} (X_{ikn} - \bar{X}_{ik}) \, (X_{jkn} - \bar{X}_{jk})$$

$$t_{ij} = \sum_{n=1}^{n} (X_{in} - \bar{X}_i)\ (X_{jn} - \bar{X}_j)$$

where g = the number of groups, n_g = the number of objects in group g, X_{ikn} = the measurement, for variable i, on the n^{th} object in group k, n = total number of objects; and i and j run from 1 to p, the number of variables. The W and T matrices are

$$W = \begin{bmatrix} W_{11} & W_{12} \\ W_{21} & W_{22} \end{bmatrix}$$

$$T = \begin{bmatrix} T_{11} & T_{12} \\ T_{21} & T_{22} \end{bmatrix}$$

where W_{11} and T_{11} are r x r, and r is the number of variables included in the discriminant functions.

The elements a_{ij} are derived from matrix A, and the elements b_{ij} from matrix B:

$$A = \begin{bmatrix} W_{11}^{-1} & & W_{11}^{-1} & W_{12} & & \\ W_{21} & W_{11}^{-1} & W_{22} & -W_{21} & W_{11}^{-1} & W_{12} \end{bmatrix} = a_{ij}$$

C-3

$$B = \begin{bmatrix} T_{11}^{-1} & & T_{11}^{-1} & T_{12} & & \\ & & & & & \\ T_{21} & T_{11}^{-1} & T_{22} & -T_{21} & T_{11}^{-1} & T_{12} \end{bmatrix} = b_{ij}$$

The optimum input variables (spectral channels or ratios) are chosen on the basis of the largest F-statistic, where, for the entry of the j^{th} variable,

$$F_j = \frac{a_{jj} - b_{jj}}{b_{jj}} \cdot \frac{n-r-g+1}{g-1}$$

where

n = total number of cases

g = number of themes

The degrees of freedom are g-1 and n-r-g+1. An iterative technique is used to determine the best linear combination of spectral bands (or ratios).

b. Hybrid Approach

As a preliminary step in using the hybrid classifier algorithm, all the possible input variables are analyzed to determine the minimum number of inputs necessary to separate the themes. For each of the variables, the means ($\bar{X}_i$) and standard deviations ($\hat{\sigma}_i$) of the themes are computed. The themes are compared pairwise for each variable, and are deemed separable if

$$\frac{\bar{X}_1 - \bar{X}_2}{c\ (\hat{\sigma}_1 + \hat{\sigma}_2)} > 1$$

The hybrid classification technique combines two existing classification schemes, the Parallelepiped algorithm and the Bayesian Maximum Liklihood Function (Addington, 1975). In this classification scheme, the means and covariance matrix are computed for each theme specified, assuming gaussian distributions. These statistics define the themes; the number of standard deviations about the mean can be specified by the analyst to represent the ideal decision boundaries for each class. In p-dimensional space, these decision boundaries are hyper-ellipsoids. The Parallelepiped algorithm approximates the hyperellipsoids with hyperrectangles. If an unknown pixel falls within one of them, it is considered unknown; and if it falls into an area where hyperrectangles overlap, it is considered ambiguous.

Computationally (Addington, 1975), each picture element (pixel) of the multi-spectral imagery data is considered as the transpose of a p-dimensional vector $\bar{X}^T = (X_1\ X_2 \ldots X_p)^T$, where p is the number of spectral bands. The mean and standard deviation of the j^{th} class out of a possible m classes are m and $\hat{\sigma}_j$, respectively. The Parallelepiped algorithm assigns a pixel to class j_o is and only if

$$\mu_{i,j_o} - \delta\hat{\sigma}_{i,j_o} \leq X_i \leq \mu_{i,j_o} + \delta\hat{\sigma}_{i,j_o}$$

for each i = 1, 2, ... p and δ = constant defining the confidence interval.

The Bayesian algorithm is used to resolve ambiguities or to assign unknowns which arise through use of the Parallelepiped algorithm. In the former case, the statistical liklihood that a pixel falls into each of the ambiguous classes is computed; in the latter, the liklihood for all classes is computed. The class with the maximum liklihood is then chosen as the class to which the

pixel is assigned. The likelihood of $\overline{X}^T$ being a member of class j is defined by the normal multivariate probability density function P_j, where

$$P_j = \frac{1}{(2\pi)^{p/2} \left| k_j \right|^{1/2}} \exp \left\{ -1/2 \ (\overline{X} - \& \ \overline{\mu}_j)^T \ K_j^{-1} \ (\overline{X} - \overline{\mu}_j) \right\}$$

where K_j is the covariance matrix (p x p) of the j^{th} class and $|K_j| = \det (K_j)$. In practice, it is not P_j which is computed, but $\ln P_j$. This is appropriate since ln is a monotonic increasing function and only the maximum P_j is desired.

3. UNSUPERVISED CLUSTER ANALYSIS

An unsupervised iterative clustering algorithm, CLUS, was used to classify the study area and assess the homogeneity of the LANDSAT spectral data for each of the lithologic units exposed in the Coconino plateau (see Section II-D-6).

CLUS is an iterative technique (Rubin and Friedman, 1967) in which the "best" partition of n objects into g groups is based on evaluation of variance and covariance matrices. This method is applicable to the general problem of classification even when the number of groups is unknown. The algorithm followed is one in which the data itself (p measurements on n objects) is used to suggest "natural categories"; that is, to find the clusters.

The best partition of n objects into g groups is defined as that partition, out of all possible partitions of the objects into g groups, for which a numerical valued criterion function achieves its maximum value. Several criterion functions exist in the CLUS program. They all depend on the fundamental relationship T = W + B, where W is the pooled within-group matrix of cross products of deviations, T is the matrix of cross products of deviations for the total sample, and B is the matrix of cross products of deviations of groups

from the grand means weighted by group size (Cooley and Lohnes, 1962). The elements of the W and T matrices are a previously defined (see III-C-2); the elements of B are

$$b_{ij} = \sum_{k=1}^{g} n_g \, (\bar{X}_{ik} - \bar{X}_i) \, (\bar{X}_{jk} - \bar{X}_j)$$

with the same nomenclature as used in III-C-2.

The "best" classification is the one which maximizes the between-group and minimizes the within-group variation.

The CLUS algorithm includes five criteria which may be used to determine the "best" classification. One criterion function is the logarithm of the ratio between the determinant of T and B (log $|T| / |B|$) where T/B = 1 + W so that maximizing log $|T| / |B|$ is the requirement. The value of this criterion function may be used as an informal indicator of the best number of groups, by examining its change in value as the number of groups is increased (Rubin and Friedman, 1967).

A second criterion uses Mahalonobis D^2, a multi-dimensional Euclidean distance function in which the distance between groups is compared with the distance within groups; the aim is to maximize variation between groups as compared with the distance within groups.

A third procedure examines the trace of W (Tr. W) and attempts to minimize this function (i.e. minimize the sum of squares within groups).

The other two criteria are approximations to log $|T| / |B|$ and to Mahalonobis D^2.

The CLUS algorithm also contains routines for improving the initial grouping; for example, it is possible to apply or suppress hill-climbing routines,

forcing passes, and reassignment passes (Rubin and Friedman, 1967). One may also start from a single group, from a chosen or previously obtained grouping, or from a random start.

Although iterative unsupervised classification techniques, such as CLUS, provide an optimum classification, these procedures are time consuming and require large amounts of computer care. Classification of MSS data by such algorithms must therefore be based initially on the classification of a random, representative, small sample of the population under study.

4. REFERENCES

1. Addington, J. (1975), A Hybrid Classifier Using the Parallelepiped and Bayesian Techniques, in Proc. of Amer. Soc. of Photogrammetry, 41st Annual Mtg., March 9-14, 1975, Washington, D.C., pp. 772-784.
2. Block, F. (1972), A Multivariate Chemical Classification of Rocks from the Montregian Petrographic Provice, Quebec, Canada, Unpubl. Ph.D. Thesis, Dept. of Geosciences, The Pennsylvania State University, University Park, PA, p. 172.
3. Cooley, W.W. and Lohnes, P.R. (1962), Multivariate Procedures for the Behavioral Sciences, John Wiley and Sons, Inc., p. 211.
4. Griffiths, J.C. (1968), Geological Data for Classification, in Proc. of a Sympos. on Decision Making in Mineral Exploration, Vancouver, Canada. Reprinted in Western Miner, Feb. and April 1968: Contribution No. 67-37, College of Earth and Mineral Sciences, The Pennsylvania State University, University Park, PA.

5. Hempel, C.G. (1952), Fundamentals of Concept Formation in Empirical Science, Vol. 1-11 of the INternational Encyclopedia of Unified Science, University of Chicago Press, Chicago, pp. 93.

6. Imbrie, J. and Purdy, E.G. (1962), Classification of Modern Behamian Carbonate Sediments, in Ham, W.E. (ed.), Classification of Carbonate Rocks, A Symposium: Memoir 1, Amer. Assoc. Petroleum Geologist, pp. 253-272.

7. Rubin, J. and Friedman, H.P. (1967), A Cluster Analysis and Taxonomy System for Grouping and Classifying Data, I.B.M. Corporation, New York Scientific Center, 590 Madison Avenue, New York, NY 10022, p. 221.